

**COMPARISON OF MODELS FOR SPACER GRID PRESSURE LOSS IN NUCLEAR FUEL  
BUNDLES FOR ONE AND TWO-PHASE FLOWS**

A Thesis

Presented in Partial Fulfilment of the Requirements for the

Degree of Master of Science

with a

Major in Nuclear Engineering

in the

College of Graduate Studies

University of Idaho

by

Alan B. Maskal

Major Professor: Fatih Aydogan, Ph.D.

Committee Members: Fred S. Gunnerson, Ph.D., Donald M. McEligot, Ph.D.

Department Administrator: Richard N. Christensen, Ph. D

May 2017

**AUTHORIZATION TO SUBMIT THESIS**

The thesis of Alan B. Maskal, submitted for the degree of Master of Science with a Major in Nuclear Engineering and titled, "COMPARISON OF MODELS FOR SPACER GRID PRESSURE LOSS IN NUCLEAR FUEL BUNDLES FOR ONE AND TWO-PHASE FLOWS," has been reviewed in final form. Permission, as indicated by the signatures and dates below, is now granted to submit final copies to the College of Graduate Studies for approval.

Major Professor: \_\_\_\_\_ Date: \_\_\_\_\_  
Fatih Aydogan, Ph.D.

Committee Members: \_\_\_\_\_ Date: \_\_\_\_\_  
Fred S. Gunnerson, Ph.D.

\_\_\_\_\_ Date: \_\_\_\_\_  
Donald M. McEligot, Ph.D.

Department  
Administrator: \_\_\_\_\_ Date: \_\_\_\_\_  
Richard N. Christensen, Ph. D.

## ABSTRACT

Spacer grids maintain the structural integrity of the fuel rods within fuel bundles of nuclear power plants. They can also improve flow characteristics within the nuclear reactor core. However, spacer grids add reactor coolant pressure losses, which require estimation and engineering into the design. Several mathematical models and computer codes were developed over decades to predict spacer grid pressure loss. Most models use generalized characteristics, measured by older, less precise equipment. The study of OECD/US-NRC BWR Full-Size Fine Mesh Bundle Tests (BFBT) provides updated and detailed experimental single and two-phase results, using technically advanced flow measurements for a wide range of boundary conditions.

This thesis compares the predictions from the mathematical models to the BFBT experimental data by utilizing statistical formulae for accuracy and precision. This thesis also analyzes the effects of BFBT flow characteristics on spacer grids. No single model has been identified as valid for all flow conditions. However, some models' predictions perform better than others within a range of flow conditions, based on the accuracy and precision of the models' predictions. This study also demonstrates that pressure and flow quality have a significant effect on two-phase flow spacer grid models' biases.

## **ACKNOWLEDGEMENTS**

The author would like to gratefully acknowledge the assistance, guidance and mentorship of Dr. Fatih Aydogan, in guiding me to achievement that I thought was impossible without his guidance.

## **DEDICATION**

I would like to dedicate this thesis to my four incredible children, Erika, Brian, Sara, and Katie for their understanding while I had to spend many hours of research and writing instead of with them. They provided the motivation necessary to maintain the effort to finish this degree.

## TABLE OF CONTENTS

<b>Authorization to Submit</b> .....	ii
<b>Abstract</b> .....	iii
<b>Acknowledgements</b> .....	iv
<b>Dedication</b> .....	v
<b>Table of Contents</b> .....	vi
<b>List of Figures</b> .....	x
<b>List of Tables</b> .....	xii
<b>Introduction</b> .....	1
<b>Chapter 1. Literature Review</b> .....	5
1.1. Introduction.....	5
1.2. Test Facility and Equipment.....	5
1.3. Formats and General Losses.....	6
1.4. Single-Phase Spacer Grid Pressure Loss Models.....	7
1.5. Two-Phase Spacer Grid Pressure Loss Models.....	12
1.6. Two-Phase Test Theory and Structure.....	14
1.7. Conclusions .....	15
1.8. References .....	16
<b>Chapter 2. Test Equipment</b> .....	18
2.1. Test Facility .....	18
2.2. Fuel Bundle and Spacer .....	20
2.3. Pressure Measurement.....	22
2.4. Void Measurement.....	24
2.5. References .....	25

<b>Chapter 3. General Parameters and Losses</b> .....	26
3.1. Introduction.....	26
3.2. Fuel Bundle Geometry.....	26
3.3. Single-Phase Flows and Parameters.....	28
3.4. Two-Phase Flows, Parameters and Measurement Method.....	29
3.5. General Spacer Loss Equation.....	29
3.5.1. Single-Phase General Losses.....	30
3.5.2. Two-Phase General Losses.....	31
3.5.3. Flow Regimes.....	36
3.6. Nomenclature.....	38
3.7. References.....	45
<b>Chapter 4. Single-Phase Pressure Loss Models</b> .....	46
4.1. Introduction.....	46
4.2. Single-Phase Pressure Loss Model Structure.....	47
4.3. Specific Single-Phase Pressure Loss Models.....	48
4.3.1. Empirical Models.....	48
4.3.2. Semi-Empirical Models.....	54
4.4. References.....	59
<b>Chapter 5. Single-Phase Experiment and Results</b> .....	61
5.1. Experiment Theory and Structure.....	61
5.1.1. Experiment Structure.....	61
5.1.2. Experiment Purpose and Theory.....	63
5.1.2.1. Purpose.....	63
5.1.2.2. Test Conditions.....	63
5.1.2.3. Possible Measurement Errors.....	64

5.2 Results.....	65
5.2.1. Criteria .....	65
5.2.2. Flow Characteristics .....	66
5.2.3. Graphical Analysis of Single-Phase Spacer Pressure Loss Models .....	66
5.2.4. Tabular Summary of the Results .....	73
5.3. Observations.....	74
5.3.1. General Observations.....	74
5.3.2. Single-Phase Spacer Grid Pressure Loss Model Observations .....	76
5.4. References .....	77
<b>Chapter 6. Two-Phase Spacer Grid Pressure Loss Models .....</b>	<b>78</b>
6.1. Introduction.....	78
6.2. Two-Phase Pressure Loss Model Structure .....	78
6.3. Two-Phase Pressure Loss Models.....	79
6.3.1. Theory.....	79
6.3.2. Specific Two-Phase Spacer Grid Pressure Loss Models .....	80
6.4. References .....	84
<b>Chapter 7. Two-Phase Experiment and Results.....</b>	<b>85</b>
7.1. Experiment Theory and Structure .....	85
7.1.1. Experiment Structure.....	85
7.1.2. Experiment Purpose and Theory .....	87
7.1.2.1. Purpose .....	87
7.1.2.2. Two-Phase Properties .....	87
7.1.2.3. Single-Phase Pressure Loss Coefficients .....	88
7.1.2.4. Possible Measurement Errors.....	88



7.2. Results.....	91
7.2.1. Criteria .....	91
7.2.2. Flow Characteristics .....	91
7.2.2.1. BFBT Flow Regimes .....	91
7.2.2.2. Two-Phase Reynolds Numbers and Void Fractions .....	93
7.2.3. Combined Properties Results .....	93
7.2.4. Graphical Analysis of the Flow Characteristics .....	98
7.2.5. Quality and Pressure Characteristics Effect.....	103
7.2.5.1. Tabular Summary .....	103
7.2.5.2. Graphical Analysis of Two-Phase Spacer Grid Pressure Loss Models.....	122
7.3. Observations.....	132
7.3.1. Two-Phase Spacer Multipliers and Single-Phase Coefficients Observations.....	132
7.3.2. General Observations and Trends.....	135
7.4. References .....	137
<b>Chapter 8. Conclusions .....</b>	<b>138</b>

## LIST OF FIGURES

### Chapter 2

Figure 1: Diagram of the Test Facility (Neykov et al., 2006) .....	18
Figure 2: Test Fuel Bundle (Neykov et al., 2006).....	19
Figure 3: Overview of the Fuel Bundle (Neykov et al., 2006).....	20
Figure 4: Spacer Cross Section (Neykov et al., 2006) .....	21
Figure 5: General View of the Spacer (Neykov et al., 2006) .....	21
Figure 6: Dimensions of the Spacer Grid (Neykov et al., 2006) .....	22
Figure 7: Test Section 301 (dpT1) (Neykov et al., 2006) .....	23
Figure 8: Void Measurement Equipment (Neykov et al., 2006).....	24

### Chapter 3

Figure 9: Rod Bundle Cross Section (Neykov et al., 2006).....	26
Figure 10: Constricted Area Diagram (Idel'chik, 1986) .....	27
Figure 11: Common Vertical Flow Patterns (Todreas and Kazimi, 2012).....	37

### Chapter 4

Figure 12: Spengos Drag Coefficients for Grid Spacers (Spengos, 1959) .....	49
Figure 13: Drag Coefficients for Transverse Grid Spacers based on Spacer Hydraulic Diameter (DeStourder, 1961).....	50
Figure 14: Spacer Drag Coefficients for the Tong and Weisman Correlation (Tong and Weisman, 1970).....	52
Figure 15: Spacer Drag Coefficients for the Rehme Correlation (Rehme, 1973).....	53
Figure 16: Form Loss Factors for the Rehme and Trippe Correlation (Rehme and Trippe. 1980).....	54
Figure 17: Chun and Oh Form Drag Coefficients (Chun and Oh, 1998).....	56

## Chapter 5

Figure 18: “Empirical Results” at 200 KPa Test Pressure .....	67
Figure 19: “Semi-Empirical Results” at 200 KPa Test Pressure.....	68
Figure 20: “Empirical Results” at 1 MPa Test Pressure .....	69
Figure 21: “Semi-Empirical Results” at 1 MPa Test Pressure .....	70
Figure 22: “Empirical Results” at 7.15 MPa Test Pressure .....	71
Figure 23: “Semi-empirical Results” at 7.15 MPa Test Pressure .....	72

## Chapter 6

Figure 24: B factor for the Chisholm Equation (Rooney et al., 1974) .....	84
---	----

## Chapter 7

Figure 25: Flow Regimes for 7.16 MPA BFBT Tests .....	92
Figure 26: Flow Regimes for 8.65 MPA BFBT Tests .....	92
Figure 27: Effect of the Reynolds Number on the Accuracy of the 2 Phase Multiplier.....	99
Figure 28: Effect of the Flow Quality on the Accuracy of the 2 Phase Multiplier.....	100
Figure 29: Effect of the Pressure on the Accuracy of the 2 Phase Multiplier .....	101
Figure 30: Effect of the Void Fraction on the Accuracy of the 2 Phase Multiplier .....	102
Figure 31: Effect of Quality and Pressure on Accuracy – $K_{Schikorr}$ .....	123
Figure 32: Effect of Quality and Pressure on Accuracy - $K_{IN}$ .....	124
Figure 33: Effect of Quality and Pressure on Accuracy – $K_{CO}$ .....	125
Figure 34: Effect of Quality and Pressure on Accuracy – $K_{Shiralkar}$ .....	126
Figure 35: Effect of Quality and Pressure on Accuracy – $K_{Rehme-Tripp}$ .....	127
Figure 36: Effect of Quality and Pressure on Accuracy – $K_{Rehme}$ .....	128
Figure 37: Effect of Quality and Pressure on Accuracy – $K_{DeStourder}$ .....	129
Figure 38: Effect of Quality and Pressure on Accuracy – $K_{Spengos}$ .....	130
Figure 39: Effect of Quality and Pressure on Accuracy - $K_{Idel'chik}$ .....	131

## LIST OF TABLES

### Chapter 4

Table 1: Summary of Single-Phase Spacer Grid Pressure Loss Models .....	46
---	----

### Chapter 5

Table 2: Single-Phase Test Data (Neykov et al., 2006) .....	62
---	----

Table 3: Bias of Calculated Results (Difference in %).....	73
--	----

Table 4: Standard Deviation of Calculated Equations Bias (%) .....	74
--	----

### Chapter 6

Table 5: Summary of Two-Phase Spacer Grid Pressure Loss Multipliers .....	78
---	----

### Chapter 7

Table 6: Two-Phase Flow Characteristics .....	86
---	----

Table 7: Combined Test Results Bias .....	95
---	----

Table 8: Combined Test Results Standard Deviation .....	96
---	----

Table 9: Accuracy of the 2 Phase Multiplier Based on 7% Quality and 7.16 MPa.....	104
---	-----

Table 10: Precision of the 2 Phase Multiplier Based on 7% Quality and 7.16 MPa.....	105
---	-----

Table 11: Accuracy of the 2 Phase Multiplier Based on 10% Quality and 7.16 MPa.....	106
---	-----

Table 12: Precision of the 2 Phase Multiplier Based on 10% Quality and 7.16 MPa.....	107
--	-----

Table 13: Accuracy of the 2 Phase Multiplier Based on 14% Quality and 7.16 MPa.....	108
---	-----

Table 14: Precision of the 2 Phase Multiplier Based on 14% Quality and 7.16 MPa.....	109
--	-----

Table 15: Accuracy of the 2 Phase Multiplier Based on 19% Quality and 7.16 MPa.....	110
---	-----

Table 16: Precision of the 2 Phase Multiplier Based on 19% Quality and 7.16 MPa.....	111
--	-----

Table 17: Accuracy of the 2 Phase Multiplier Based on 24% Quality and 7.16 MPa.....	112
---	-----

Table 18: Precision of the 2 Phase Multiplier Based on 24% Quality and 7.16 MPa.....	113
--	-----

Table 19: Accuracy of the 2 Phase Multiplier Based on 7% Quality and 8.65 MPa.....	114
--	-----

Table 20: Precision of the 2 Phase Multiplier Based on 7% Quality and 8.65 MPa.....	115
---	-----

Table 21: Accuracy of the 2 Phase Multiplier Based on 14% Quality and 8.65 MPa.....	116
Table 22: Precision of the 2 Phase Multiplier Based on 14% Quality and 8.65 MPa.....	117
Table 23: Accuracy of the 2 Phase Multiplier Based on 24% Quality and 8.65 MPa.....	118
Table 24: Precision of the 2 Phase Multiplier Based on 24% Quality and 8.65 MPa.....	119
Table 25: Highest Accuracy and Highest Precision Two-Phase Models at each Quality Ratio and Pressure .....	121

## INTRODUCTION

The nuclear fuel rod bundles used in nuclear power plants such as Pressurized Water Reactors (PWR) and Boiling Water Reactors (BWR) require spacer grids to maintain the integrity and spacing of the slender fuel rods. In addition to maintaining critical geometry, these spacer grids can provide benefits such as enhanced cooling through increased mixing and turbulence, which may increase heat distribution, leading to higher Departure from Nucleate Boiling (DNB) conditions in PWRs. The spacer grids also enhance the critical power ratios by increasing the liquid layer's thickness in BWRs. However, spacers also cause a pressure drop which must be engineered into the performance and operation of fuel bundles.

The flow within a fuel bundle involves a number of complicated factors, such as cross flow, (de)entrainment of liquid layers, bubble or droplet break up/join together. Numerous models, both in mathematical form, and computer codes, such as computational fluid dynamics, (CFD), have been developed for analysis of flow, and specifically flow through complicated nuclear fuel bundle channels. Complete flow characterization requires specialized three dimensional CFD. However, the useful CFD models for specific fuel bundles are developed in industry, proprietary, and require extensive programming and cost to implement. In the public domain, a number of one-dimensional mathematical models have been developed. These models have been used in textbooks, and system and sub-channel computer codes, within the nuclear industry since the 1960's. These equations can benefit decision-making, if the equations are valid in the application for which the equation is used.

These historical one-dimensional models and codes depend on data from measurement, either from an actual or simulated bundle. The Japanese Nuclear Power and Energy Corporation (NUPEC) realized that at the time of the models' initial development, the available technology's precision led to general measurements. Many flow properties and fuel bundle

components were combined, instead of measuring those properties and components individually.

In the late 1980's, this situation led NUPEC to conduct the BWR Full-Size Fine Mesh Bundle Tests (BFBT), which used updated technological measurement techniques and focused on specific locations within the fuel bundle and spacer. These tests led to the OECD/US-NRC Benchmark Study, which in the early 2000's analyzed the extensive data gathered. The objective of that study was not only to use detailed, updated measurements to revise codes and models, it was also to obtain data to separate the effects of different flow characteristics. If a flow characteristic or property, with a measurable effect on the predicted measurement's accuracy, can be identified, this data could enable refinement of the model's accuracy and application over a wider range of conditions, including outside the conditions used for the original validation. However, the BFBT benchmark study's published results from mathematical models and flow characteristics are limited.

The motivation for this study is to continue further research into application of data from the BFBT to available, published models. The objective of the study is to determine if historical models are valid using the BFBT refined data, and to determine if specific flow characteristics affect the models' accuracy. This study focuses on the pressure loss across a spacer grid, because pressure loss is a critical effect within the fuel bundle, and the spacer grid is a critical component. This study's historical models have been published either before, or soon after, the OECD/US-NRC Benchmark Study could be applied to them. The BFBT provides the data necessary to isolate the point of measurement, and precisely characterize the flow for many components. Applying the BFBT data to established mathematical models can provide useful information about the accuracy and precision of available models for the performance of nuclear fuel bundles.

This study consists of compiling available and established historical single and two-phase spacer grid pressure loss models, then comparing those models' pressure loss estimations to the established NUPEC BFBT experimental data. The objective is to determine how the conditions and flow characteristics, used to develop the historical models, apply to conditions outside the historical models' range of development. In addition, this study attempts to identify flow characteristics that correlate with the models' estimated accuracy.

This objective of this study is accomplished by focusing on applying the detailed, measured BFBT flow characteristics of pressure, flowrate and void fraction, over a range of pressures and flows, to available one-dimensional mathematical models of spacer grids, in order to obtain a predicted spacer pressure loss. These results are compared to the experimental results for single and two-phase flows, from BFBT tests' measured data on an average configuration of a spacer grid. If historical models can provide valid estimations, they can be used to identify if more extensive modeling is required, and assist in design and operational engineering at a lower expenditure of time and resources.

This study begins by describing the equipment used in the experiment, a BWR simulator using a full-size, real-life nuclear fuel bundle, then describes the general pressure losses within the channel, and how the spacer grid's pressure losses are isolated. Next, a compilation of the available single-phase spacer grid pressure loss models is presented in a common format. The BFBT experimental data is used for input into the historical models, and the output is an estimate, which is compared to an experimental measurement, in order to determine the accuracy and precision of the historical models.

For clarification, the single-phase models results and discussion are presented separately from the two-phase results and discussion. The main difference between single and two-phase flows is the increased complexity of the flow. The additional complexity requires determination of important ratios between phases, particularly void fraction, velocity ratio, and



the patterns of flow within different sections of the fuel bundle. These flow characteristics, and other fluid properties are inputs for equations used to produce a predicted loss, and then to determine the accuracy and precision of the models' predicted results, when applied to the BFBT experimental database. Both single-phase and two-phase spacer grid pressure loss models are compared using flow characteristics. However, the complexity of two-phase flow leads to both additional applicable characteristics, and extensive development and analyses of those additional characteristics. Separating the analyses of single and two-phase flows enables this study to maintain focus throughout development of the two-phase parameters.

The two-phase portion of the thesis begins with an explanation of the two-phase model, and then presents a compilation of the available two-phase spacer grid loss models. The BFBT data is input into the models to establish a reference prediction. Next, the historical models' initial results are grouped in different formats, using the flow characteristics, to identify the flow characteristics with significant effects on accuracy using graphical analysis. Finally, the two-phase spacer grid pressure loss models are grouped by the effective flow characteristics. These results are analyzed in tabular and graphical form to determine the accuracies of historical models.

The conclusion from the analyses of both the single and two-phase spacer grid pressure loss models is no single universal model, that meets all BFBT boundary conditions accurately, was identified. However, by using the BFBT experimental data, this study identifies specific boundary conditions within the BFBT, for which some one-dimensional spacer grid models can be useful. The study also concludes pressure and flow quality are dominant factors contributing to the accuracy and precision of the two-phase spacer grid pressure loss models.

## CHAPTER 1: LITERATURE REVIEW

### 1.1. Introduction:

This chapter describes the selected measurement data, experimental set-up, the format of experiments and an overview of existing mathematical spacer grid models in the literature. A concise discussion of the sources this study uses provides this overview.

### 1.2. Test Facility and Equipment:

The Nuclear Power Engineering Corporation of Japan (NUPEC) BWR Full-size Fine-Mesh Bundle Tests (BFBT) benchmark study, as published by Neykov et al. in 2006 in Volume I: Specifications, provides the data this study is based on. The BFBT benchmark study, with its precise spacer and flow data, provides the necessary quality of data to meet requirements. The requirements are: The measurements are both focused on a spacer and have the detail necessary to allow isolating spacer pressure loss, the flow properties provide adequate data to enter variables into historical one and two-phase spacer loss models for each test run, and detailed flow properties are available to characterize the flow extensively, enabling comparison between tests and models.

This study is based on an OECD/NRC BFBT benchmark workshop conducted in 2002, (Neykov et al., 2006) that determined the variables, used in development of models to predict flow within nuclear fuel bundles, had not been updated with technological advances to replace generalized theories, measurements and characteristics. These variables, such as temperature, pressure, viscosity, and void fraction, have critical effects on the flow. By precisely determining those characteristics' effects, models can likely be developed, that can be applied to a wider range of flows and geometries. The BFBT tests, conducted in Japan from 1987 to 1995, used updated technology to measure a range of flow properties, at precise points, for this purpose.

The BFBT benchmark study focused on computer codes and sub-channel flows, and that portion of the BFBT study is proprietary. However, the information provided by Neykov's 2006 publication of the BFBT study provides adequate data to conduct a study using one-dimensional historical models. The value of the "Volume I: Specifications," is it provides precise enough data on the geometry of the fuel bundle, and spacer, so they can be accurately used for input into the models and flow characteristics. It also provides the overall structure of the tests, which consist of a range of flow characteristic combinations, providing a good comparison of results. The disadvantage of the published version of the benchmark study is the results data is limited to the spacer grid used in this study, instead of all the results and developments from the BFBT benchmark study.

### 1.3. Formats and General Losses

This thesis involves a compilation of models, produced by a number of authors, ranging over sixty years. These models used specific nomenclature appropriate for their use and time. Different models used different symbols for the same factors, English units and metric units were used, the names of some properties such as density and specific weight were defined differently between models, and some variables are undefined. This is illustrated by very different nomenclature used by Todreas and Kazimi (2012) for the two-phase spacer pressure loss correlation compared to the equation provided by Lahey and Moody (1993).

A common format is desirable to avoid confusion and ensure the models are being applied and compared correctly. Todreas and Kazimi provide a wide range of nomenclature in *Nuclear Systems Volume I*, (Todreas and Kazimi, 2012) and the majority of the nomenclature used in this study came from this text. An additional advantage of this textbook is examples of calculations are provided, that resolve questions about nomenclature. However, this textbook uses the same nomenclature for different factors or does not define all the nomenclature used, such as some variations of the two-phase multiplier. Another issue is the

nomenclature is clear enough in an individual section of the Todreas and Kazimi textbook, because the textbook's section is focused enough to keep it in context. For this study, identifying the locations of the measurement, and identifying other components of the measurement, require more detail to be applied accurately. This lack of detail was resolved primarily through addition of subscripts and superscripts, and expanding the abbreviations used in this study, such as "liq" instead of "l" for liquid, which can be confused with a "1."

The general losses were all calculated from applying the models and equations from the Todreas and Kazimi textbook to the BFBT data. Tong and Weisman's textbook on Pressurized Water Reactors (PWR) (Tong and Weisman, 1970) could have been used for single-phase general losses, and Lahey and Moody's textbook on Boiling Water Reactors (BWR) (Lahey and Moody, 1993) could have been used for both single and two-phase general losses. Those textbooks provide clear equations and their work predates Todreas and Kazimi. However, Todreas and Kazimi provide extensive examples, which resolve questions on the factors of the general loss equations. These examples provide common factors to compare the results, enabling better focus on the spacer loss. As an example, this study used Todreas and Kazimi's equations and diagrams, to describe flow regimes, to clarify the large volume of approaches, equations and diagrams in available literature describing flow regimes. Although deduction is required to apply Todreas and Kazimi's examples to a section of a fuel bundle instead of an entire length of a fuel bundle, the calculations can be performed with confidence in the results.

#### 1.4. Single-Phase Spacer Grid Pressure Loss Models

As stated before, the single-phase pressure loss models come from models produced over a period of 60 years and multiple authors. From all the sources and models reviewed, the models and source information used in this study were chosen based on being distinct enough to separate them from other models. The other reason is enough information is

available to ensure the available characteristics are applied properly to the model. Research into the historical models' sources identified the tests used to validate the various original models all used water, or a theoretical method such as CFD.

The models' original published source was used with one exception; however, in most cases the nomenclature in this study and the original nomenclature are not the same, for reasons stated in the prior section. This study configured the factors of the equations to a common format, patterned after the Klaus Rehme paper (1973). This common format enables a clearer and more confident understanding of the models, allowing better focus on the results. The Todreas and Kazimi textbook also provides detailed examples of three of the models, providing additional clarification on the terms used and their application.

The models, and sources of the models, are presented in the chronological order they were developed, by category. The first category is labeled as empirical, using a correlation coefficient chosen from charts, using factors identified by the author. The second category is labeled as semi-empirical, using correlation coefficients calculated from equations. I. Idel'chik produced one of the initial models, published in the 1940's, basing his model on obstructions in a channel. However, the version of the Idel'chik model used in this study is a revised version he published in his 1986 textbook, *Handbook of Hydraulic Resistance*. (Idel'chik, 1986).

A. C. Spengos (1959) published "Tests on Models of Nuclear Reactor Elements," the first available report focused on the spacers in a nuclear fuel bundle. The Spengos study was based on a gas cooled reactor. Spengos provided a geometrically accurate simulation in lower turbulence ranges that for the period, was a major advancement. He provided a detailed explanation of the test equipment, the measurements used, and the derivation of his model. His model is difficult to apply, because Spengos incorporated a spacer separation distance into the charts for his drag coefficients, and this spacer separation cannot be applied directly

to the BFBT, so the best case was chosen and applied consistently. In addition, the material used for the spacers and channel was Plexiglas, with no adjustments for the different properties of real spacer material. This study used the Spengos model mainly for comparison purposes.

A. N. DeStourder (1961) published the first universally applicable model based on nuclear fuel bundle spacer grids, "Drag Coefficients for Fuel Element Spacers," in a format similar to the common format used in this study. He developed his model from observation of a wide range of spacer grid types used for gas cooled reactors. DeStourder's paper is concise and easy to understand. However, DeStourder does not provide a clear description of how he isolated the spacer pressure loss. Unfortunately, later published versions of the chart he used to determine drag coefficients eliminate the detail of the spacers he used, along with the information it provided. He uses a best fit line through a number of plots for the loss coefficient, and as the Reynolds Number declines, the different spacers have more widely divergent plots. While he mostly studied wire type spacers, he also used a type of spacer grid similar to the BFBT spacer. This model is still used in textbooks.

Tong and Weisman published a model based on a combination of pressure losses at the inlet and outlet of the spacer in *Thermal Analysis of Pressurized Water Reactors*, (1970) based on a Kays and London chart reproduced in the textbook, that combines the turbulence with the geometry. The chart was originally developed in 1955, and is referred to in other publications, including DeStourder's; however, Tong and Weisman is the earliest version available that used it in an equation for grid spacers. The chart was originally validated on flow through heat exchangers, and the textbook does not identify if it was validated on nuclear fuel bundle spacers. However, the model's application is clear and it remained in this textbook's revisions, so it's applicability to the BFBT fuel bundle and flows are within this study.

K. Rehme's initial work, "Pressure Drop Correlations for Fuel Element Spacers," (1973), provides results from tests for a gas cooled reactor simulator in a very clear format. He used a wide variety of spacer grids, including the type used in the BFBT. To isolate the spacer losses, Rehme eliminated the frictional losses with the same equation used in this study; however, the effects of gravity were eliminated by using a horizontal bundle, while the BFBT simulator was vertical. Also, the chart for the drag coefficient was developed at a time when a lower accuracy was acceptable, so judgement is required to determine the correlation factors.

In 1980 Rehme published "Pressure Drop and Velocity Distribution in Rod Bundles with Spacer Grids" (1980) with G. Trippe, based on turbulent flows in a Liquid Metal Fast Breeder Reactor. The Rehme/Trippe paper discusses a number of topics, is more focused on computer codes, and does not have the range of spacers of the original Rehme study. However, the publication does have a refined adjustment chart with more detail on the geometry of a limited number of spacer grids, one of which matches the spacer grid in this study.

One of the first published models, where the drag coefficient was calculated, was "An Experimental and Analytical Study of the Synthesis of Grid Spacer Loss Coefficients," by B.S. Shiralkar and D.W. Radcliffe as "General Electric Technical Report NEDE-13181". (1971) This report is based on the spacer grids used in production BWRs at the time. Shiralkar's tests were conducted on horizontal simulators using anemometers within the bundle and air as a coolant, however it is difficult to determine how the authors isolated grid spacer loss. Shiralkar's report provides an excellent description of a grid spacer similar to the BFBT, and the calculations for determining the loss. However, this study is not available from any identifiable open source, and Shiralkar used only highly turbulent flows, with a limited drag coefficient.

A more useful description of the Shiralkar model was provided by M. Glueck in "Validation of the Sub-Channel Code F-COBRA-TF, Part I. Recalculation of Single-Phase and Two-Phase Pressure Loss Measurements." (2008) He applied the Shiralkar model to the BFBT benchmark, where he focused on individual channel flow. He expanded Shiralkar's original study to include an equation to calculate drag at lower Reynolds Numbers, and makes it much more applicable to the flow characteristics provided in this study. However, with the high Reynolds Numbers from the BFBT's flow, Glueck's coefficient approaches a limiting value, and the majority of BFBT test flows use Shiralkar's original equation.

"A Pressure Drop Model for Spacer Grids with and without Flow Mixing Vanes" (Chun and Oh, 1998) took a new approach to spacer grid loss in the late 1990's, by separating losses into different parameters based on the geometry of a spacer grid. Their article is a concise, clear, description of the model and application, although the equations needed to be re-written to the common format used in this thesis. The grid configuration pressure loss factor is also based on a set of coefficients from a table. Application of the grid form table is difficult to understand and requires judgement. The validation of Chun and Oh's model was based on PWRs, however the technique used for the validation is unclear from the information provided by the authors.

In a later refinement of the Chun and Oh Model, Chun and Oh worked with W.K. In, and published "Empirical and Computational Pressure Drop Correlations for PWR Spacer Grids," (In et al, 2002) which was also based on PWRs. The form pressure loss factors, previously identified from a chart, were changed to an equation, and they simplified other factors. Todreas and Kazimi provide clear examples which apply this model. The validation of this model appears to be from Computational Fluid Dynamics from the article by In et al.

The latest version of a spacer grid pressure loss coefficient is "Proposal for Pressure Drop Prediction for a Fuel Bundle with Grid Spacers using Rehme Pressure Drop Correlations,"



(Schikorr et al., 2010) based on a simulator for a Fast Breeder Reactor. His model is an equation-based version of Rehme's model, with the equation for a drag coefficient coming from the article "Thermohydraulic Optimization of Homogeneous and Heterogeneous Advanced Pressurized Reactors," (Cigarini and Dalle Donne, 1988), which was based on a PWR. Both papers are extensive and cover a number of topics. The Schikorr et al. paper states their model in a very clear and applicable format, and the drag coefficient from Cigarini and Dalle Donne is clearly applicable to this study.

### 1.5. Two-Phase Spacer Grid Pressure Loss Models

Two-phase spacer grid pressure loss models and their published sources vary from single-phase models in two-main aspects. First, a two-phase model consists of multiplying a single-phase spacer pressure loss coefficient by a multiplier based on characteristics of the two-phase flow. A publication will only provide a multiplier, which can be used with any single-phase coefficient from other published sources. Second, few sources exist on the two-phase spacer grid pressure loss multiplier. The majority of multipliers are based on friction and other losses; however, using the same criteria as single-phase models, nine distinct two-phase spacer grid pressure loss models were identified.

A number of models were published based on pressure loss from an expansion of flow from a narrower channel type models in 1961. One of the first published compilations is "Natural Circulation Tests with Water at 800 to 2000 PSIA under Non-Boiling, Local Boiling and Bulk Boiling Conditions," (Mendler et al., 1961), which was a Westinghouse report based on boiling within PWRs. This report provides a clear definition of one of the two-phase multipliers and its variables; however, the report covers other topics and the two-phase pressure loss model is not the focus. The only applicable multiplier with clearly identifiable variables was initially described as the "fog flow" model, which was an earlier term based on properties of two-phase systems in refrigerant condensers. Further origins are unclear. This

model appears in Lahey and Moody's textbook, *The Thermal-Hydraulics of a Boiling Water Nuclear Reactor*, (1993) as the "homogenous multiplier." However, for clarification in this study, it will be referred to as the "Mendler" multiplier.

The Mendler multiplier then appeared in a compilation by P.A. Lottes, "Expansion Losses in Two-Phase Flow," (1961) in the same year. Lottes provided his own two-phase multiplier based on an expansion of flow from a narrow channel, along with the Mendler multiplier, the "Richardson" multiplier and the "Romie" multiplier. The advantage of the Lottes compilation is it is concise and provides the equations clearly with the variables well defined. The Lottes and the Romie multipliers are provided in a fully developed form using the pressure loss from different void coefficients before and after the spacer. Although the Romie multiplier is found in a number of publications, it was provided to Lottes through a company report and by conversation. All additional publications using the Romie multiplier refer back to the Lottes paper.

The two-phase multipliers in the Lottes paper are based only on expansions of flow from a narrow channel, and Lotte's paper applies a general pressure loss factor to all the equations with only an abbreviated explanation. In order to apply to spacer loss with confidence, Lahey and Moody provide a detailed explanation of the expansion pressure loss coefficient and how it is separated out to provide more familiar forms of the multipliers used in spacer loss in their BWR textbook. The textbook further provides a simplified version of the Lottes and Romie multipliers, that assumes the change in the void coefficient before and after the spacer is negligible, to provide more familiar forms of the multipliers. Lahey and Moody also provide data to verify the correct application of the Mendler multiplier. Lahey and Moody's textbook also provides a correction factor for the Mendler multiplier, which it identifies as the McAdams correlation. The Todreas and Kazimi textbook provides a good explanation of the value to use in the McAdams correlation.

D.R.H. Beattie (1973) provided a number of two-phase loss multipliers in “A Note on the Calculation of Two-Phase Pressure Losses,” one of which was dedicated to spacer pressure loss. The model provided is both well-defined and in its form can be clearly applied in the thesis. It is a variation of the Mandler multiplier, however Beattie does not identify how the equation was derived or how it was validated.

The Chisolm multiplier appears in a number of publications. However, it has an important factor,  $B$ , which is usually not well defined or is simplified in later publications, leading to inaccurate application of the multiplier. The best source for a description of this multiplier is “Flow of Steam-Water Mixtures through Sharp Edged Orifices,” (Rooney, Chisholm and Cornwell, 1974) which was a publication for a conference. The Chisholm multiplier is a combination of the Mandler and Martinelli multipliers. This multiplier was originally based on orifice flow, however it works well with spacers. The conference publication explains the derivation of the unnamed parameter,  $B$ , along with providing both a chart and equation to obtain  $B$ . The paper was concise and provided very clear information to apply the model, along with detailed explanation of the model’s validation using a simulator and water.

#### 1.6. Two-Phase Test Theory and Structure

A number of the single-phase pressure loss correlations utilized Reynolds Numbers and viscosity. The single-phase study used only liquid properties of water, and the flow was characterized based on the liquid phase. However, for two-phase flow, M.M. Awad and Y.S. Muzychka provide a clear definition of two-phase viscosity in “Effective Property Models for Homogenous Two-Phase Flows,” (2008) for use in calculating the two-phase Reynolds Number. The compilation portion of their paper, describing the two-phase properties is clear and can be applied without difficulty, although their paper covers other topics as well.

P. Venkateswararao et al. (1982) provided characterization maps for the flow regimes in their study, “Flow Pattern Transition for Gas-Liquid Flow in a Vertical Rod Bundle.” While their

paper covered many topics on flow mapping, along with equations to predict a flow regime, its value to this study is it provided flow regime maps reprinted from works by Bergles, and Williams and Peterson, that are no longer available. Lahey and Moody state that only empirically derived flow regime maps, not equations, are reliable. Lahey and Moody also state that flow regime maps are good for a very narrow range of pressures, so it was critical to obtain validated flow regime maps, which applied to the pressures close to the BFBT data. A large number of sources were reviewed and while many flow regime maps and equations have been produced, the majority of maps and models are either at standard pressures or the pressures are unlabeled.

#### 1.7. Conclusions:

Information to conduct the analyses and comparison necessary for this thesis is available. Analysis of the pressure loss across a nuclear fuel bundle spacer requires detailed characterization of the flow, which exists in BFBT Vol. I, where precise data on the measured losses has been provided. Available publications have provided models with clearly defined variables, which enable the BFBT flow properties to be used and compared. The BFBT conditions, which were not the conditions originally used for validation of these models, can be applied to these mathematical models to determine the differences between predicted and measured results.

The available literature produced ten distinct single-phase models and nine distinct two-phase multipliers. The available flow measurements and literature produced the single-phase flow characteristics of pressure and turbulence, measured by Reynolds Number, for single-phase comparisons. The two-phase flow provided a wider range of characteristics such as pressure, turbulence, flow quality, void fraction and flow regime, enabling more comparisons. The available data and literature enables both graphical and tabular analyses, which leads to the discussion and conclusions produced within this study.

## 1.8. References

Awad, M.M. and Muzychka, Y.S., 2008. Effective Property Models for Homogenous Two-Phase Flows. *Experimental Thermal and Fluid Science*, Vol. 33, No. 1, pp. 106-113.

Beattie, D. R. H., 1973. A Note on the Calculation of Two-Phase Pressure Losses." *Nuclear Engineering and Design*, Vol. 25, No. 3, pp. 395-402.

Chun, T.H. and Oh D.S., 1998. A Pressure Drop Model for Spacer Grids with and without Flow Mixing Vanes. *Journal of Nuclear Science and Technology*, Vol.35, No. 7, pp. 508-510.

Cigarini, M. and Dalle Donne, M., 1988. Thermohydraulic Optimization of Homogeneous and Heterogeneous Advanced Pressurized Reactors. *Nuclear Technology*, Vol. 80, No. 1, pp. 107-132.

DeStourder, A. N., 1961. Drag Coefficients for Fuel Element Spacers. *Nucleonics*, Vol. 19, No. 6, pp. 74-79.

Glueck, M., 2008. Validation of the Sub-Channel Code F-COBRA-TF, Part I. Recalculation of Single-Phase and Two-Phase Pressure Loss Measurements. *Nuclear Engineering and Design*, Vol. 238, No. 9, pp. 2308-2316.

Idel'chik, I. E., 1986. *Handbook of Hydraulic Resistance*, 2<sup>nd</sup> ed. Hemisphere Publishing Corporation, New York, ISBN: 978-0-8911-6284-1.

In, W.K., Oh, D.S. and Chun, T.H., 2002. Empirical and Computational Pressure Drop Correlations for PWR Spacer Grids. *Nuclear Technology*, Vol. 139, No. 1, pp. 72-79.

Lahey Jr., R. T. Jr. and Moody, F. J., 1993. *The Thermal-Hydraulics of a Boiling Water Nuclear Reactor*, 2nd Ed. American Nuclear Society Publishing, La Grange Park, Illinois, ISBN: 0-89448-037-5.

Lottes, P., 1961. Expansion Losses in Two-Phase Flow. *Nuclear Science and Engineering*, Vol. 9, No. 1, pp. 26-31.

Mendler, O.J., Rathbun, A.S.; Van Huff, N.E., and Weiss, A., 1961. Natural Circulation Tests with Water at 800 to 2000 PSIA under Non-Boiling, Local Boiling and Bulk Boiling Conditions. *Journal of Heat Transfer*, Vol. 83, No. 3, pp. 261-273.

Neykov, B., Aydogan, F., Hochreiter, L., Ivanov, K., Utsuno, H., Kasahara, F., Sartori, E., and Martin, M., 2006. NUPEC BWR Full-size Fine-mesh Bundle Test (BFBT) Benchmark, Vol. I: Specifications. OECD, Nuclear Energy Agency, NEA No. 6212, ISBN: 92-64-01088-2.

Rehme, K., 1973. Pressure Drop Correlations for Fuel Element Spacers. *Nuclear Technology*, Vol. 17, No. 1, pp. 15-23.

Rehme, K. and Trippe, G., 1980. Pressure Drop and Velocity Distribution in Rod Bundles with Spacer Grids. *Nuclear Engineering Design*, Vol. 62, No. 1, pp. 349-359.

Rooney, D.H., Chisholm, D. and Cornwell, R.S., 1974. Flow of Steam-Water Mixtures through Sharp Edged Orifices. Heat and Fluid Flow in Steam and Gas Turbine Plant Conference, Institute of Mechanical Engineering, London, England, Conference Publication 3-1973, pp. 1-8.

Schikorr, M., Bubelis, E., Mansani, E. L., and Litfin, K., 2010. Proposal for Pressure Drop Prediction for a Fuel Bundle with Grid Spacers using Rehme Pressure Drop Correlations. Nuclear Engineering and Design, Vol. 240, No. 7, pp. 1830-1842.

Shiralkar, B.S., and Radcliffe, D.W., March 1971. An Experimental and Analytical Study of the Synthesis of Grid Spacer Loss Coefficients. General Electric Technical Study NEDE-13181.

Spengos, A. C., 1959. Tests on Models of Nuclear Reactor Elements, IV. Model Study of Fuel Element Supports. UMRI-2431-4-P, University of Michigan Research Institute, Ann Arbor.

Todreas, N. E., and Kazimi, M. S., 2012. Nuclear Systems, 2nd Ed. CRC Press Publishing, Boca Raton, Florida, ISBN: 978-1-4398-0887-0.

Tong, L.S., and Weisman, J., 1970. Thermal Analysis of Pressurized Water Reactors, 1st Ed. American Nuclear Society Publishing, La Grange Park, Illinois, ISBN: 978-0-8944-8038-6.

Venkateswararao, P., Semiat, R. and Dukler, A.E., 1982. Flow Pattern Transition for Gas-Liquid Flow in a Vertical Rod Bundle. International Journal of Multiphase Flow, Vol. 8, No. 5, pp. 509-524.

## CHAPTER 2: TEST EQUIPMENT

### 2.1. Test Facility

The analysis of historical models and flow properties is performed using the experimental data from NUPEC's extensive BWR Simulator tests in Japan. The tests measured detailed flow characteristics in a BWR fuel bundle, including pressure loss and void fraction over multiple heights in a simulated vertical fuel bundle. The NUPEC Test Facility Diagram is shown in Figure 1 (Neykov et al., 2006).

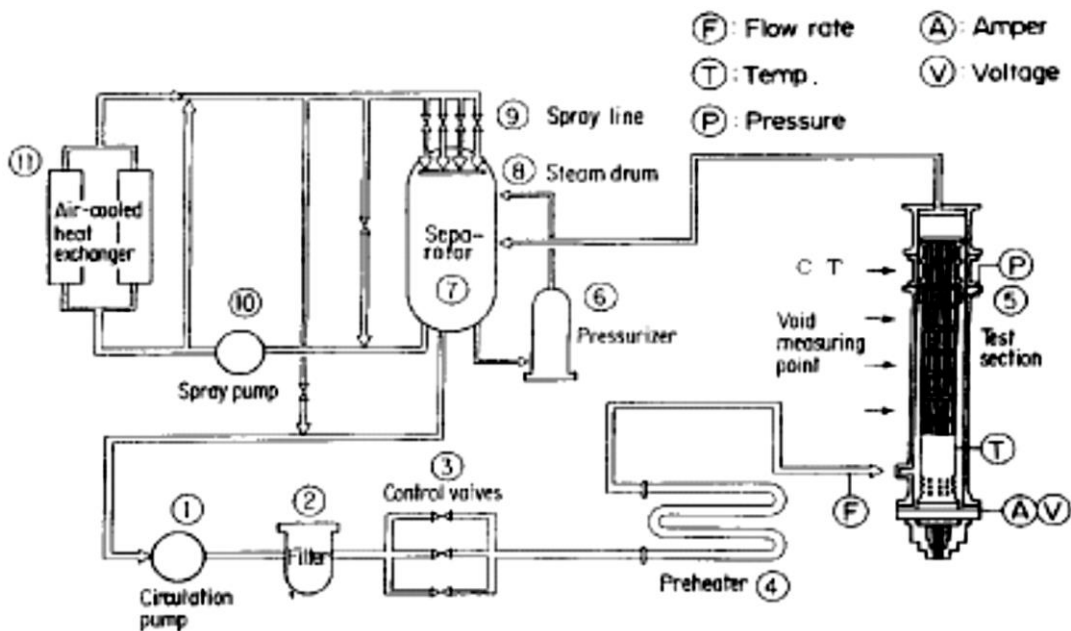


**Figure 1: Diagram of the Test Facility (Neykov et al., 2006)**

The objective of NUPEC's experiments was to simulate a full-size BWR fuel bundle, shown in Figure 2 (Neykov et al., 2006).

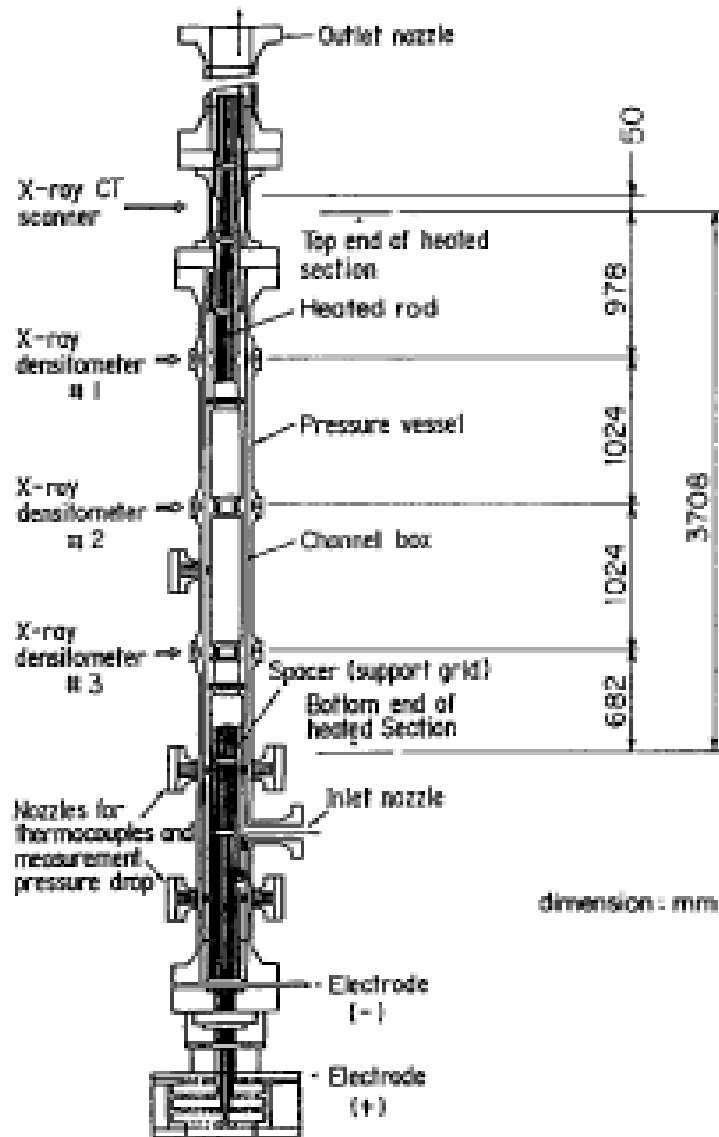


**Figure 2: Test Fuel Bundle (Neykov et al., 2006)**

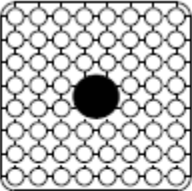
The simulated fuel bundle substituted electrically heated rods, instead of nuclear fuel rods, to heat the water to test temperatures. However, all other components within the test fuel bundle were the same as a BWR fuel bundle, including the spacers. The water was circulated at test pressures, temperatures, void fractions and flowrates.



## 2.2. Fuel Bundle and Spacer

The fuel rod bundle chosen for this study is the C2A (an 8x8 High Burn-Up bundle design).

The bundle cross-section is shown in Figure 3 with its specifications:

Item	Data			
Test assembly				
	4	C2A	C2B	C3
Simulated fuel assembly type	High burn-up 8x8			
Number of heated rods	60			
Heated rods outer diameter (mm)	12.3			
Heated rods pitch (mm)	16.2			
Axial heated length (mm)	3708			
Number of water rods	1			
Water rods outer diameter (mm)	34.0			
Channel box inner width (mm)	132.5			
Channel box corner radius (mm)	8.0			
In channel flow area (mm <sup>2</sup> )	9463			
Spacer type	Ferrule			
Number of spacers	7			
Spacer pressure loss coefficients	1.2			
Spacer location (mm)	455, 967, 1479, 1991, 2503, 3015, 3527 (Distance from bottom of heated length to spacer bottom face)			
Radial power shape	A	A	B	A
Axial power shape	Uniform	Cosine	Cosine	Inlet-peak

○ : Heated rod ● : Water rod no flow in water rods

A: Simulation pattern for beginning of operation

B: Simulation pattern for middle of operation

**Figure 3: Overview of the Fuel Bundle (Neykov, et al., 2006)**

The spacers in this fuel test section are ferrule style spacers, which means they have individual rings to hold the rods in place. The spacer frontal view diagram is shown below in Figure 4 with the side lengths and a frontal view of the ferrules. Better views and dimensions are provided below in Figures 5 and 6 respectively.

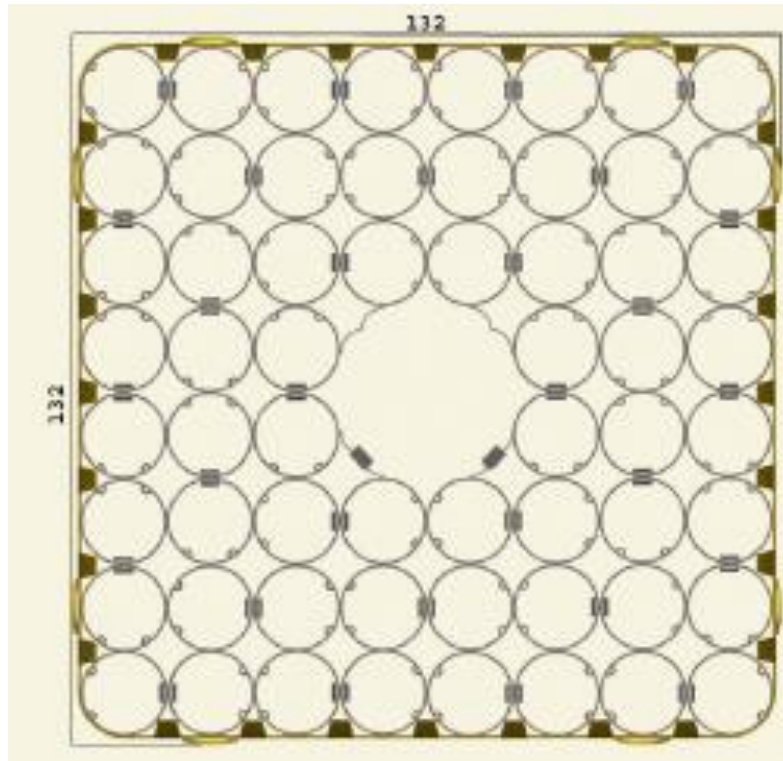


Figure 4: Spacer Cross Section (Neykov et al., 2006)

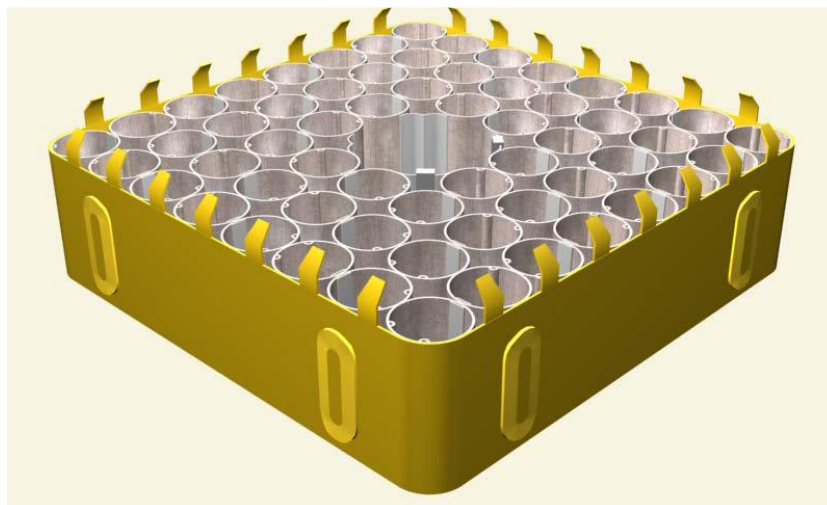
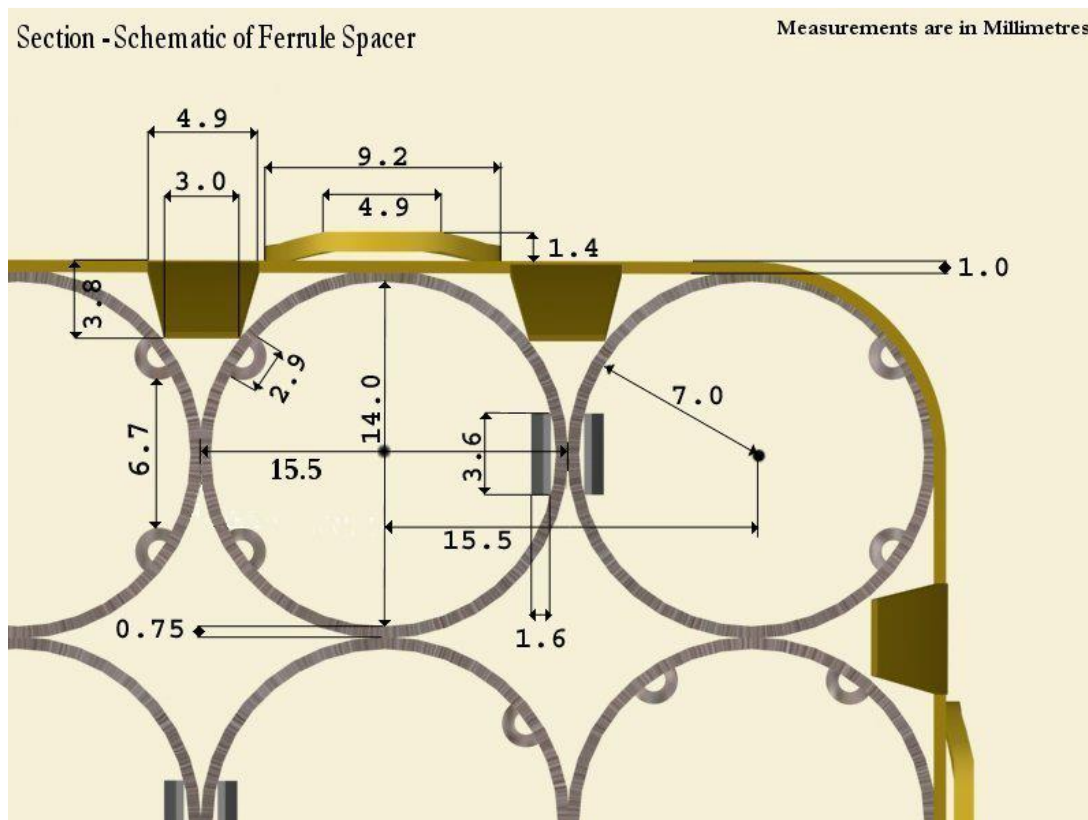


Figure 5: General View of the Spacer (Neykov et al., 2006)



**Figure 6: Dimensions of the Spacer Grid (Neykov et al., 2006)**

A ferrule type spacer is a relatively standard spacer design with no mixing vanes. This spacer geometry was used to analyze the mathematical models identified in this study.

### 2.3. Pressure Measurement

Many flow characteristics are measured within the test section. Pressure, temperature, flowrate and void fraction are the measured characteristics for this study, and the other parameters were derived from them. A diagram of the test section and the heights of the pressure taps are shown in Figure 7. The pressure loss measurement used in this study is taken across dpT1, circled in Figure 7, of the fuel simulator bundle. This section for this study's measurements from the BFBT test was recorded as "section 301" in the BFBT test results.

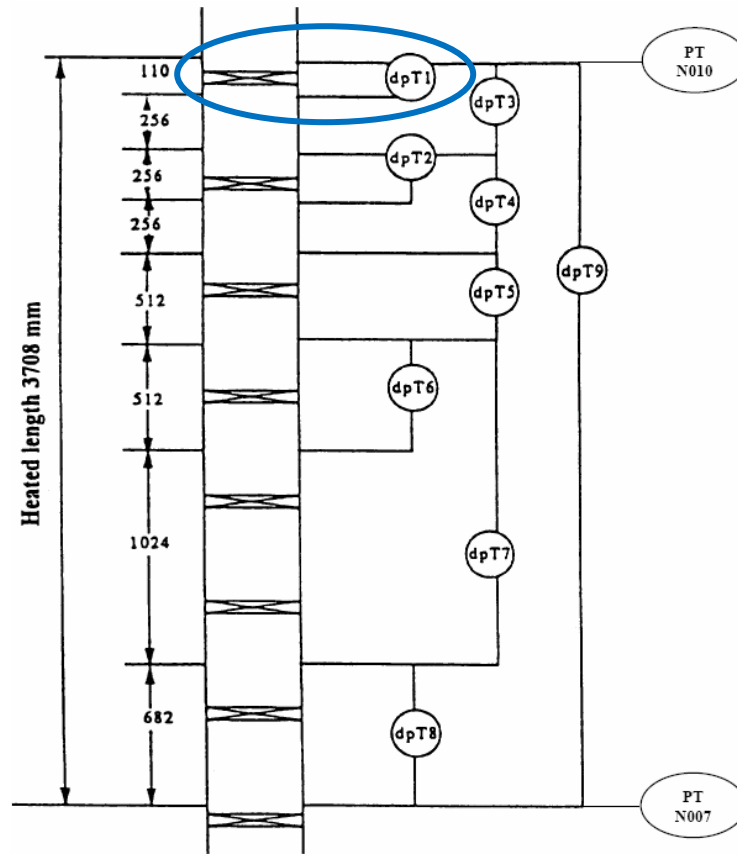


**Figure 7: Test Section 301 (dpT1) (Neykov et al., 2006)**

The dpT1 pressure section and the associated pressure taps, were chosen as the test location for this study, based on the minimum additional bundle space compared to the spacer grid. The distance between the two-pressure taps is 0.110 meters and the spacer height is 0.031 meters, positioned approximately midway within the test section. These dimensions reduce the amount of bundle friction before and after the spacer, and gravitational effects, while reducing flow effects in the immediate vicinity of the spacer, providing a better focus on the spacer loss estimate. Therefore, the pressure drop across dPT1 is predominantly due to spacer grid pressure drop.

This section was used for the pressure loss measurements of both single and two-phase flow. While measuring two-phase flow, the flow across the entire section was two-phase, and the pressure measurement included both the vapor and liquid fractions of the mixture. The

temperature was measured by thermocouples on the spacers and the flowrate was measured prior to entering the fuel bundle's inlet. (Neykov et al., 2006)

#### 2.4. Void Measurement

Various measuring equipment was used for the BFBT (Neykov et al., 2006) to measure the volume of the two phases. To measure the cross sectional average transient void distribution, the BFBT used three rotating X-ray densitometers, at various elevations along the fuel bundle. A rotating X-ray CT scanner, at steady state conditions, 50 mm above the heated length, measured the final void distribution using a fine mesh. The void measurement was used to provide flow quality at measured locations. A diagram of the measurement system is shown in Figure 8 (Neykov et al., 2006).

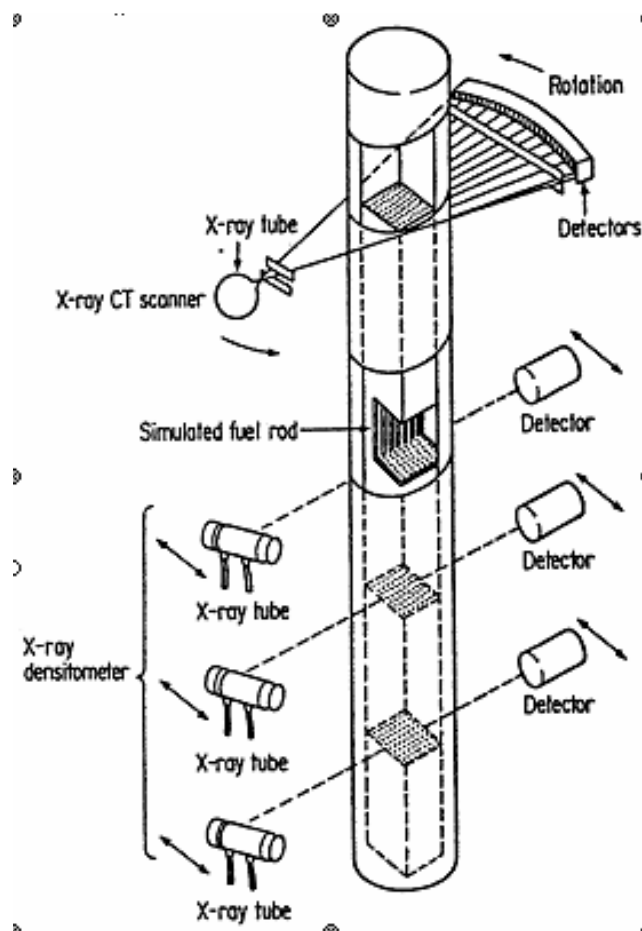


Figure 8: Void Measurement Equipment (Neykov et al., 2006).

## 2.5 References

Neykov, B., Aydogan, F., Hochreiter, L., Ivanov, K., Utsuno, H., Kasahara, F., Sartori, E., and Martin, M., 2006. NUPEC BWR Full-size Fine-mesh Bundle Test (BFBT) Benchmark, Vol. I: Specifications. OECD, Nuclear Energy Agency, NEA No. 6212, ISBN: 92-64-01088-2.

## CHAPTER 3: GENERAL PARAMETERS AND LOSSES

### 3.1. Introduction

This study involves a compilation of models from a number of sources. Clarifying the nomenclature and symbols into a common format is critical, for the reasons identified in the literature review.

The spacer pressure loss models ( $\Delta P_{SP}$ ) are based only on the pressure loss across the spacer. To isolate the pressure losses from only the spacer grid, the general pressure losses across section 301 are identified and removed from the total pressure loss across section 301. Although the calculations are for losses, the calculations in this study and most of the references in this study produce positive values, which are later subtracted from the total pressure.

### 3.2. Fuel Bundle Geometry

Figure 4 previously displayed the associated spacer grid in this bundle. Figure 9 displays a cross section of the frontal view of the rod bundle, which is an 8x8 BWR bundle, with a central water rod. (Neykov et al., 2006) Figure 10 displays a diagram of an idealized constricted channel, which will be used to illustrate the parameters. (Idel'chik, 1986)

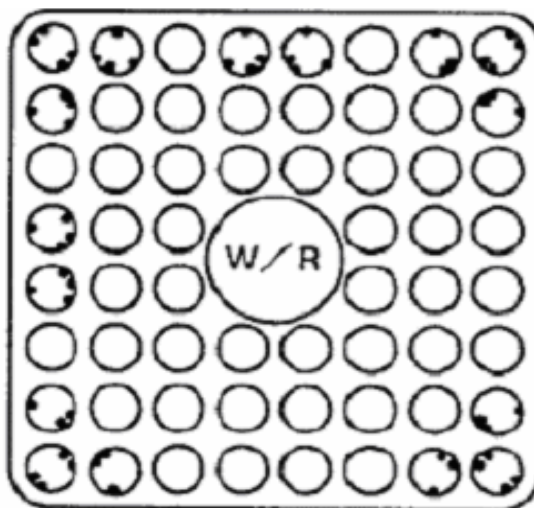
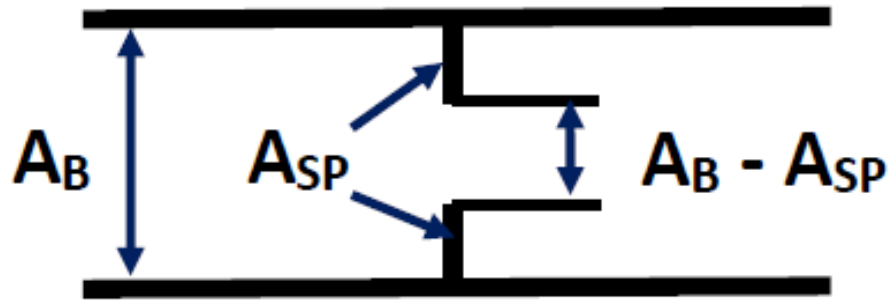


Figure 9: Rod Bundle Cross Section (Neykov et al., 2006)



**Figure 10: Constricted Area Diagram (Idel'chik, 1986)**

The following section describes the fuel bundle parameters used in this study and provides a common format. The fuel bundle parameter description is based on Figures 4, 9 and 10. The parameter ( $A_{SP}$ ) is the spacer frontal area including supporting components, also called the frontal projection. ( $A_{rod}$ ) is the rod cross section frontal area, both water and fuel rods, and ( $A_B$ ) is the total cross section of the channel before and after the spacer, minus the area of the fuel and water rods. ( $WP_B$ ) is the wetted perimeter of the fuel bundle, before and after the spacer, which includes the perimeter of the inside walls of the channel, plus the circumference of the water and fuel rods. ( $WP_{SP}$ ) is the wetted perimeter of the spacer, which is the length of the all the spacer grid components' sides, that come in contact with the flow, including the fuel and water rod perimeters within the spacer.

The parameters in the remainder of this section and section 3.3, are based on definitions in equation form, using the previously described geometric parameters. The blockage ratio ( $\epsilon$ ) is the ratio of the grid frontal projection to fuel bundle area before and after the spacer. It is calculated by equation (1) (Todreas and Kazimi, 2012):

$$\epsilon = A_{SP}/A_B \quad (1)$$

Similar to the blockage ratio is the contraction ratio ( $\sigma$ ). It is the ratio of the flow through area in the spacer grid to the flow through area in the bundle, before and after the spacer. It is calculated by equation (2):

$$\sigma = ((A_B - A_{SP})/A_B) \text{ or } 1 - \epsilon \quad (2)$$



### 3.3. Single-Phase Flows and Parameters

The location, where the mass flux is measured, is identified by subscripts. Mass flux through the bundle ( $G_B$ ) before and after the spacer is calculated by equation (3) (Todreas and Kazimi, 2012):

$$G_B = (\dot{m}/A_B) \quad (3)$$

where ( $\dot{m}$ ) is the mass flowrate. Mass flux through the open area of the spacer ( $G_{SP}$ ) is comparable; however, it is calculated by equation (4):

$$G_{SP} = (\dot{m}/(A_B - A_{SP})) \quad (4)$$

Hydraulic diameter is another term that is calculated at different locations. The hydraulic diameter of the fuel bundle channel ( $D_B$ ), before and after the spacer, includes the wetted circumferences of fuel and water rods, and the lengths of the sides of the fuel channel. It is calculated by equation (5):

$$D_B = (4A_B)/WP_B \quad (5)$$

The hydraulic diameter of the spacer grid cross section ( $D_{SP}$ ) includes the wetted circumferences of fuel and water rods, and spacer components' exposed perimeters in the spacer area. It is calculated by equation (6):

$$D_{SP} = (4A_{SP})/WP_{SP} \quad (6)$$

Three separate Reynolds Numbers are used. The first is the flat length Reynolds Number, ( $Re_L$ ) calculated by equation (7):

$$Re_L = (\rho U L)/\mu \quad (7)$$

where ( $L$ ) is the length of the fluid along the surface, ( $\rho$ ) is the density of the coolant, ( $U$ ) is velocity, and ( $\mu$ ) is dynamic viscosity. The Reynolds Number of the fuel bundle, ( $Re_B$ ) is based on the hydraulic diameter of the coolant channel. It is calculated by equation (8):

$$Re_B = (\rho U_B D_B)/\mu \quad (8)$$

where ( $U_B$ ) is the velocity in the fuel channel before and after the spacer. The Reynolds Number of the spacer ( $Re_{SP}$ ) is calculated by equation (9):

$$Re_{SP} = (\rho U_{SP} D_{SP})/\mu \quad (9)$$

where ( $U_{SP}$ ) is the velocity across the spacer.

#### 3.4. Two-Phase Flows, Parameters and Measurement Method

The initial calculations for two-phase flow require the determination of the void fraction, ( $\alpha$ ), the ratio of the cross sectional area of the vapor to the total cross sectional area, and the slip (velocity) ratio, ( $S$ ), which is the ratio of vapor phase velocity to liquid phase velocity. These parameters are calculated from known variables such as mass flowrate, ( $\dot{m}$ ), and other properties, determined from pressure and temperature at the point of measurement, to calculate the flow quality, ( $x$ ), which is the mass flowrate of the vapor to the total mass flowrate.

Based on the instrumentation and accuracy required, and the constant heat flux along the heated length, the flow quality for this study is calculated on a linear basis from zero at the point of boiling, to the flow quality measured at the exit of the rod fuel bundle. All other properties and the calculated parameters use the same linear basis.

#### 3.5. General Spacer Loss Equation

The pressure drop across dPT1 consists of spacer grid pressure drop and other general losses. The pressure drop based on the spacer grid is calculated by using the two-phase total pressure loss equation. To define the specific pressure loss term and isolate the fuel bundle pressure loss from the spacer grid pressure loss, this section presents a brief overview of two-phase flow pressure loss terms. The total two-phase flow pressure loss consists of the terms shown in equation (10) (Todreas and Kazimi, 2012):

$$\Delta P_{out-in} = \Delta P_{inertia} + \Delta P_{acceleration} + \Delta P_{form} + \Delta P_{gravity} + \Delta P_{friction} \quad (10)$$

where ( $\Delta P_{out-in}$ ) is the change in pressure from the pressure inlet to the outlet of the measured section; ( $\Delta P_{inertia}$ ) is the pressure change from the added force when flow begins in non-steady

state; ( $\Delta P_{\text{acceleration}}$ ) is the pressure change from the force on the vapor phase in two-phase flows; ( $\Delta P_{\text{form}}$ ) is the pressure loss from a geometric change in the channel, or the spacer in this study; ( $\Delta P_{\text{gravity}}$ ) is the pressure loss from the force necessary for vertical movement and ( $\Delta P_{\text{friction}}$ ) is the pressure loss from friction with the channel sides and rods.

### 3.5.1. Single-Phase General Losses

The single-phase portion of this study uses single incompressible phase, steady state flow, measured at the same size cross section before and after the BFBT database spacer. The incompressibility is based on the conditions of the experiment, which uses liquid water, at constant pressure, for each set of tests. The flow conditions negate the acceleration, ( $\Delta P_{\text{acceleration}}$ ), and inertia, ( $\Delta P_{\text{inertia}}$ ), terms.

The first general pressure loss factored into the test results, to isolate the spacer pressure loss, is pressure loss from gravity due to elevation rise calculated by equation (11):

$$\Delta P_{\text{gravity}} = \rho g \Delta z \quad (11)$$

where  $g$  is the acceleration of gravity and ( $\Delta z$ ) is the vertical distance the coolant rises.

The second general pressure loss, factored into the test results, is the frictional pressure drop along the channel sides, and fuel and water rods, calculated by equation (12):

$$\Delta P_{\text{friction}} = f (L/D_B) (\rho U_B^2 / 2) \quad (12)$$

where ( $f$ ) is a friction factor and ( $L$ ) is the length of the channel section, or ( $\Delta z$ ) in this case for a vertical channel. For the test data used, the flow in the bundle is turbulent at the measuring points and the friction factors are calculated by equations (13) and (14) (Todreas and Kazimi, 2012):

$$f = 0.184 \text{Re}_B^{-0.2} \quad \text{if } 3 \times 10^4 < \text{Re}_B < 1 \times 10^6 \quad (13)$$

$$f = 0.316 \text{Re}_B^{-0.25} \quad \text{if } 4 \times 10^3 < \text{Re}_B < 1 \times 10^5 \quad (14)$$

### 3.5.2. Two-Phase General Losses

The second part of this study uses two-phase, compressible, steady state flow measured at the same cross section, before and after the same BFBT spacer as the single-phase portion of this study. The compressible phase leads to a pressure loss, ( $\Delta P_{\text{acceleration}}$ ), based on the increase in force on the vapor phase, as the vapor expands in the fuel channel. This loss factor requires the change in void fraction, which is calculated from the slip ratio.

The Premoli correlation uses the difference between the flow quality, and other water flow characteristics determined at the section 301 pressure taps, on either side of the spacer, to calculate the slip ratio using equation (15): (Todreas and Kazimi, 2012)

$$S = 1 + E_{1 \text{ Prem}} \left[ \left( \frac{y}{1 + y E_{2 \text{ Prem}}} \right) - y E_{2 \text{ Prem}} \right]^{0.5} \quad (15)$$

where  $y$ ,  $E_{1 \text{ Prem}}$ , and  $E_{2 \text{ Prem}}$  are Premoli Correlation parameters that will be defined as they are used. Since the general channel losses are calculated between two pressure measurement points, the void fraction at both the inlet and outlet of the measured section of the channel (section 301) are required. The calculations for the Premoli correlation are shown for the flow quality at the inlet, ( $x_{301 \text{ in}}$ ). The flow quality, at the inlet, ( $x_{301 \text{ in}}$ ), outlet, ( $x_{301 \text{ out}}$ ), and spacer, ( $x_{\text{sp}}$ ), were calculated using the linear method described earlier, with the subscripts identifying the location of the measurement, phases and other identifiers. These multiple flow quality locations are used at both ends of the spacer to identify the total pressure loss. The “Prem” subscript denotes it is a Premoli parameter. This clarification is used because different equations use the same symbols as each other, and variations of equations exist which require precise identification.

The volumetric flow fraction, ( $\beta$ ), is used to calculate the parameter ( $y$ ). The volumetric flow fraction at the initial place of measurement, the inlet pressure tap of section dPT1, ( $\beta_{301in}$ ), is calculated by equation (16):

$$\beta_{301in} = 1/[1 + (\frac{1-x_{301in}}{x_{301in}})(\frac{\rho_{v,301in}}{\rho_{liq,301in}})] \quad (16)$$

where ( $\rho_v$ ) is the density of the vapor phase, and ( $\rho_{liq}$ ) is the density of the liquid phase. The parameter ( $y$ ) is defined at the test section 301 inlet by equation (17):

$$y_{301in} = \frac{\beta_{301in}}{(1-\beta_{301in})} \quad (17)$$

Equation (18) determines if a slip ratio is present:

$$y_{301in} \leq \frac{1-E_{2Prem,301in}}{E_{2Prem,301in}^2} \quad (18)$$

Otherwise the slip ratio is unity, where ( $\beta$ ) = ( $\alpha$ ). ( $E_{2Prem}$ ) at the inlet of section 301 is calculated by equation (19):

$$E_{2Prem,301in} = 0.0273 We_{Prem,301in} Re_{Prem,301in}^{-0.51} (\frac{\rho_{liq,301in}}{\rho_{v,301in}})^{-0.08} \quad (19)$$

where ( $We_{Prem,301in}$ ) is the Weber number of the fuel bundle at the 301 pressure measurement inlet, and ( $Re_{Prem,301in}$ ) is the Reynolds Number of the fuel bundle measured at the same point.

The Reynolds and Weber Numbers for the Premoli Correlation (Todreas and Kazimi, 2012) are calculated by equation (20) and equation (21), respectively:

$$Re_{Prem,301in} = \frac{G_m D_B}{\mu_{liq,301in}} \quad (20)$$

$$We_{Prem,301in} = \frac{G_m^2 D_B}{\gamma_{301in} \rho_{liq,301in}} \quad (21)$$

where ( $\mu_{liq}$ ) is the liquid phase dynamic viscosity and ( $\gamma$ ) is surface tension. ( $G_m$ ) is the two-phase mass flux through the fuel bundle. The assumption is the mass flowrates of the phases at the outlet will add up to the mass flowrate of the liquid initially entering the bundle, ( $\dot{m}_{liq,bundlein}$ ), so the total mass flowrate does not change and it is calculated by equation (22):

$$G_m = \frac{(\dot{m}_{liq} + \dot{m}_v)}{A_B} = \frac{\dot{m}_{liq,bundlein}}{A_B} \quad (22)$$

where  $(\dot{m}_{liq})$  is the mass flowrate of the liquid phase and  $(\dot{m}_v)$  is the mass flowrate of the vapor phase.

The parameter  $(E_{1\text{ Prem}})$ , at the section 301 inlet, is calculated by equation (23):

$$E_{1\text{ Prem},301\text{ in}} = 1.578 \text{ Re}_{\text{Prem},301\text{ in}}^{-0.19} \left( \frac{\rho_{liq,301\text{ in}}}{\rho_{v,301\text{ in}}} \right)^{0.22} \quad (23)$$

After the slip ratio is determined using equation (15), the void fraction at the section 301 inlet is calculated using equation (24): (Todreas and Kazimi, 2012)

$$\alpha_{301\text{ in}} = 1 / \left[ 1 + \left( \frac{1-x_{301\text{ in}}}{x_{301\text{ in}}} \right) \left( \frac{\rho_{v,301\text{ in}}}{\rho_{liq,301\text{ in}}} \right) (S_{301\text{ in}}) \right] \quad (24)$$

The acceleration pressure loss factor,  $(\Delta P_{\text{acceleration}})$ , is calculated from equation (25):

$$\Delta P_{\text{accel } 301} = \left[ \frac{(1-x)^2}{(1-\alpha)(\rho_{liq})} + \frac{x^2}{(\alpha)(\rho_v)} \right]_{301\text{ out}} - \left[ \frac{(1-x)^2}{(1-\alpha)(\rho_{liq})} + \frac{x^2}{(\alpha)(\rho_v)} \right]_{301\text{ in}} \quad (25)$$

The general pressure loss factor due to gravity is  $(\Delta P_{\text{gravity}})$ . The difference from single-phase flow is the density of the liquid-vapor mixture,  $(\rho_m)$ . The mixture density is calculated by equation (26):

$$\rho_m = (\alpha)(\rho_v) + (1-\alpha)(\rho_{liq}) \quad (26)$$

Since the quality was calculated linearly, the average of the properties and void fractions between the inlet and outlet of section 301,  $301_{\text{ave}}$ , provides accurate input. For a vertical fuel bundle, the gravity loss equation simplifies to equation (27):

$$\Delta P_{\text{gravity},301\text{ ave}} = \rho_{m,301\text{ave}} g (z_{301\text{ out}} - z_{301\text{ in}}) \quad (27)$$

where  $(z)$  is the elevation of the measured points. The loss from friction with the bundle walls,  $(\Delta P_{\text{friction}})$ , and the loss from the spacer and other restrictions,  $(\Delta P_{\text{form}})$ , use a two-phase multiplier. The concept uses the pressure losses for the liquid phase, then multiplies those losses by a correlation factor, or multiplier, to estimate the total loss within the two-phase system. This pressure loss for friction is shown by equation (28):

$$\Delta P_{\text{fric}}^{2P} = \Delta P_{\text{fric}}^{\text{liq}} \phi_{\text{liq}} \quad (28)$$

where  $(\Delta P_{\text{fric}}^{2P})$  is the two-phase frictional pressure loss.  $(\Delta P_{\text{fric}}^{\text{liq}})$  is the frictional pressure loss from the liquid phase, where the subscript, "fric," denotes friction, and  $(\phi_{\text{liq}})$  is the two-phase correlation factor, or multiplier, for the pressure loss ratio from the liquid phase to two-phase pressure loss. Since the slip ratio is greater than one, a separate flow pressure loss correlation model is required, instead of a model based on the (Homogenous Equilibrium Model) HEM. The two-phase frictional loss correlation, used in this study, is the Friedel Correlation for frictional flow along the unobstructed fuel channel. It is calculated by equation (29): (Todreas and Kazimi, 2012)

$$\phi_{\text{liq,Friedel}} = E_{\text{Friedel}} + \frac{3.24 F_{\text{Friedel}} H_{\text{Friedel}}}{We_{\text{Friedel}}^{0.035} Fr_{\text{Friedel}}^{0.0454}} \quad (29)$$

where  $(\phi_{\text{liq,Friedel}})$  is the two-phase multiplier based on the liquid phase for the Friedel friction correlation. The individual parameters will be explained further throughout development of the loss factor. As with gravity loss, the water properties are assumed to vary linearly along the channel, so the average value between the inlet and outlet of section 301 will provide accurate results. The parameter  $(E_{\text{Friedel}})$  for section 301 is calculated by equation (30):

$$E_{\text{Friedel},301} = (1 - x_{301 \text{ ave}})^2 + x_{301 \text{ ave}}^2 \left( \frac{(\rho_{\text{liq}} f_{v,\text{Friedel } 301})}{(\rho_v f_{\text{liq,Friedel } 301})} \right)_{301,\text{ave}} \quad (30)$$

where the liquid friction factor,  $(f_{\text{liq,Friedel}})$ , and the vapor friction factor,  $(f_{v,\text{Friedel}})$ , are calculated by equation (31) and (32) respectively:

$$f_{\text{liq,Friedel } 301} = \left[ 0.86859 \ln \left( \frac{Re_{\text{liq},301 \text{ ave}}}{1.964 \ln(Re_{\text{liq},301 \text{ ave}}) - 3.8215} \right) \right]^{-2} \quad (31)$$

$$\text{and } f_{v,\text{Friedel } 301} = \left[ 0.86859 \ln \left( \frac{Re_{v,301 \text{ ave}}}{1.964 \ln(Re_{v,301 \text{ ave}}) - 3.8215} \right) \right]^{-2} \quad (32)$$

with the liquid and vapor Reynolds Numbers, ( $Re_{liq,ave}$ ) and ( $Re_{v,ave}$ ), calculated using the viscosity for the phase, and the two-phase mass flux, by equation (33) and equation (34) respectively:

$$Re_{liq,301\ ave} = \frac{G_m D_B}{\mu_{liq,301\ ave}} \quad (33)$$

$$Re_{v,301\ ave} = \frac{G_m D_B}{\mu_{v,301\ ave}} \quad (34)$$

where ( $\mu_v$ ) is the vapor phase dynamic viscosity. The parameter ( $F_{Fried}$ ) is calculated by equation (35):

$$F_{Fried,301} = x_{301\ ave}^{0.78} (1 - x_{301\ ave})^{0.224} \quad (35)$$

The parameter ( $H_{Fried}$ ) uses the average density and viscosity and is calculated by equation (36):

$$H_{Fried,301} = \left( \frac{\rho_{liq}}{\rho_v} \right)_{301\ ave}^{0.91} \left( \frac{\mu_v}{\mu_{liq}} \right)_{301\ ave}^{0.19} \left( 1 - \frac{\mu_v}{\mu_{liq}} \right)_{301\ ave}^{0.7} \quad (36)$$

The Froude number, ( $Fr_{Fried}$ ), is calculated by equation (37):

$$Fr_{Fried,301} = \frac{G_m^2}{g D_H \rho_{m,301\ ave}^2} \quad (37)$$

The Weber number parameter is similar to the parameter used for the Premoli correlation, except the mixture density is used as shown by equation (38):

$$We_{Fried,301} = \left( \frac{G_m^2 D_H}{\gamma_{301\ ave} \rho_{m,301\ ave}} \right) \quad (38)$$

Equations (30) and equations (35) through (38) are substituted into equation (29) to calculate the two-phase Friedel friction multiplier. The general two-phase friction pressure loss per length, ( $\Delta P_{fric}^{2P}/L$ ), is calculated by dividing the liquid friction factor by the fuel bundle hydraulic diameter, which has units in length, to obtain the friction coefficient per length, then multiplying



it by the two-phase Friedel friction multiplier and the dynamic pressure factor as shown by equation (39):

$$\Delta P_{\text{Friedel},301}^{2P}/L = \phi_{\text{liq},\text{Friedel}} \left( \frac{f_{\text{liq},\text{Friedel},301}}{D_H} \right) \left( \frac{G_m^2}{2 \rho_{\text{liq},301 \text{ ave}}} \right) \quad (39)$$

Multiplying the pressure loss per unit length, by the distance between the pressure taps, (L), estimates the total fuel bundle frictional pressure loss using equation (40):

$$\Delta P_{\text{Friedel},301}^{2P} = \phi_{\text{liq},\text{Friedel}} \left( \frac{f_{\text{liq},\text{Friedel},301}}{D_H} \right) \left( \frac{G_m^2}{2 \rho_{\text{liq},301 \text{ ave}}} \right) L \quad (40)$$

### 3.5.3. Flow Regimes

An additional two-phase flow characteristic is the pattern, or regime, of the flow, or how the vapor and liquid are distributed within the channel. Large differences in the concentrations of the different phases, within a channel, can affect the pressure loss and energy distribution between flows with the same flow quality. The method which best matches this study is the Flow Pattern Map, based on the superficial velocities of the liquid and the vapor (Lahey and Moody, 1993). The boundaries between the flow pattern transitions are imprecise, and depend on a number of factors. Generally, as the pressure increases, the superficial velocity of the flow change, from one pattern to another, is lowered. So the pressure, the flow pattern map was developed for, is valid only for a narrow range.

The mass flux of the vapor and liquid phases of the two-phase mass flux are calculated respectively at the spacer by equation (41) and (42):

$$G_{\text{liq},\text{sp}} = G_m(1 - x_{\text{sp}}) \quad (41)$$

$$G_{\text{v},\text{sp}} = G_m x_{\text{sp}} \quad (42)$$

The superficial velocity of the liquid phase, ( $j_{\text{liq},\text{sp}}$ ), is calculated at the spacer by equation (43):

$$j_{\text{liq},\text{sp}} = \frac{G_{\text{liq},\text{sp}}}{\rho_{\text{liq},\text{sp}}} \quad (43)$$

While the superficial velocity of the vapor phase at the spacer, ( $j_{v,sp}$ ), is calculated by equation (44):

$$j_{v,sp} = \frac{G_{v,sp}}{\rho_{v,sp}} \quad (44)$$

These superficial flows are then plotted on an empirically developed chart, which will be demonstrated in section 7.2.2.1. A drawing of the different flow regimes is shown in Figure 11 for a vertical pipe: (Todreas and Kazimi, 2012)

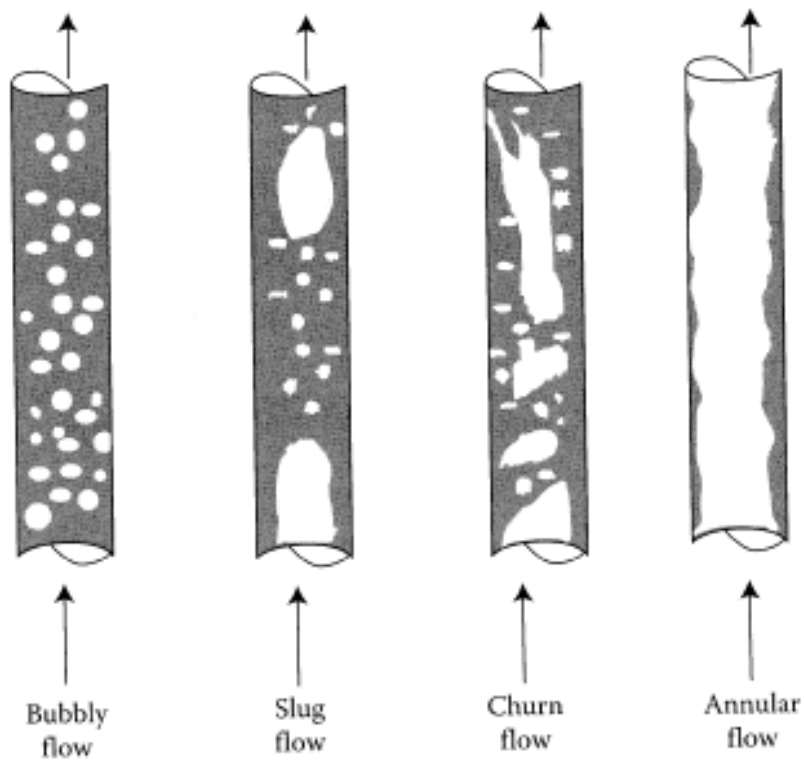


**Figure 11: Common Vertical Flow Patterns (Todreas and Kazimi, 2012)**

### 3.6. Nomenclature

The nomenclature shown below is used to describe the geometry of the fuel bundle and the measured losses provided by the BFBT study, including all losses along the fuel bundle channel.

(Factors that are dimensionless are denoted with a “\*\*”)

(For factors with multiple sub-factors, such as ( $\Delta P$ ), only the first factor will have the units listed, assume all the following sub-factors will have the same units unless otherwise listed)

$\Delta P$  – general change in pressure (Pascal (kg/m-sec<sup>2</sup>))

$\Delta P_{\text{acceleration}}$  – pressure change from the force on the vapor phase

$\Delta P_{\text{accel } 301}$  – pressure change from the force on the vapor phase across section 301 (refer to Figure 7 for section 301)

$\Delta P_{\text{EXP}}$  – the pressure change through an expansion

$\Delta P_{(\text{CO})}$  – Chun/Oh pressure loss correlation

$\Delta P_{(\text{DS})}$  - DeStourder pressure loss correlation

$\Delta P_{(I)}$  - Idel'chik pressure loss correlation

$\Delta P_{(\text{IN})}$  - In pressure loss correlation

$\Delta P_{(\text{RT})}$  – Rehme/Trippe pressure loss correlation

$\Delta P_{(\text{S})}$  - Spengos pressure loss correlation

$\Delta P_{(\text{SB})}$  – Schikorr/Bubelis pressure loss correlation

$\Delta P_{(\text{TW})}$  – Tong/Weisman pressure loss correlation

$\Delta P_{(\text{V})}$  - Rehme pressure loss correlation

$\Delta P_{\text{form}}$  - pressure change from channel obstruction

$\Delta P_{\text{friction}}$  – pressure change from channel friction

$\Delta P_{\text{fric}}^{2P}$  two-phase frictional pressure loss

$\Delta P_{\text{fric}}^{\text{liq}}$  – frictional pressure loss only from the liquid phase

$\Delta P_{\text{Friedel},301}^{2P}$  – two-phase Friedel frictional pressure loss (across section 301)

$\Delta P_{\text{gravity}}$  – pressure change from elevation change

$\Delta P_{\text{gravity}, 301 \text{ ave}}$  – pressure change from elevation change (across section 301)

$\Delta P_{\text{inertia}}$  - the pressure change from the added force initiating flow

$\Delta P_{\text{out-in}}$  - the change in pressure from the pressure inlet to the outlet

$\Delta P_{\text{sp}}$  – The single-phase pressure change across the spacer

$\Delta P_{\text{sp}}^{2P}$  – The two-phase pressure change across the spacer

$\Delta P_X^{2P}$  - general two-phase pressure loss correlation, x is a place holder

$\emptyset$  – \*General 2 phase pressure multiplier

$\emptyset_{\text{liq}}$  – \*2 phase multiplier based on the liquid phase

$\emptyset_{\text{liq},\text{Friedel}}$  - \*2 phase multiplier based on the liquid phase for the Friedel correlation

$\emptyset_{\text{liq},\text{sp}}$  – \*General 2 phase spacer pressure multiplier based on the liquid phase

$\emptyset_{\text{liq},\text{sp}}^{\text{Lottes}}$  – \*Lottes 2 phase spacer pressure multiplier

$\emptyset_{\text{liq},\text{sp}}^{\text{Lottes exp}}$  – \*Lottes 2 phase spacer pressure multiplier, expanded version for different void

fractions

$\emptyset_{\text{liq},\text{sp}}^{\text{Romie exp}}$  - \*Romie 2 phase spacer pressure multiplier, expanded version

$\emptyset_{\text{liq},\text{sp}}^{\text{Romie}}$  - \*Romie 2 phase spacer pressure multiplier

$\emptyset_{\text{liq},\text{sp}}^{\text{Richardson}}$  - \*Richardson 2 phase spacer pressure multiplier

$\emptyset_{\text{liq},\text{sp}}^{\text{Mendler}}$  - \*Mendler 2 phase spacer pressure multiplier

$\emptyset_{\text{liq},\text{sp}}^{\text{Mendler corr}}$  - \*Mendler 2 phase spacer pressure multiplier, corrected version

$\emptyset_{\text{liq},\text{sp}}^{\text{Beattie}}$  - \*Beattie 2 phase spacer pressure multiplier

$\emptyset_{\text{liq},\text{sp}}^{\text{Chisholm}}$  - \*Chisholm 2 phase spacer pressure multiplier

$\Delta z$  – the difference in elevation (m)

$\Theta$  – \*area modifier for the spacer flow

$\lambda_{\text{turb}}$  – \*lower Reynolds Number Shiralkar drag coefficient

$\varepsilon$  - rod roughness (m)

$\sigma$  – \*standard deviation

$\sigma$  - \*contraction ratio – spacer flow through area/bundle flow through area

$\epsilon$  - \*blockage ratio - grid area/bundle flow through area

$\lambda_{\text{turb}}$  – \*Shiralkar turbulent friction coefficient

$f$  - \*unnamed friction coefficient

$f_{(D)}$  – \*friction coefficient for the Chun/Oh and In correlations

$\alpha$  – void fraction ( $\text{m}^2/\text{m}^2$ )

$\alpha_{\text{sp}}$  – void fraction at the spacer

$\alpha_{301 \text{ in}}$  – void fraction at the inlet of section 301

$\beta$  – volumetric flow fraction ( $(\text{m}^3/\text{sec})/(\text{m}^3/\text{sec})$ )  $\beta = \alpha$  only if no slip ratio is present

$\beta_{301 \text{ in}}$  – volumetric flow fraction at the inlet of section 301

$\rho$  – density ( $\text{kg}/\text{m}^3$ )

$\rho_m$  – two-phase density

$\rho_v$  – vapor phase density

$\rho_{\text{liq}}$  - liquid phase density

$\rho_{v,301 \text{ in}}$  – vapor phase density at the inlet of section 301

$\rho_{\text{liq},301 \text{ in}}$  – liquid phase density at the inlet of section 301

$\rho_{\text{liq},301 \text{ ave}}$  – liquid phase average density across section 301

$\rho_{m,301 \text{ ave}}$  – average two-phase density across section 301

$\rho_{v,\text{sp}}$  – vapor phase density at the midpoint of the spacer

$\rho_{\text{liq},\text{sp}}$  – liquid phase density at the spacer midpoint

$\mu$  – dynamic viscosity ( $\text{kg}/\text{m}\cdot\text{sec}$ )

$\mu_{\text{liq}}$  – liquid phase dynamic viscosity

$\mu_v$  – vapor phase dynamic viscosity

$\mu_{liq,301 in}$  – dynamic viscosity of the liquid phase at the inlet of section 301

$\mu_{liq,301 ave}$  – dynamic viscosity of the liquid phase across section 301

$\mu_{v,301 ave}$  – dynamic viscosity of the vapor phase across section 301

$\mu_{liq,sp}$  – liquid phase dynamic viscosity at the spacer

$\mu_{v,sp}$  - vapor phase dynamic viscosity at the spacer

$\mu_{m,sp}$  – two-phase dynamic viscosity at the spacer

$v_v$  – specific volume vapor phase ( $m^3/kg$ )

$v_{liq}$  – specific volume liquid phase

$\gamma$  – surface tension – (Newton( $kg\cdot m/sec^2$ ) - $sec/m^2$ ,  $kg/m\cdot sec$ )

$\gamma_{ave 301}$  – average surface tension across section 301

$\gamma_{301 in}$  – surface tension at the inlet of section 301

$A$  – cross sectional area ( $m^2$ )

$A_B$  – flow through area of the channel (Bundle)

$A_{rod}$  – cross sectional area of fuel and water rods

$A_{SP}$  - frontal area of spacer

$B$  – \*Chisholm two-phase spacer pressure multiplier coefficient

BWR – Boiling Water Reactor

$C_x$  - \*general drag coefficient

$C_{d,0 IN}$  - \*In form-drag coefficient

$C_{d,i}$  - \*Chun/Oh form-drag coefficient

$C_{d,grid}^{fric}$  - \*In grid frictional drag coefficient

$C_{d,turb}^{fric}$  - \*In turbulent flow frictional drag coefficient

$C_{d,rod}^{fric}$  - \*In rod frictional drag coefficient

$C_{DS}$  - \*DeStourder drag coefficient

$C_{f,lam}^{fric}$  - \*Chun/Oh laminar flow frictional drag coefficient

$C_{f,turb}^{fric}$  - \*Chun/Oh turbulent flow frictional drag coefficient

$C_S$  - \*Spengos drag coefficient

$C_{SH}$  - \*Shiralkar drag coefficient

$C_V$  - \*Rehme drag coefficient

$C_{V(D)}$  - \*Schikorr/Bubelis drag coefficient

$D_B$  - hydraulic diameter of the fuel bundle before and after the spacer (m)

$D_{SP}$  - hydraulic diameter of the spacer

$E_{1 Prem}$  - \*specific parameter of the Premoli Correlation

$E_{1 Prem,301 in}$  - \*specific parameter of the Premoli Correlation at the inlet of section 301

$E_{2 Prem}$  - \*specific parameter of the Premoli Correlation

$E_{2 Prem, 301 in}$  - \*specific parameter of the Premoli Correlation at the inlet of section 301

$E_{Fried,301}$  - \*specific parameter of the Friedel Correlation across section 301

$F_{Fried,301}$  - \*specific parameter of the Friedel Correlation across section 301

$Fr_{Fried,301}$  - \*Froude number of the Friedel Correlation across section 301

$f_{(SH)}$  - \*higher turbulence Shiralkar drag coefficient

$f_{liq,Fried 301}$  - \*Friedel liquid phase friction factor across section 301

$f_{v,Fried 301}$  - \*Friedel vapor phase friction factor across section 301

$g$  - acceleration due to gravity (9.81 m/sec<sup>2</sup>)

$G_B$  - mass flowrate through the fuel bundle open area (flux) (kg/sec - m<sup>2</sup>)

$G_{liq,sp}$  - mass flux of the liquid phase through the spacer open area

$G_{SP}$  - mass flux through the spacer

$G_{v,sp}$  - mass flux of the vapor phase through the spacer open area

$G_m$  - 2 Phase mass flux through the fuel bundle

$H_{Fried,301}$  - \*specific parameter of the Friedel Correlation (across section 301)

$H_{SP}$  - \*height, or length, of a spacer along the fuel channel (m)

- $j_{liq,sp}$  – superficial velocity of the liquid phase (m/sec)
- $j_{v,sp}$  – superficial velocity of the vapor phase (m/sec)
- $K_{(B,IN)}$  – \*In combined fuel bundle pressure loss coefficient
- $K_c$  – \*Tong/Weisman contraction pressure loss coefficient
- $K_{(CO)}$  – \*Chun/Oh pressure loss coefficient
- $K_e$  - \*Tong/Weisman expansion pressure loss coefficient
- $K_f$  - \*Shiralkar friction pressure loss coefficient
- $K_{fric,grid}$  – \*Chun/Oh grid frictional pressure loss coefficient
- $K_{fric,rod}$  - \*Chun/Oh rod frictional pressure loss coefficient
- $K_{form,grid}$  – \*Chun/Oh spacer form pressure loss coefficient
- $K_{form,mixing}$  - \*Chun/Oh mixing vane form pressure loss coefficient
- $K_{(Idel'chik)}$  or  $K_{(I)}$  - \* Idel'chik pressure loss coefficient
- $K_{(RT)}$  or  $\xi$  – \*Rehme/Trippe pressure loss coefficient
- $K_{(SH)}$  - \*Shiralkar pressure loss coefficient
- $K_{(V)}$  - \*Rehme pressure loss coefficient
- $K_{EXP}$  - \*single-phase pressure loss coefficient through an expansion
- $K_{sp}$  – \*single-phase spacer pressure loss coefficient
- $K_U$  - \*single-phase velocity transition coefficient
- $L$  – length (m)
- $L_{turb}$  – length to turbulent transition
- $\dot{m}$  - mass flowrate (kg/s)
- $\dot{m}_{liq}$  – mass flowrate of the liquid phase
- $\dot{m}_v$  – mass flowrate of the vapor phase
- $\dot{m}_{liq\ bundle\ in}$  – mass flowrate of the liquid phase going into the bundle
- $P$  – general pressure (Pascal (kg/m-sec<sup>2</sup>))



PWR – pressurized water reactor

$Re_B$  – \*Reynolds Number (bundle) of the fuel channel before and after the spacer

$Re_L$  - \*Reynolds Number (length of flat surface)

$Re_{SP}$  - \*Reynolds Number (spacer)

$Re_{Prem,301 in}$  - \*Reynolds Number of the fuel bundle at the inlet of section 301

$Re_{liq,ave 301}$  – \*average Reynolds Number of the liquid phase between points (across section 301)

$Re_{v,ave 301}$  – \*average Reynolds Number of the vapor phase between points(across section 301)

$Re_{2P sp}$  – \*two-phase Reynolds Number of the fuel bundle at the spacer

$S$  – \*slip (velocity) ratio ((m/sec)/(m/sec))

$S_{301 in}$  – \*slip ratio at the inlet of section 301

$U$  - undesignated velocity (m/sec)

$U_B$  - velocity in the fuel channel where there is no spacer

$U_{SP}$  - velocity at the spacer

$WA_{rod}$  - the wetted area of the rods along the height of the spacer ( $m^2$ )

$We_{Prem, 301 in}$  - \*Weber number of the fuel bundle at the inlet of section 301

$We_{Fried,301}$ - \*Weber number of the Friedel Correlation for the fuel bundle across section 301

$WP_B$  -wetted perimeter bundle, walls of the channel plus the perimeter of the rods (m)

$WP_{SP}$  - wetted perimeter spacer, cross-sectional perimeter of spacer components that contact the flow (m)

$x$  – flow quality ((kg/s)/(kg/s))

$x_{301 in}$  - flow quality at the inlet of section 301

$x_{301 out}$  - flow quality at the outlet of section 301

$x_{sp}$  - flow quality at the midpoint of the spacer

$x_{301,ave}$  – average flow quality across section 301

$y$  – \*specific parameter of the Premoli Correlation

$y_{301 in}$  – \*specific parameter of the Premoli Correlation at the inlet of section 301

$z_{301 in}$  – elevation of section 301 inlet (m)

$z_{301 out}$  – elevation of section 301 outlet (m)

### 3.7. References

Idel'chik, I. E., 1986. Handbook of Hydraulic Resistance, 2<sup>nd</sup> ed. Hemisphere Publishing Corporation, New York, ISBN: 978-0-8911-6284-1.

Lahey Jr., R. T. Jr. and Moody, F. J., 1993. The Thermal-Hydraulics of a Boiling Water Nuclear Reactor, 2nd Ed. American Nuclear Society Publishing, La Grange Park, Illinois, ISBN: 0-89448-037-5.

Neykov, B., Aydogan, F., Hochreiter, L., Ivanov, K., Utsuno, H., Kasahara, F., Sartori, E., and Martin, M., 2006. NUPEC BWR Full-size Fine-mesh Bundle Test (BFBT) Benchmark, Vol. I: Specifications. OECD, Nuclear Energy Agency, NEA No. 6212, ISBN: 92-64-01088-2.

Todreas, N. E., and Kazimi, M. S., 2012. Nuclear Systems, 2nd Ed. CRC Press Publishing, Boca Raton, Florida, ISBN: 978-1-4398-0887-0.

## CHAPTER 4: SINGLE-PHASE PRESSURE LOSS MODELS

### 4.1. Introduction

This chapter identifies the one-dimensional single-phase spacer pressure loss models available in open literature, that focus specifically on pressure loss across the spacer. These models were chosen based on enough available data to distinguish the specific model from any other model, and enough data to verify the model is used correctly. The section begins with the general theory and structure of the single-phase spacer pressure loss model then provides ten specific single-phase pressure loss models. The following one-dimensional single-phase models, listed in Table 1, can be grouped into two different categories.

**Table 1: Summary of Single-Phase Spacer Grid Pressure Loss Models**

Model	Category	Description
<b>Idel'chik</b>	Empirical	Early loss coefficient from Fluid Dynamics
<b>Spengos</b>	Empirical	Early study based on horizontal Plexiglas spacers using water as coolant
<b>DeStourder</b>	Empirical	Early compilation based on a wide variety of spacers and studies
<b>Tong/Weisman</b>	Empirical	From one of the initial texts on PWRs, used the contraction through the spacer.
<b>Rehme</b>	Empirical	Based on Fast Breeder Reactors, however used water for the experiments
<b>Trippe-Rehme</b>	Empirical	Provided refined factors for the earlier Rehme equation
<b>Shiralkar</b>	Semi-Empirical	Provided one of the first semi-empirical equations based on turbulent flow
<b>Chun/Oh</b>	Semi-Empirical	Losses were divided into three factors, based on PWRs
<b>In/Chun/Oh</b>	Semi-Empirical	Added refinements to the Chun/Oh equation
<b>Schikorr/ Bubelis</b>	Semi-Empirical	Provided an semi-empirical equation for the Rehme correlation

The first category is referred to as empirical models. These models are based on experimental observations and have a “drag” or bias coefficient, developed from test data, to correlate flow pressure, and the geometric, or form, modifier to the measured pressure loss. These coefficients ( $C_x$ ), are available in graphs or tables based on plots of experimental data, and are selected using the chart’s plotting factors, for substitution into the pressure loss coefficient. The Idel’chik model is an exception, it has a coefficient calculated from only the blockage ratio.

The second category (ii) is referred to as semi-empirical models, because the models use equations to calculate “drag” and form coefficients. The equations for the drag coefficients ( $C_x$ ) are based on factors determined by the authors of the model.

#### 4.2. Single-Phase Pressure Loss Model Structure

With the removal of gravity and friction pressure loss, the only pressure loss is from the spacer grid, given in the general form as equation (45): (Todreas and Kazimi, 2012)

$$\Delta P_{sp (general)} = K_{sp} ((\rho U_{SP}^2)/2) \quad (45)$$

where ( $\Delta P_{spacer (general)}$ ) is the pressure loss from the spacer grid, and ( $K_{sp}$ ) is a general loss coefficient at the spacer that will be developed further in the study, and named for the specific model. It is multiplied by the dynamic pressure factor, ( $\rho U_{SP}^2/2$ ), where ( $U_{SP}$ ) is the velocity of the coolant across the spacer. Equation (45) assumes a portion of the pressure decrease, from the increase in flowrate through the spacer, will not be recovered. This proportional decrease will correlate with the general loss coefficient ( $K_{SP}$ ), as the coolant decelerates at the spacer outlet. The general loss coefficient factors are shown in equation (46): (Rehme, 1973)

$$K_{sp} = C_x (\theta) \quad (46)$$

where ( $C$ ) is the drag coefficient, ( $\Theta$ ) is an area, or form, modifier based on the geometry of the spacer, and the subscript ( $x$ ) represents the specific version of the coefficients, named for the specific model. Substituting equation (46) into equation (45) provides a standard format appearing frequently in literature to describe the historical models, shown in equation (47):

$$\Delta P_{sp (X)} = C_x (\theta)((\rho U_{SP}^2)/2) \quad (47)$$

Or by using mass flux in the dynamic pressure loss factor, the pressure loss across the spacer can be calculated by equation (48):

$$\Delta P_{sp (X)} = C_x (\theta)(G_{sp}^2/2\rho) \quad (48)$$

where ( $G_{sp}$ ) is the mass flux through the spacer grid. The drag coefficient is not present in all of the spacer pressure loss correlation models, but the area modifier and the general loss coefficient are always present.

### 4.3. Specific Single-Phase Spacer Pressure Loss Models

#### 4.3.1 Empirical Models

Idel'chik (1986) developed one of the first pressure loss coefficients, based on fluid dynamics and obstructions in piping, calculated by equation (49):

$$K_{(Idel'chik)} = [((0.5\epsilon)^{1/2} + \epsilon)/(1 - \epsilon)]^2 \quad (49)$$

Substituting the Idel'chik pressure loss coefficient (49), which consists only of form loss with no friction coefficient, ( $C_x$ ), provides pressure loss equation (50):

$$\Delta P_{(I)} = [((0.5\epsilon)^{1/2} + \epsilon)/(1 - \epsilon)]^2 (G_B^2/2\rho) \quad (50)$$

In the late 1950s, Spengos (1959) analyzed water flow through a variety of horizontal Plexiglas spacers. He developed the following pressure loss equation (51):

$$\Delta P_{(S)} = n C_S (\epsilon/(1 - \epsilon)) (G_{SP}^2/2\rho) \quad (51)$$

where ( $C_S$ ) is the drag coefficient, which Spengos developed from observation, identified in Figure 4. The coefficient “n” is the number of supports/foot length. This “n” coefficient and its application is unique to any model. It is calculated in units of “supports per foot length,” however it is substituted into equation (51) as a dimensionless coefficient. Further, the distance between spacers is calculated in inches, so it can be used to identify which line to use in Figure 12. The spacer used in this study equates to the spacer designated as “9.6 inches, with rods,” plotted by solid squares in Figure 4. The Support Reynolds Number in Figure 12 (Spengos, 1959) is the Reynolds Number of the spacer ( $Re_{SP}$ ).

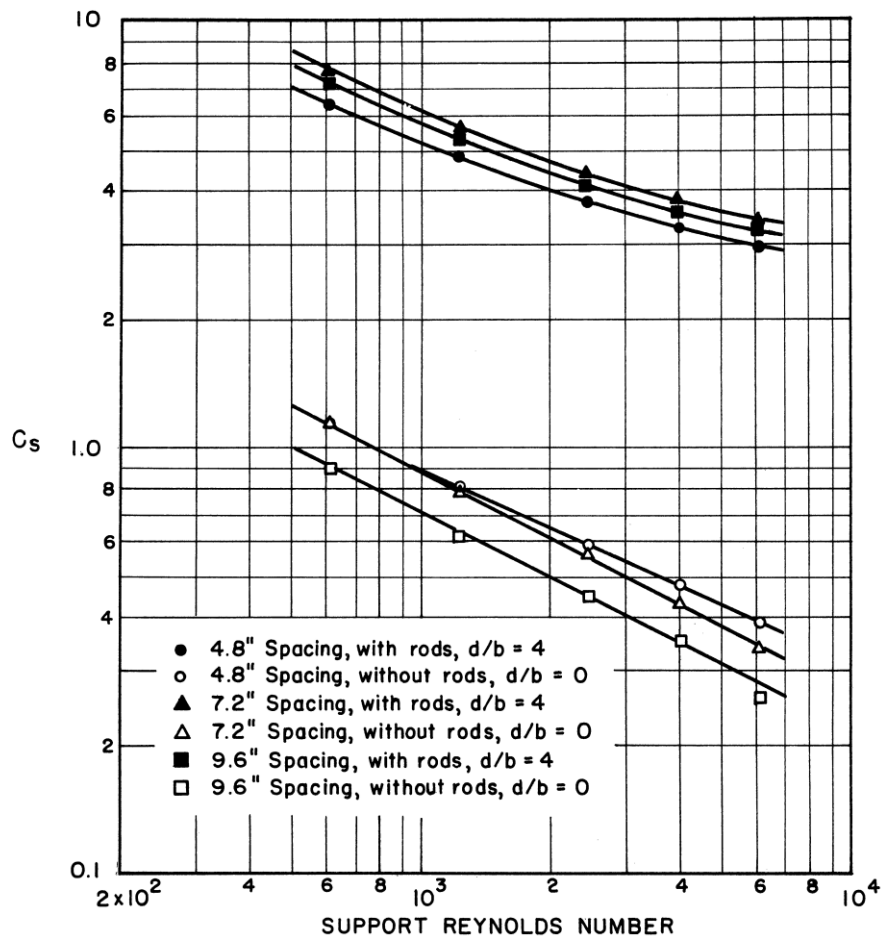


Figure 12: Spengos Drag Coefficients for Grid Spacers (Spengos, 1959)

A. N. DeStourder, (1961) based his empirical correlation on a wide variety of spacers and reactor types to develop the following pressure loss equation (52):

$$\Delta P_{(DS)} = C_{DS} (\epsilon) (G_{SP}^2 / 2\rho) \quad (52)$$

The drag coefficient ( $C_s$ ) is calculated from Figure 13 based on the Honeycomb type of the spacer grid, and  $\epsilon$  is the blockage ratio calculated from equation (1). In some publications, the DeStourder drag coefficient table is displayed without the types of spacers. Using a drag coefficient, without considering the conditions and spacer grid, may provide a misleading bias.

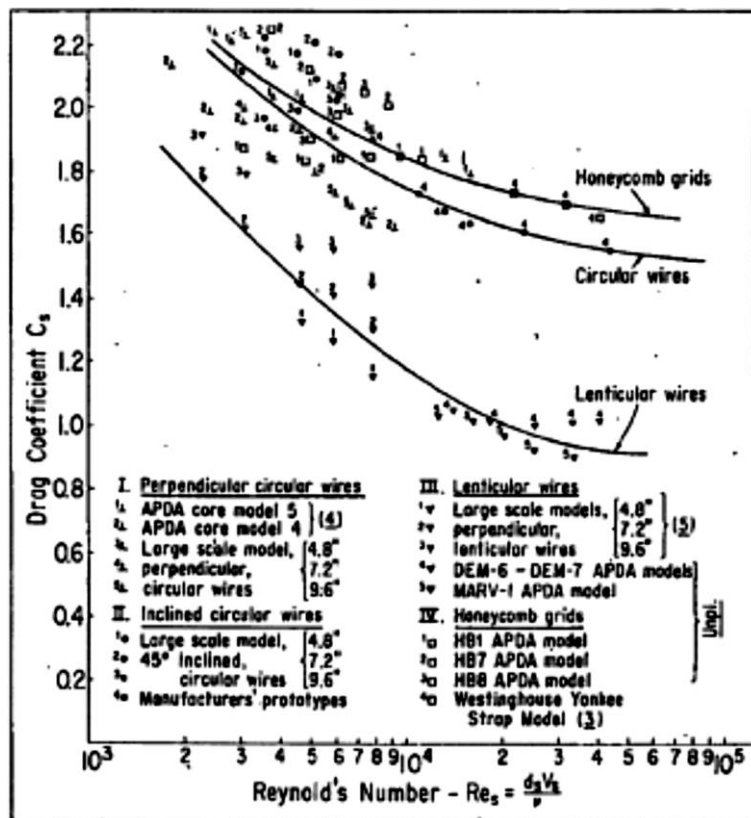


Figure 13: Drag Coefficients for Transverse Grid Spacers based on Spacer Hydraulic Diameter (DeStourder, 1961)

The drag coefficients, for the spacer grid used in this study, are identified based on the experimental data for the Honeycomb spacer grids. Also, the calculations for the Spengos and DeStourder equations are based on the Reynolds Number and flowrate across the spacer. Many correlation equations use the fuel rod bundle parameters as the basis for the variables. A conversion factor allows the use of the mass flux ( $G_B$ ) or velocity ( $U_B$ ) in the bundle, to calculate the mass flux through the spacer, with almost any equation originally based on flowrate through the bundle as shown in equation (53):

$$G_{SP}^2/2\rho = (A_B/(A_B - A_{SP}))^2(G_B^2/2\rho) \quad (53)$$

Dividing through by ( $A_B$ ) provides equation (54):

$$G_{SP}^2/2\rho = (1/(1 - \epsilon)^2)(G_B^2/2\rho) \quad (54)$$

Substituting equation (54) into the DeStourder equation (52) provides equation (55):

$$\Delta P_{(DS)} = C_{DS} \epsilon / (1 - \epsilon)^2 (G_B^2 / 2\rho) \quad (55)$$

This conversion factor only allows multiplication by the bundle mass flux, ( $G_B$ ), instead of the spacer, ( $G_{SP}$ ). The area modifier is a separate factor. In the DeStourder Equation, the area modifier is still provided by equation (56):

$$\theta = A_{SP} / A_B \text{ or } \epsilon \quad (56)$$

Tong and Weisman (1970) provided a correlation equation based on combined drag coefficients and area modifiers at the entrance and exit of the spacer. This is shown in pressure loss equation (57):

$$\Delta P_{(TW)} = (K_c + K_e) (1 / (1 - \epsilon)^2) (G_B^2 / 2\rho) \quad (57)$$

where ( $K_c$ ) and ( $K_e$ ) are the loss coefficients from the sudden contraction and expansion respectively, of the coolant. The pressure loss coefficients' value is identified from the Reynolds Number of the spacer and the contraction ratio, from the table reprinted in the Tong and Weisman text, shown in Figure 14 (Tong and Weisman, 1970):



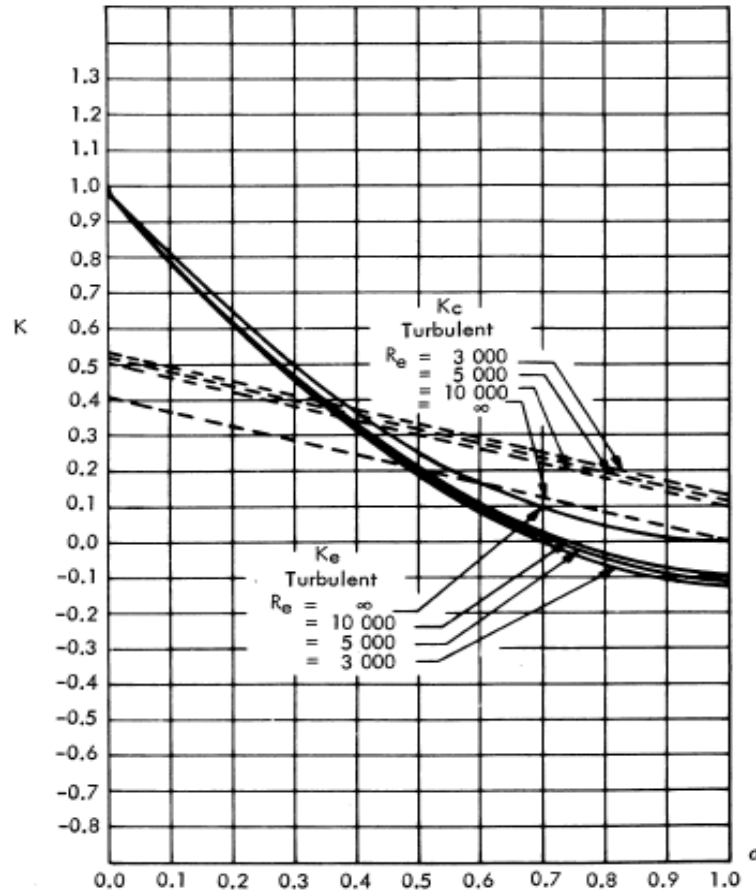


**Figure 14: Spacer Drag Coefficients for the Tong and Weisman Correlation (Tong and Weisman, 1970)**

The horizontal axis of the chart in Figure 14 is based on the contraction ratio ( $\sigma$ ) or  $(1-\epsilon)$ , and the Reynolds Number is based on  $Re_{sp}$ . A velocity conversion factor, equation (54), was added to equation (57), since the original equation's velocity was based on the spacer grid.

Klaus Rehme (1973) developed empirical drag coefficients for a wider range of Reynolds Numbers, and developed the area modifier further. His research was performed on fast breeder reactor fuel bundles, but the experimentation was conducted using water as a coolant.

Rehme's study used the square of the blockage ratio ( $\epsilon$ ) for a form loss correlation as shown in equation (58):

$$(A_{SP}/A_B)^2 = \epsilon^2 \quad (58)$$

leading to Rehme's pressure loss coefficient equation (59) (Rehme, 1973):

$$K_{(V)} = C_v \epsilon^2 \quad (59)$$

where  $K_{(V)}$  is the Rehme Pressure Loss Coefficient, and  $C_v$  is the Rehme drag coefficient, which is identified from Figure 15 (Rehme 1973). Placing equation (59) into the pressure loss equation provides Rehme's pressure loss equation (60):

$$\Delta P_v = C_v \epsilon^2 (G_B^2/2\rho) \quad (60)$$

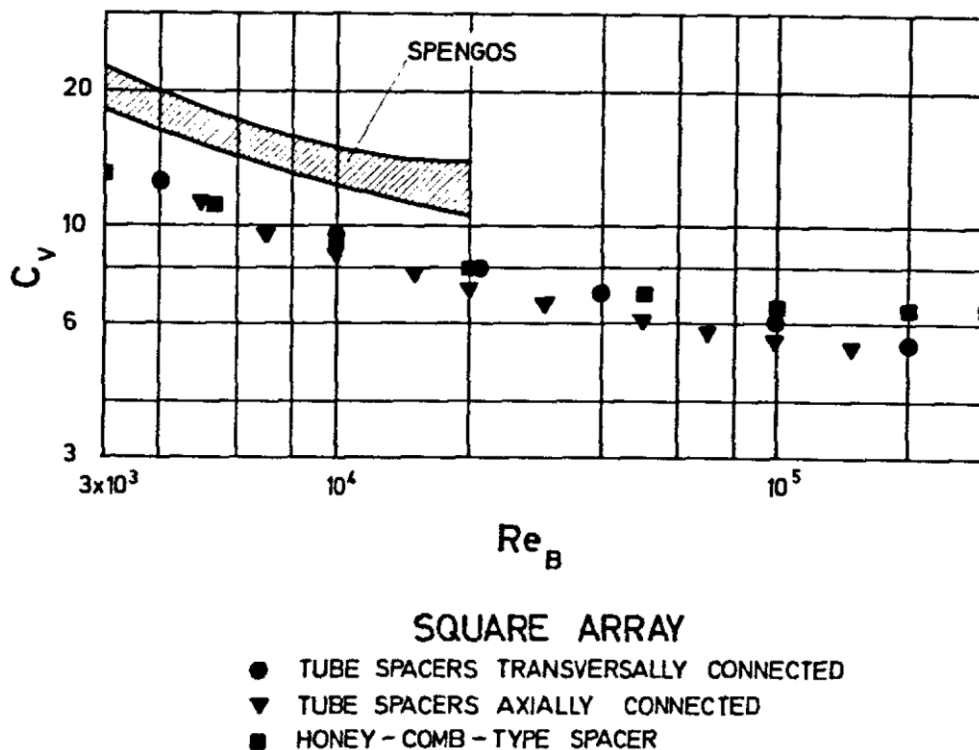


**Figure 15: Spacer Drag Coefficients for the Rehme Correlation (Rehme, 1973)**

In 1979, Rehme worked with Trippe to revise the original spacer grid model. The new model combines the area modifier and the drag coefficient to identify the pressure loss coefficient directly. These pressure loss coefficients apply within a defined range of blockage ratios. The Rehme-Tripp (Rehme and Trippe, 1980) pressure loss correlation is shown in equation (61):

$$\Delta P_{RT} = K_{RT}(G_B^2/2\rho) \quad (61)$$

$(K_{(RT)})$  is ( $\xi$ ), from Figure 16 (Rehme and Trippe. 1980) for blockage ratios from 0.2 to 0.45. The “SII” spacer type shown from Figure 16 most closely matches the spacer, used in this study, for the validation against BFBT experimental data.

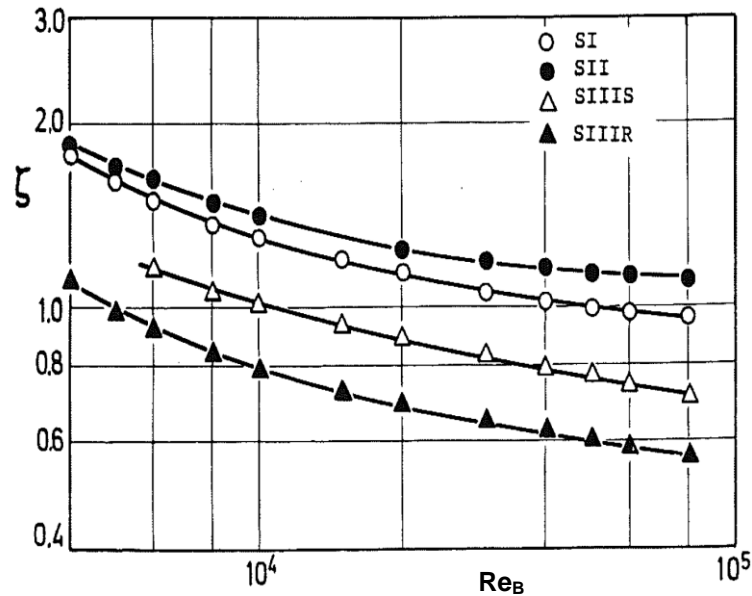


**Figure 16: Form Loss Factors for the Rehme and Trippe Correlation (Rehme and Trippe. 1980)**

#### 4.3.2 Semi-Empirical Models

The second category of equations is semi-empirical correlations. This category uses form and spacer friction coefficients, computed from equations, to decrease dependency on tables/figures which require repeated data extraction and interpolation. The objective is to increase accuracy and precision, and to provide a wider applicability of the loss correlation equation.

Shiralkar (Glueck, 2008) developed one of the earliest semi-empirical pressure loss equations for BWR fuel bundle flows. The total pressure loss coefficient ( $K_{SH}$ ) is calculated from two other pressure loss coefficients provided in equation (62): (Glueck, 2008)

$$K_{(SH)} = K_f + K_{(I)} \quad (62)$$

where ( $K_{(l)}$ ) is the Idel'chik pressure loss coefficient, which was described earlier. ( $K_f$ ) is the friction pressure loss coefficient, provided by equation (63):

$$K_f = [C_{(SH)} (H_{SP})(WP_B/4A_B)] [(WP_{SP}/WP_B) (1/(1 - \epsilon)^3) - 1] \quad (63)$$

The drag coefficient ( $C_{(SH)}$ ) was originally given as  $f_{(SH)}$ , which is equal to 0.015 for the entire range of Reynolds Numbers based Shiralkar's fuel bundle. However, a later study by Glueck expanded this figure for Reynolds Numbers below  $10^5$  by equation (64):

$$\lambda_{turb} = 0.0055 \left[ 1 + [(20000 (\epsilon/D_B)) + (10^6/Re_B)]^{1/3} \right] \quad (64)$$

where, ( $\lambda_{turb}$ ) is the drag coefficient when ( $Re_B$ )  $< 10^5$ , and ( $\epsilon$ ) is the rod roughness, which is generally  $2.5 \times 10^{-6}$  meters for a BWR rod. The original basis for Shiralkar's model was the BWR, which concentrated on high, turbulent flow above a ( $Re_B$ ) of  $10^5$ . When ( $Re_B$ )  $> 10^5$ , the value for ( $C_{(SH)}$ ) is ( $f_{(SH)}$ ), 0.015, and the pressure loss correlation ( $K_{(l)}$ ) is used in the calculation. When ( $Re_B$ )  $< 10^5$ , the value for ( $C_{(SH)}$ ) is ( $\lambda_{turb}$ ), and the pressure loss correlation ( $K_{(l)}$ ) is not used in the calculation. So depending on ( $Re_B$ ), ( $C_{(SH)}$ ) will equal  $f_{(SH)}$  or ( $\lambda_{turb}$ ), and the Idel'chik Pressure Loss Coefficient will be used in the calculation. Shiralkar's pressure loss correlation is provided by equation (65):

$$\Delta P_{(SH)} = (K_I + K_f)(G_B^2/2\rho) \quad (65)$$





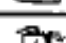




Chun and Oh (1998) developed a semi-empirical correlation model for PWRs, then verified the equation with PWR model simulation codes. The total pressure loss coefficient consisted of four separate parameters based on the spacer design, shown in equation (66):

$$K_{(CO)} = K_{form,grid} + K_{fric,grid} + K_{fric,rod} + K_{form,mixing} \quad (66)$$

where ( $K_{form,grid}$ ) is the loss from the spacer grid form, ( $K_{fric,grid}$ ) is the friction on the grid, ( $K_{fric,rod}$ ) is the friction on the fuel and water rod, and ( $K_{form,mixing}$ ) is the form loss due to a mixing vane, which was not used in this study (Chun and Oh, 1998). The form loss for the spacer grid is calculated by equation (67):

$$K_{form,grid} = \sum_i C_{(d,i)} (A_{SP}/A_B) \quad (67)$$

where ( $C_d$ ) is a form loss coefficient, which comes from the table in Figure 17 (Chun and Oh, 1998):

	Grid Elements	Shape		$C_d^{(4)}$
$K_{form}^{grid}$	Strip	Blunt		0.9
		Stream shape		0.45
	Spring	Horizontal		0.45
		Vertical		1.2
	Dimple	Horizontal		0.45
		Oval		0.76
	Nugget	Upstream		1.17
		Downstream		0.42
$K_{form}^{mixing}$	Mixing Vane	-		1.17

**Figure 17: Chun and Oh Form Drag Coefficients (Chun and Oh, 1998)**

The next loss parameter is the frictional loss in the grid, given by ( $K_{fric,grid}$ ) (Chun and Oh, 1998). It is based on turbulent and laminar friction, along with the height of the spacer, and the factor is calculated by equation (68):

$$K_{grid,fric} = [C_{f,lam}^{fric} (L_{turb}/H_{SP}) + C_{f,turb}^{fric} ((H_{SP} - L_{turb})/H_{SP})] ((H_{SP} W_{P_{SP}})/A_B) \quad (68)$$

where ( $C_{f,lam}^{fric}$ ) is the laminar frictional drag coefficient, and ( $C_{f,turb}^{fric}$ ) is the turbulent frictional drag coefficient. ( $L_{turb}$ ) is the length, along the spacer, where the flow becomes turbulent, based on a flat plate Reynolds Number ( $Re_L$ ) of 50,000. ( $C_f^{fric}$ ) is calculated by equation (69) and equation (70):

$$C_{f,lam}^{fric} = 1.328/Re_L^{1/2} \quad (69)$$

$$C_{f,turb}^{fric} = 0.455/(\log Re_L)^{2.58} \quad (70)$$

The parameter ( $K_{\text{fric,rod}}$ ) (Chun and Oh, 1998) is based on friction from all the rods within the spacer, and is calculated by equation (71):

$$K_{\text{rod,fric}} = f_{(D)}(H_{\text{SP}}/D_{\text{B}}) \quad (71)$$

Where ( $f_{(D)}$ ) is a drag coefficient based on the ( $\text{Re}_{\text{SP}}$ ), calculated by equation (72) and (73): (Chun and Oh, 1998)

$$f_{(D)} = 0.184 \text{Re}_{\text{SP}}^{-0.2} \quad \text{if } 3 \times 10^4 < \text{Re}_{\text{SP}} < 1 \times 10^6 \quad (72)$$

$$f_{(D)} = 0.316 \text{Re}_{\text{SP}}^{-0.25} \quad \text{if } \text{Re}_{\text{SP}} < 3 \times 10^4 \quad (73)$$

The rod friction parameter modifies the fuel bundle hydraulic diameter, ( $D_{\text{B}}$ ), so only the wetted perimeter of the rods ( $\text{WP}_{\text{Rods}}$ ) are included, and it does not include the sides of the fuel bundle. Substituting the modified equation (5), for the fuel bundle hydraulic diameter into equation (71), the rod friction parameter is shown by

$$K_{\text{rod,fric}} = f_{(D)}(H_{\text{SP}} \text{WP}_{\text{Rods}})/(4 A_{\text{B}}) \quad (74)$$

The symbol for the drag coefficient will remain ( $f_{(D)}$ ) in this equation, for reasons shown later. Since there is no mixing vane in this study's tests, the Chun/Oh Pressure Loss Correlation is provided by equation (75) (Chun and Oh, 1998):

$$\Delta P_{(\text{CO})} = (K_{\text{form,grid}} + K_{\text{fric,grid}} + K_{\text{fric,rod}})(1/(1 - \epsilon)^2)(G_{\text{B}}^2/2\rho) \quad (75)$$

This pressure loss correlation was obtained by multiplying the total pressure loss summation coefficient, ( $K_{(\text{CO})}$ ), by the bundle flowrate to spacer flowrate conversion factor, equation (54), then substituting both these terms into the basic spacer grid pressure loss equation (45).

Chun and Oh later worked with In to refine the pressure loss correlation equation, substituting a calculation method for the spacer form loss parameter. The following description of the In/Chun/Oh equation only applies to the changes from the Chun/Oh model.

In's total spacer pressure loss coefficient consists of the summation of the parameters in equation (76) (In et al., 2002):

$$K_{(B,IN)} = C_{d,0 IN}(\epsilon) + C_{d,grid}^{fric} \left( (H_{SP} WP_{SP})/A_B \right) + C_{d,rod}^{fric} (WA_{rod}/A_B) \quad (76)$$

where  $WA_{rod}$  is the wetted area of the fuel and water rods within the spacer. The frictional loss coefficients for the In, Chun and Oh models are identified by the subscript "d" as in  $(C_d)$ , instead of  $(C_f)$ , in the Chun and Oh model. The spacer form drag coefficient,  $(C_{d,0 IN})$ , is the significantly different parameter, compared to Chun and Oh's previous model. The In correlation for spacer form loss is calculated by (77):

$$C_{d,0 IN} = 2.75 - 0.27 \log_{10} (Re_B) \quad (77)$$

The grid friction loss coefficient varies from the original Chun/Oh equation by changing the flat plate Reynolds Number ( $Re_L$ ) for turbulence transition length ( $L_{turb}$ ) to 30,000. In addition, the drag coefficient for turbulent flow is calculated by equation (78):

$$C_{d,turb}^{fric} = 0.523 / (\ln^2(0.06 Re_L)) \quad (78)$$

In/Chun/Oh used only equation (72), not equation (73), for a rod friction factor, and  $(C_{d,rod}^{fric})$  does not equal  $(f_{(D)})$ . The drag coefficient is combined with the friction factor as indicated below in equation (79):

$$C_{d,rod}^{fric} (WA_{rod}/A_B) = C_{d,rod}^{fric} (4H_{SP}/D_B) = f_{(D)} (H_{SP}/D_B) = f_{(D)} \left( (H_{SP} WP_{rods})/4A_B \right) \quad (79)$$

by substituting  $(WA_{rod})$  for  $(H_{SP} WP_{rods})$ , and then dividing out  $(WA_{rod}/A_B)$ ,  $(C_{d,rod}^{fric})$  is calculated by equation (80):

$$C_{d,rod}^{fric} = f_{(D)}/4 \quad (80)$$

By multiplying the summation of the three sub- pressure coefficients loss,  $(K_{form,grid})$ ,  $(K_{fric,grid})$  and  $(K_{fric,rod})$ , by the spacer flowrate conversion factor, equation (54), the In Pressure Loss Correlation is calculated by equation (81):

$$\Delta P_{(IN)} = K_{(B,IN)} (1/(1 - \epsilon)^2) (G_B^2/2\rho) \quad (81)$$

The most recent semi-empirical correlation equation is a conversion of the Rehme equation's drag coefficient to semi-empirical form by Schikorr et al. Schikorr's experiment used water based simulations, across numerous test facilities in Europe. The general form of the pressure loss correlation (Schikorr et al., 2010) is calculated by equation (82):

$$\Delta P_{(SB)} = C_{V(D)} (\epsilon^2)(G_B^2/2\rho) \quad (82)$$

where the difference is the equation for  $(C_{V(D)})$ , which is the Schikorr-Bubelis drag coefficient, (Cigarini and Donne 1988) based on Fast Breeder Reactor Fuel Bundles, calculated by equation (83):

$$C_{V(D)} = 3.5 + (73.14/Re_B^{0.264}) + (2.79 \times 10^{10}/Re_B^{2.79}) \quad (83)$$

with a maximum drag coefficient  $(C_{V(D)})$ , of  $2/\epsilon$ . (Schikorr et al., 2010).

#### 4.4. References

Chun, T.H., and Oh D.S., 1998. A Pressure Drop Model for Spacer Grids with and without Flow Mixing Vanes. *Journal of Nuclear Science and Technology*, Vol.35, No. 7, pp. 508-510.

Cigarini, M. and Dalle Donne, M., 1988. Thermohydraulic Optimization of Homogeneous and Heterogeneous Advanced Pressurized Reactors. *Nuclear Technology*, Vol. 80, No. 1, pp. 107-132.

DeStourder, A. N., 1961. Drag Coefficients for Fuel Element Spacers. *Nucleonics*, Vol. 19, No. 6, pp. 74-79.

Glueck, M., 2008. Validation of the Sub-Channel Code F-COBRA-TF, Part I. Recalculation of Single-Phase and Two-Phase Pressure Loss Measurements. *Nuclear Engineering and Design*, Vol. 238, No. 9, pp. 2308-2316.

Idel'chik, I. E., 1986. *Handbook of Hydraulic Resistance*, 2<sup>nd</sup> ed. Hemisphere Publishing Corporation, New York, ISBN: 978-0-8911-6284-1.

In, W.K., Oh, D.S. and Chun, T.H., 2002. Empirical and Computational Pressure Drop Correlations for PWR Spacer Grids. *Nuclear Technology*, Vol. 139, No. 1, pp. 72-79.

Rehme, K., 1973. Pressure Drop Correlations for Fuel Element Spacers. *Nuclear Technology*, Vol. 17, No. 1, pp. 15-23.

Rehme, K. and Trippe, G., 1980. Pressure Drop and Velocity Distribution in Rod Bundles with Spacer Grids. *Nuclear Engineering Design*, Vol. 62, No. 1, pp. 349-359.



Schikorr, M., Bubelis, E., Mansani, E. L., and Litfin, K., 2010. Proposal for Pressure Drop Prediction for a Fuel Bundle with Grid Spacers using Rehme Pressure Drop Correlations. *Nuclear Engineering and Design*, Vol. 240, No. 7, pp. 1830-1842.

Spengos, A. C., 1959. Tests on Models of Nuclear Reactor Elements, IV. Model Study of Fuel Element Supports. UMRI-2431-4-P, University of Michigan Research Institute, Ann Arbor.

Todreas, N. E., and Kazimi, M. S., 2012. *Nuclear Systems*, 2nd Ed. CRC Press Publishing, Boca Raton, Florida, ISBN: 978-1-4398-0887-0.

Tong, L.S., and Weisman, J., 1970. *Thermal Analysis of Pressurized Water Reactors*, 1st Ed. American Nuclear Society Publishing, La Grange Park, Illinois, ISBN: ISBN: 978-0-8944-8038-6.

## CHAPTER 5: SINGLE-PHASE EXPERIMENT AND RESULTS

### 5.1. Experiment Theory and Structure

#### 5.1.1. Experiment Structure

The BFBT experimental structure consists of twelve increasing flowrates for each of three target pressures, 200 KPa, 1 MPa, and 7.15 MPa. These thirty-six tests provide a wide range of data on varying conditions, since with the increase in flowrate there is an increase in the Reynolds Number, leading to an increase in turbulence, providing detailed data for pressure loss across the real, full-scale spacer grid and flow characteristics of the coolant.

The pressures and flowrates from the experimental conditions were close to the planned values, with minor, insignificant variations. The measured and calculated variables of pressure, temperature, flowrate, density and viscosity, for the flow conditions from each test number, are used as inputs for the established variables of each historical spacer grid pressure loss model. These variables include the calculations for both general and spacer losses. The experimental measurements at pressure section dPT1, recorded as “dp 301” for this set of tests, are shown in Table 2 (Neykov et al., 2006) for each of the target pressures and flowrate, for each test number:

**Table 2: Single-Phase Test Data (Neykov et al., 2006)**

Test #	Planned Pressure MPa	Measured Pressure MPa	Planned Flow rate (Kg/sec)	Measured Flow Rate (Kg/sec)	Measured Pressure Loss dp301 (KPa)
P70001	0.2	0.2	2.5	2.5	0.11
P70002	0.2	0.2	3.8	3.7	0.18
P70003	0.2	0.2	5.0	5.0	0.31
P70004	0.2	0.2	6.3	6.3	0.46
P70005	0.2	0.2	7.6	7.5	0.63
P70006	0.2	0.2	8.8	8.8	0.83
P70007	0.2	0.2	10.1	10.0	1.05
P70008	0.2	0.2	11.3	11.3	1.29
P70009	0.2	0.2	13.9	13.8	1.86
P70010	0.2	0.2	15.1	15.1	2.16
P70011	0.2	0.2	16.4	16.2	2.46
P70012	0.2	0.2	17.6	17.4	2.81
P70013	0.98	1.0	2.5	2.5	0.06
P70014	0.98	0.99	3.8	3.8	0.14
P70015	0.98	0.99	5.0	5.1	0.27
P70016	0.98	0.98	6.3	6.2	0.38
P70017	0.98	0.98	7.6	7.5	0.54
P70018	0.98	0.99	8.8	8.7	0.73
P70019	0.98	0.99	10.1	10.0	0.94
P70020	0.98	0.99	11.3	11.4	1.21
P70021	0.98	1.0	13.9	13.8	1.72
P70022	0.98	0.98	15.1	15.1	2.03
P70023	0.98	0.98	16.4	16.3	2.36
P70024	0.98	0.98	17.6	17.6	2.72
P70025	7.2	7.17	2.5	2.5	0.08
P70026	7.2	7.15	3.8	3.9	0.18
P70027	7.2	7.15	5.0	5.1	0.3
P70028	7.2	7.16	6.3	6.3	0.46
P70029	7.2	7.16	7.6	7.5	0.64
P70030	7.2	7.16	8.8	8.7	0.79
P70031	7.2	7.16	10.1	10.0	1.11
P70032	7.2	7.16	11.3	11.2	1.37
P70033	7.2	7.15	13.9	13.9	2.06
P70034	7.2	7.15	15.1	15.0	2.41
P70035	7.2	7.16	16.4	16.3	2.81
P70036	7.2	7.15	17.6	17.6	3.25

dp 301 – The measured Pressure Loss across the Test Section for Differential Pressure 301

## 5.1.2. Experiment Purpose and Conditions

### 5.1.2.1. Purpose

As previously noted, the purpose of this study is to compare predicted pressure losses from historical equations, using input conditions from the BFBT bundle experiments and the BFBT test section dimensions, to the measured pressure losses. The first objective was to identify whether the historical equations are accurate and precise, using more detailed measurements and different conditions, than the conditions used to develop the equations. The next objective is to identify whether the more precisely measured flow properties demonstrated any trends for further development. The desired result is to identify the percent bias of the predicted pressure loss, from the measured pressure loss, over the range of flowrates from the experiment's pressure test grouping. To accomplish this comparison, a predicted spacer grid pressure loss was generated, for each of the pressure loss models, for all thirty-six tests. While water was used as a coolant in the majority of the historical tests, a wide variety of bundle types and flowrates were used in those tests, providing a variety of historical conditions used to validate the original models and to compare to measured losses and flow characteristics.

### 5.1.2.2. Test Conditions

The pressure and the Reynolds Number were chosen as the parameters for comparison. The Reynolds Number was chosen because it converts the measured flowrates and other available properties into a standard measure of turbulence. The pressure ranges were chosen because there is a range of clearly identifiable Reynolds Number data points, for each of the three pressures used in the study. There was not enough data to identify the effect of a range of pressures at an established Reynolds Number or flowrate, or data points for any other single-phase flow characteristic.

To analyze the flow characteristic of Reynolds Number, the Reynolds Number based on the fuel bundle's hydraulic diameter ( $Re_B$ ) was the common factor for comparison of the historical spacer pressure loss models' predictions, to the measured spacer pressure loss from the BFBT experimental set. These biases are plotted across the range of Reynolds Numbers for each test set. To analyze the flow characteristic of pressure, the test sets are grouped based on the target input pressures of 200 KPa, 1 MPa, and 7.15 MPa, providing a data plot for each model, at each test pressure. The bias of each historical model, for each measured Reynolds Number to the BFBT measurement, is displayed graphically later in Section 5.2.3. The purpose is to show the bias, from the predicted pressure loss to the measured pressure loss, in percentage, over the increasing turbulence of the pressure test grouping. In addition to the Reynolds Number and the pressure parameters, the empirical and semi-empirical models are graphed separately for comparison.

#### 5.1.2.3. Possible Measurement Errors

The accuracy of the instrumentation measuring the flowrate and pressure was +/- 1.0 %. The flowrate affects the flow velocity and mass flux, while the pressure affects the flow properties of density and viscosity. Based on the factors for spacer grid pressure loss, a +1% change in flowrate will affect the experimental pressure loss +0.3%, and a -1% change in flowrate will affect the experimental pressure loss -0.3% across all the flowrates. The increase in the all the historical models' calculated pressure loss is less than +2% from a 1% increase in flowrate. The possible measurement error for each model's performance is listed beneath the tables for the final results in section 5.2.4.

The viscosity and density increase from a 1% pressure increase is approximately 0.035% and .022%, respectively, in the 7.15 MPa pressure range. At the 2 lower pressure ranges, the changes are below .001 %. The maximum change in viscosity will affect the measured and calculated pressures less than 0.0001%. The maximum density error will affect the

measured pressure loss less than 0.001%, and calculated pressures less than 0.02%. These errors are less than 2% proportionally of an error in flowrate measurement, including within the final results.

The maximum deviations in the results, from combined pressure and flow errors, are listed beneath the tables for the final results in section 5. The results are already in percentage, so for example, a +/- 1% possible measurement error of the bias means a 10% bias's true value could be between 9% and 11%. All the historical models are calculated from the same BFBT factors, so all calculations increase or decrease proportionally, and the results are analyzed strictly by comparison. Therefore, the maximum measurement error, in any combination, will have no effect on the final results.

## 5.2 Results

### 5.2.1. Criteria

To analyze the results, the criteria consist of accuracy and precision. Accuracy is the difference between the averaged sum of the experimental and the predicted measurements, which is designated as the bias, or difference. The average bias is based on the average of the twelve test runs for each target pressure, and is produced from the average of the measured difference to the predicted difference, in percentage, using equation (84):

$$\text{Bias (\%)} = \left[ \frac{\sum_{(i)} \left( \frac{x_{(i)} - t_{(i)}}{t_{(i)}} \times 100 \right)}{n} \right] \text{ OR } \left[ \frac{\sum(\text{predicted value difference (\%)})}{12} \right] \quad (84)$$

where  $(x_{(i)})$  is the  $i$ th predicted pressure loss measurement for the  $i$ th flowrate,  $(t_{(i)})$  is the pressure loss measurement from the test for the  $i$ th flowrate, and  $n$  is the number of samples for the given pressure.

Precision measures the range of variation about the average difference of a model, or how close to the average bias the measured data points are. This study used standard deviation of the sample,  $(\sigma_{(\text{predicted})})$  measuring the percent differences, from the experimental results to

the predicted results, based on the twelve predicted values for each target pressure. This will determine how precise the bias is, in percent standard deviation, produced by equation (85):

$$\sigma_{(\text{predicted } \%)} = \sqrt{\frac{\sum_{(i)} \left[ \left( \frac{x_{(i)} - t_{(i)}}{t_{(i)}} \times 100 \right) - \left( \frac{\sum_{(i)} \left( \frac{x_{(i)} - t_{(i)}}{t_{(i)}} \times 100 \right)}{n} \right) \right]^2}{(n-1)}} \quad (85)$$

with the terms simplified, the standard deviation for the twelve tests for each pressure group is shown by equation (86):

$$\sigma_{(\text{predicted } \%)} = \sqrt{\frac{\sum \left[ \left( \frac{(x_{(i)} \text{ predicted value})}{\text{difference } (\%)} \right) - \left( \frac{(\text{average predicted value})}{\text{difference } (\%)} \right) \right]^2}{(12-1)}} \quad (86)$$

### 5.2.2. Flow Characteristics

Reynolds Numbers for the 200 KPa test flowrates ranged from 4660 to  $3.9 \times 10^4$ . For the 1 MPa Test flowrates, the Reynolds Numbers ranged from  $2.2 \times 10^4$  to  $1.5 \times 10^5$ , and for the 7.15 MPa Test flowrates, the Reynolds Numbers ranged from  $3.7 \times 10^4 < (Re_B) < 2.6 \times 10^5$ . Laminar flow in a square or rectangular channel occurs approximately until  $(Re_B) > 2300$ , then a transition area continues until  $(Re_B) > 10^4$ , and flow becomes fully turbulent. This data identifies the experimental flows as mostly turbulent with a small number of flows as transitioning to turbulent. The relation to the Single-Phase Spacer Pressure Loss Models is with an increasing turbulent Reynolds Number, the drag coefficients approach limiting values, then the pressure loss factor is a constant.

### 5.2.3. Graphical Analysis of Single-Phase Spacer Pressure Loss Models

The plots of the bias, are in Figures 18, 19, 20, 21, 22 and 23. The Reynolds Number is calculated for each of the measured flowrates and pressures for each of the ten single-phase models. The empirical and semi-empirical models are also graphically compared to each other in successive figures.

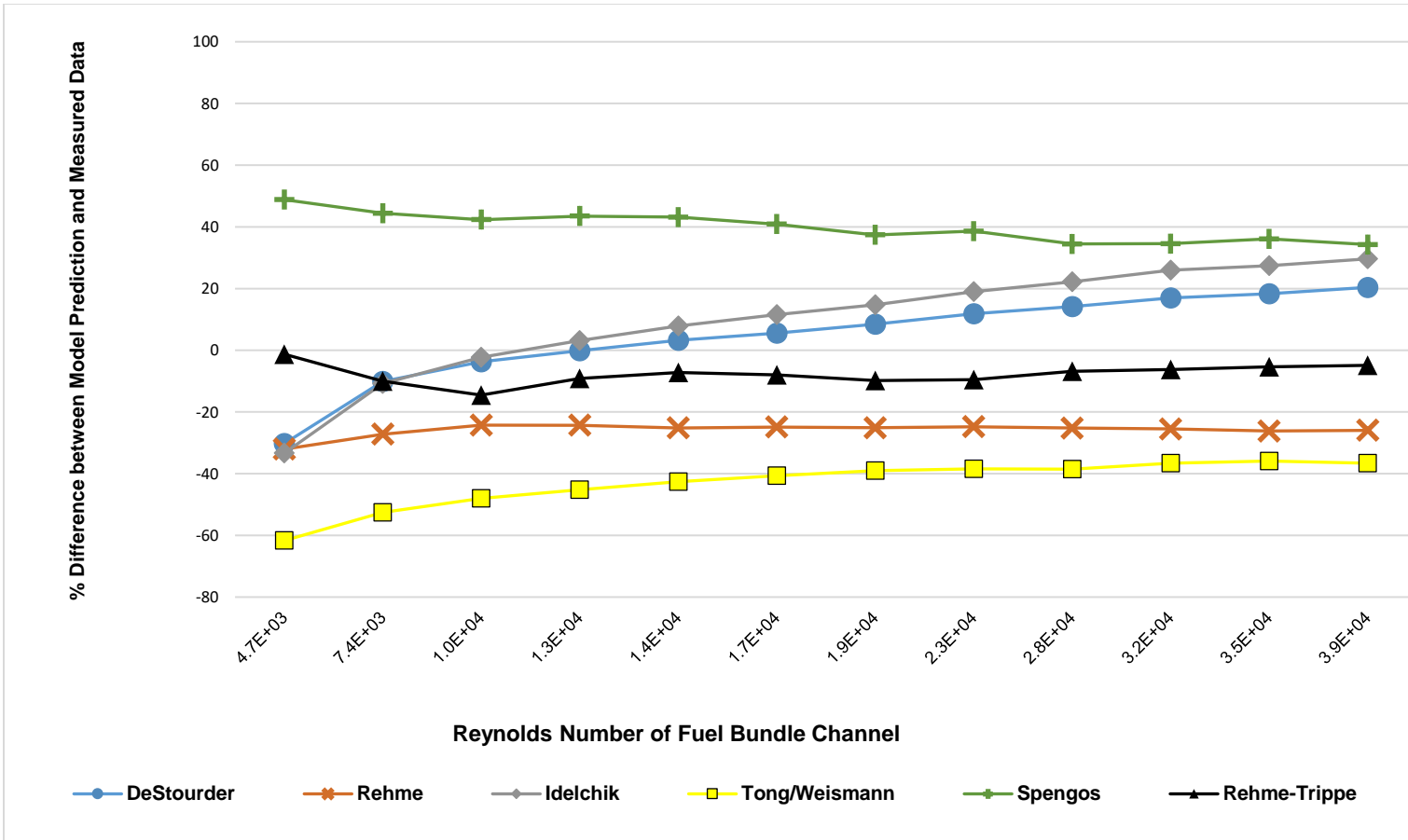


Figure 18: "Empirical" Results at 200 kPa Test Pressure



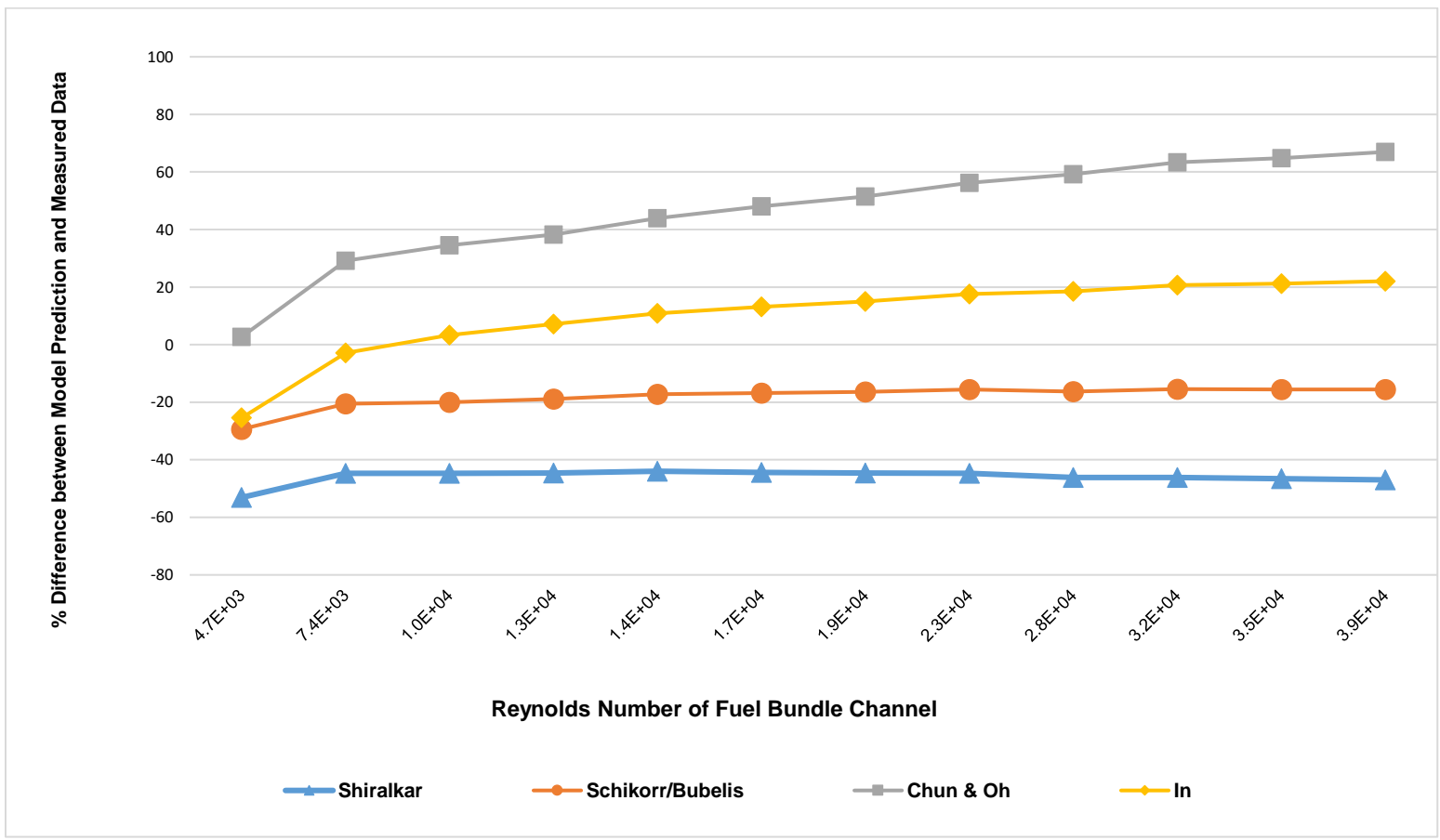


Figure 19: "Semi-Empirical" Results at 200 KPa Test Pressure

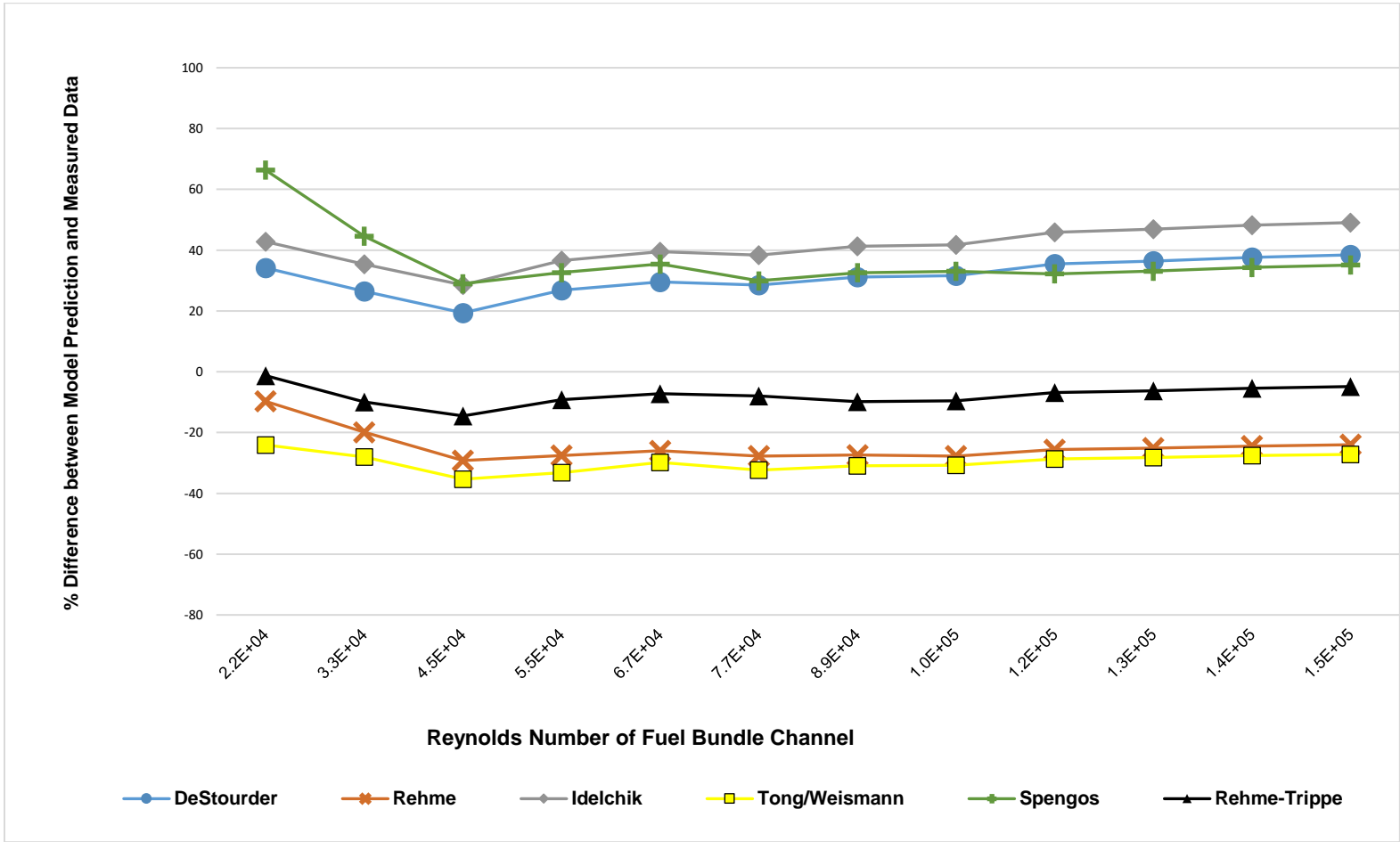


Figure 20: "Empirical" Results at 1 MPa Test Pressure

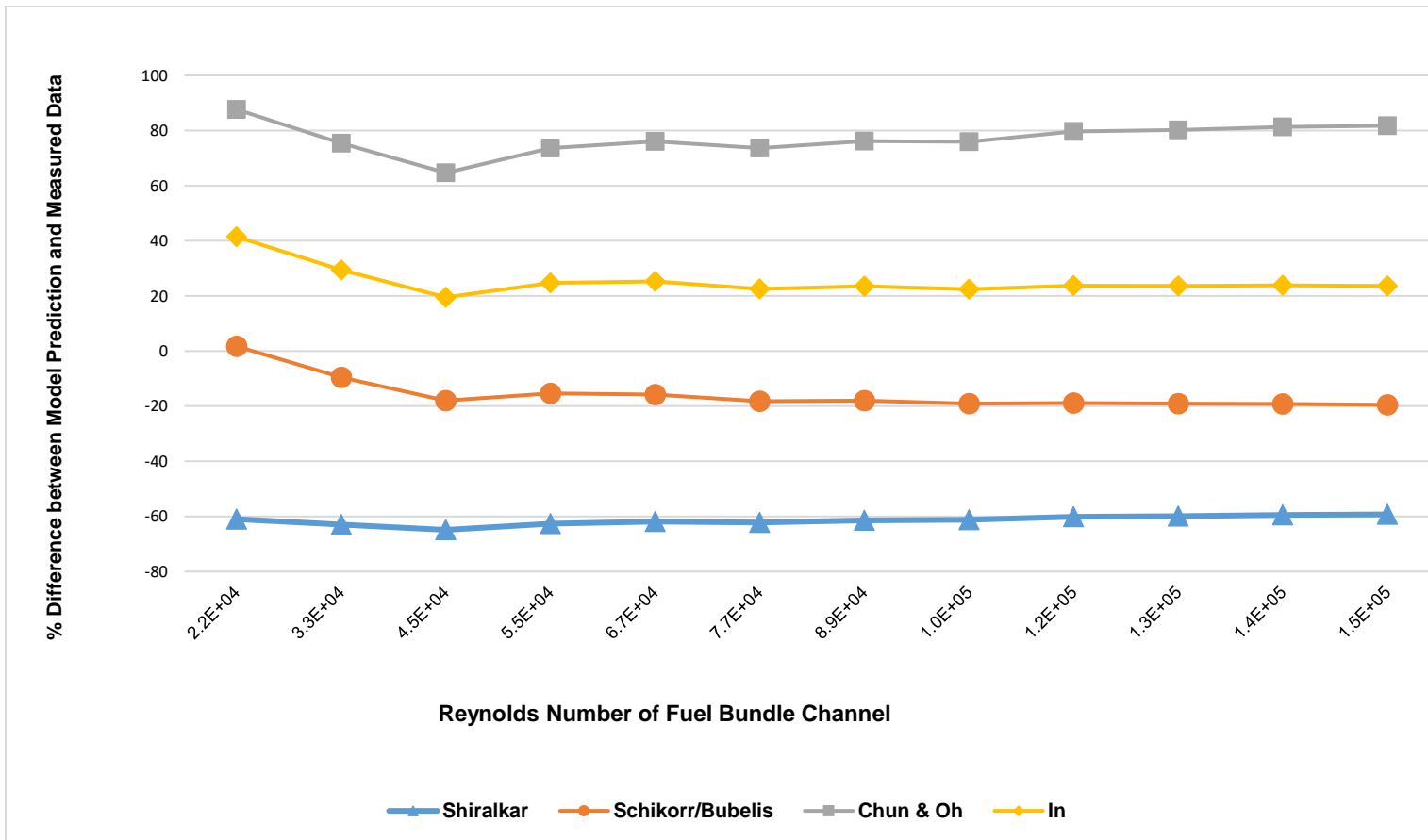


Figure 21: "Semi-Empirical" Results at 1 MPa Test Pressure

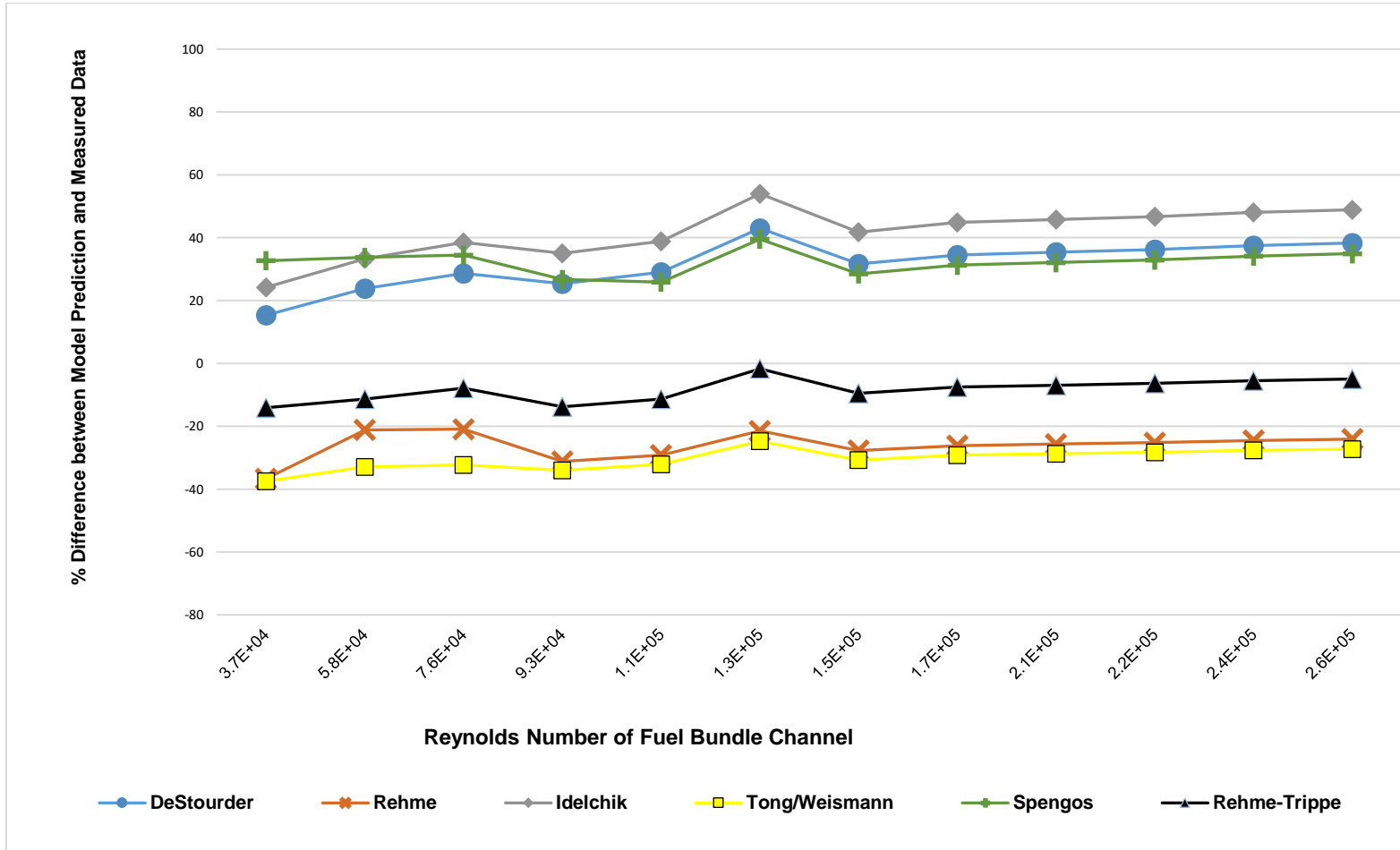


Figure 22: "Empirical" Results at 7.15 MPa Test Pressure

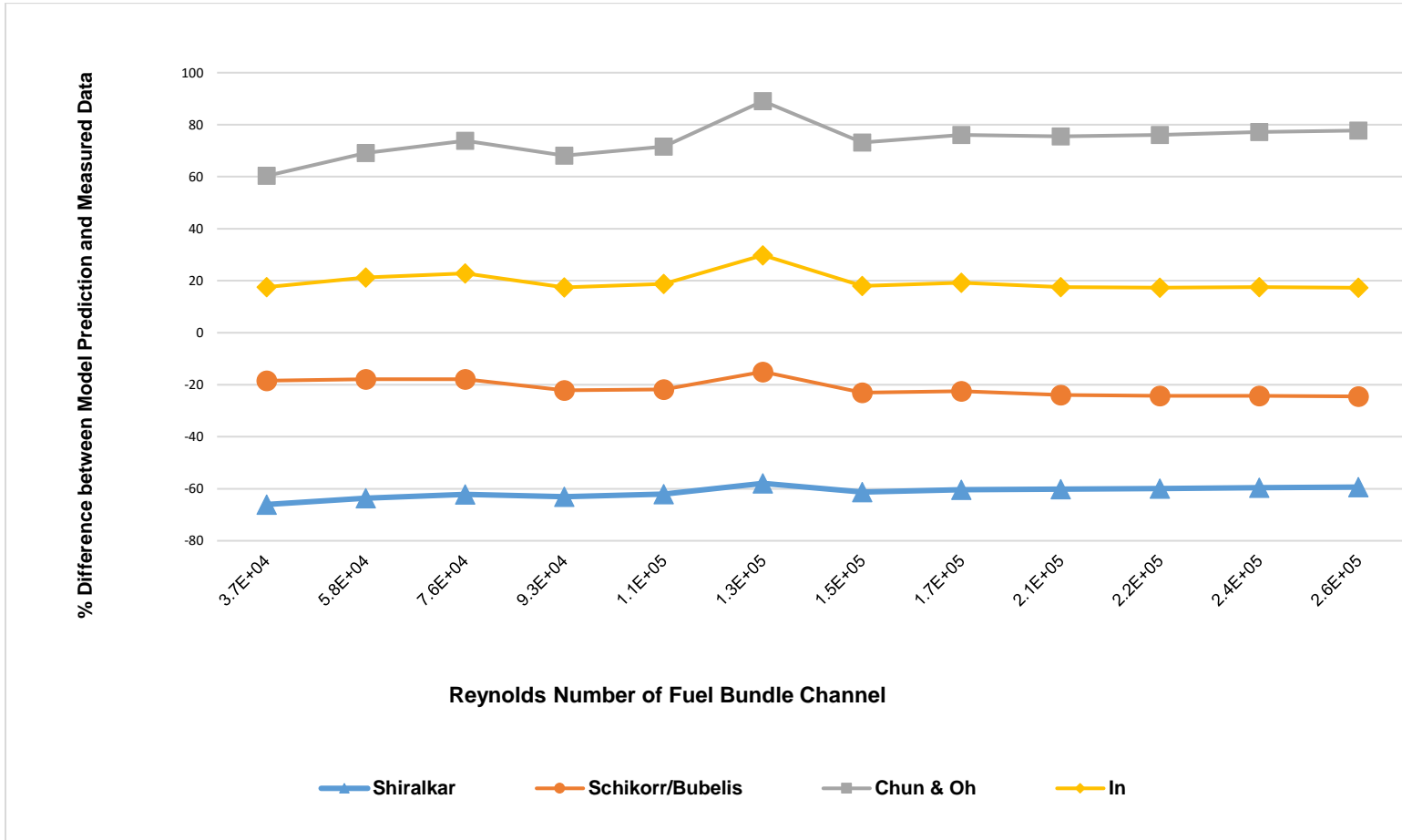


Figure 23: “Semi-Empirical” Results at 7.15 MPa Test Pressure

#### 5.2.4. Tabular Summary of the Results

The summary of the results of the bias, in percentage, is in Table 3, showing the agreement of the predicted to the measured values. The summary of the standard deviation results of the average bias is in Table 4, showing the scatter of the predicted values to the measured value.

**Table 3: Bias of Calculated Results (Difference in %)**

Model	Inlet Pressure			Ave Bias
	200 KPa	1 MPa	7.15 MPa	
<b>Empirical Based</b>				
Idel'chik	9.59	41.19	41.66	30.81
Spengos	39.86	36.52	32.23	36.20
DeStourder	4.56	31.32	31.56	22.48
Tong/Weisman	-42.99	-29.69	-30.47	-34.38
Rehme	-25.89	-24.54	-26.16	-25.53
Trippe/Rehme	-18.82	-7.74	-8.42	-11.66
<b>Semi-Empirical Based</b>				
Shiralkar	-45.89	-61.41	-61.28	-56.19
Chun/Oh	46.67	77.16	73.99	65.91
In/Chun/Oh	10.17	25.29	19.57	18.32
Schikorr/Bubelis	-18.15	-15.75	-21.30	-18.40

**Error of Measurement from instrumentation – Percentage from Original Data**  
**Errors will proportionally increase or decrease variance across all models as shown below:**

Idel'chik: +/- 2.88 % 200 KPa Range of True Bias = 6.71% to 12.47%

Spengos: +/- 2.84 %

DeStourder: +/- 2.67 %

Tong Weisman: +/- 1.43 %

Rehme: +/- 1.53 %

Trippe/Rehme: +/- 1.88 %

Shiralkar: +/- 2.51 %

Chun/Oh: +/- 3.53 %

In/Chun/Oh: +/- 2.88 %

Shickorr/Bubelis: +/- 1.59 %

**Table 4: Standard Deviation of Calculated Equations Bias (%)**

Model	Inlet Pressure			Ave ST Deviation
	200 KPa	1 MPa	7.15 MPa	
<b>Empirical Based</b>				
Idel'chik	18.36	5.99	8.16	10.84
Spengos	4.70	10.16	3.79	6.22
DeStourder	14.38	5.55	7.58	9.17
Tong/Weisman	7.77	3.06	3.50	4.77
Rehme	2.10	5.26	4.57	3.98
Trippe/Rehme	5.81	3.3	3.72	4.28
<b>Semi-Empirical Based</b>				
Shiralkar	2.46	1.64	2.23	2.11
Chun/Oh	18.21	5.65	6.84	10.32
In/Chun/Oh	13.36	5.56	3.67	7.6
Schickorr/Bubelis	3.95	6.16	3.18	4.43

**Error of Measurement from instrumentation – Percentage from Original Data Errors will proportionally increase or decrease variance across all models as shown below:**

Idel'chik: +/- 0.37 % 200 KPa Range of True  $\sigma$ = 17.99% to 18.74%

Spengos: +/- 0.21 %

DeStourder: +/- 0.29 %

Tong Weisman: +/- 0.16 %

Rehme: +/- 0.11 %

Trippe/Rehme: +/- 0.12 %

Shiralkar: +/- 0.05 %

Chun/Oh: +/- 0.43 %

In/Chun/Oh: +/- 0.26 %

Shickorr/Bubelis: +/- 0.15 %

### 5.3. Observations

#### 5.3.1. General Observations

An unusual pressure loss appears in the test bundle at  $1.3 \times 10^5$  ( $Re_B$ ) in the 7.15 MPa pressure group. This loss is reflected in all the historical models and will likely affect the variance to a small amount.

None of the established historical models accurately predicts the pressure loss, or provides a precise bias, better than any other model, for all the tested pressures and flows. No significant overall advantage is demonstrated between empirical or semi-empirical groups of models.

The graphical analysis of predicted pressure loss results in Figs. 18 through 23, for the ten single-phase pressure loss models using flow characteristics of the BFBT, demonstrates less variance of the bias as pressure and Reynolds Number increases. The majority of

models demonstrate a range of biases over the Reynolds Numbers, with the largest variance at the lowest Reynolds Number. The Rehme-Trippe Model indicates a comparative advantage in accuracy in Table 3, by demonstrating a consistent bias below 10%, or an agreement between the measured and predicted pressure loss, within 10% in the higher 2 pressures. The Shiralkar Model indicates a comparative advantage in precision in Table 4, by demonstrating a consistent standard deviation below 2.5% in all the pressure groupings.

Table 3 does not identify any significant groupings in the criteria of accuracy; however, some possible trends are indicated. Except for the Spengos model, the lowest average biases are in the lower two pressure groupings, with four of the models' lowest average bias in the 200 KPa pressure group and five of the models' lowest average bias in the 1 MPa pressure group. Three of four semi-empirical models demonstrate their highest bias in the 1 MPa range, however three empirical models had the highest bias in the 200 KPa pressure group, and three models had the highest bias in the 7.15 MPa pressure group. The above average and below average biases show no indicators. There are no other discriminators between any characteristics, and the amount of data is not large enough for a general conclusion.

Table 4 identifies groupings in the criterion of precision. The test results from seven of the ten models identify the highest standard deviations in the 200 KPa pressure group, and the other three models' highest deviations occur in the 1 MPa pressure group. Only the Rehme model's lowest standard deviation occurs in the 200 KPa group, while six of the ten models demonstrate the highest precision in the 1 MPa group. In the two higher pressure ranges, sixteen of the twenty results are below the average standard deviation for their models. Only the Rehme model has an above average standard deviation in the 7.15 MPa group. No significant differences between the ranges of semi-empirical or empirical models were observed.



### 5.3.2. Single-Phase Spacer Grid Pressure Loss Model Observations

The measures of performance only use comparison. There is no model or publication which establishes a baseline standard to determine a universal performance measure for general one-dimensional spacer grid pressure loss models, and the criteria for the performance of a model will be determined by the application. The objective for any pressure loss model, in an application, is that the model produces a result that has both a bias and a standard deviation within specifications.

Table 3 identifies advantages with the accuracy of the Rehme/Trippe model. The Rehme/Trippe model demonstrates the lowest average bias for all thirty-six tests, -11.66%; and the average standard deviation is 4.28%, which is the third lowest of the ten models. The DeStourder Model demonstrates the lowest bias at the 200 KPa pressure grouping, -4.56%, however the standard deviation is 14.38%, which is the eighth lowest. The Rehme/Trippe Model demonstrates the lowest bias at the 1MPa pressure grouping, -7.74%, and the standard deviation is 3.3%, which is the third lowest. The Rehme/Trippe Model also demonstrates the lowest bias at the 7.15 MPa pressure grouping, -8.42%, and the standard deviation is 3.72%, which is the fifth lowest.

Table 4 identifies advantages with the precision of the Shiralkar model. The Shiralkar model demonstrates the lowest average standard deviation for all thirty-six tests, 2.11%, however the average bias is -56.19%, which is the ninth lowest of the ten models. The Rehme Model demonstrates the lowest standard deviation, 2.10%, at the 200 KPa pressure grouping, however the bias is -25.89%, which is the sixth lowest. The Shiralkar Model demonstrates the lowest standard deviation at the 1 MPa and 7.15 MPa pressure groupings, 1.64% and 2.23% respectively, and the second lowest standard deviation at the 200 KPa pressure grouping, 2.46%. However, the bias is the ninth lowest for all the pressure groups, -45.89% for the 200 KPa group, -61.41% for the 1 MPa group, and -61.28% for the 7.15 MPa group.

#### 5.4. References

Neykov, B., Aydogan, F., Hochreiter, L., Ivanov, K., Utsuno, H., Kasahara, F., Sartori, E., and Martin, M., 2006. NUPEC BWR Full-size Fine-mesh Bundle Test (BFBT) Benchmark, Vol. I: Specifications. OECD, Nuclear Energy Agency, NEA No. 6212, ISBN: 92-64-01088-2.

## CHAPTER 6: Two-Phase Spacer Grid Pressure Loss Models

### 6.1. Introduction

The one-dimensional two-phase pressure loss models follow a different format from the single-phase models. Two-phase models calculate the frictional and spacer grid pressure loss in the liquid phase, then multiply that loss by a conversion factor based on two-phase flow characteristics, to estimate the losses within both phases. This is the same concept shown in the Friedel correlation for frictional losses in the fuel channel before and after the spacer. This use of two factors leads to a greater number of combinations, and the methods to effectively compare the combinations are more complex.

While many two-phase multipliers exist, the majority are based on frictional losses within the channel. Only a few are derived for losses at a spacer grid, and most of the spacer grid two-phase flow multipliers originated from form pressure losses for flows through obstructions, expansions, and contractions. Table 5 provides a summation of the different one-dimensional two-phase pressure loss multipliers below:

**Table 5: Summary of Two-Phase Spacer Grid Pressure Loss Multipliers**

<b>Multiplier</b>	<b>Description</b>
<b>Lottes</b>	Based on all losses occurring proportionally in the liquid phase
<b>Expanded Lottes</b>	Same as the Lottes, void coefficients at pressure taps used
<b>Romie</b>	Based on maintaining a momentum balance with the densities
<b>Expanded Romie</b>	Similar to the Romie multiplier with the assumption of no phase changes
<b>Richardson</b>	Balanced the pressure loss with kinetic energy and no phase change
<b>Mendler</b>	Based on densities using the Homogenous Equilibrium Model.
<b>Mendler Corrected</b>	Mendler model with a correction factor for viscosity ratio.
<b>Beattie</b>	Based on density of the liquid to the mixture, with empirical corrections
<b>Chisholm</b>	Based on density of the liquid to the mixture, with Lockhart-Martinelli correction

### 6.2. Two-Phase Pressure Loss Model Structure

The pressure change at a spacer follows the same general format by using the single-phase pressure loss coefficient ( $K_x$ ) to calculate the two-phase pressure loss ( $\Delta P_x^{2P}$ ) using a

two-phase multiplier ( $\Phi_{liq,x}$ ), as the Friedel Correlation accomplished earlier section 4.6.2. This format is described by equation (87): (Todreas and Kazimi, 2012)

$$\Delta P_{sp}^{2P} = K_{sp} \frac{G_m^2}{2 \rho_{liq,sp}} \Phi_{liq,sp} \quad (87)$$

where ( $\Delta P_{sp}^{2P}$ ) is the two-phase pressure loss at the spacer, ( $K_{sp}$ ) is the single-phase spacer pressure loss coefficient and ( $\Phi_{liq,sp}$ ) is the general two-phase spacer pressure loss multiplier based on the liquid phase. With this format, the previously developed single-phase spacer pressure loss models are required to determine the two-phase pressure losses.

### 6.3. Two-Phase Pressure Loss Models

#### 6.3.1 Theory

Lottes (1961) provided one of the initial compilations of two-phase spacer grid pressure loss multipliers. The focus of the Lottes paper was deriving two-phase losses through expansions. This pressure loss was based on the general pressure balance equation (88) and the conservation of momentum equation (89):

$$P_1 + \rho \frac{U_1^2}{2} = P_2 + \rho \frac{U_2^2}{2} + K_U \rho \frac{U_1^2}{2} \quad (88)$$

$$\rho_1 U_1 A_1 = \rho_2 U_2 A_2 \quad (89)$$

where (P) is pressure, (U) is velocity, (A) is area and ( $K_U$ ) is the single-phase velocity transition coefficient, based on the assumption of incompressible flow and the contraction ratio, ( $\sigma$ ). The contraction ratio and the blockage ratio, ( $\epsilon$ ), were explained in detail in the first part of this study and the calculation for the single-phase velocity transition coefficient is shown in equation (89).

$$K_U = (1 - \sigma)^2 \text{ or } K_U = \epsilon^2 \quad (89)$$

Substituting equation (89) into the general pressure balance provides equation (90): (Lottes, 1961)

$$-\Delta P_{EXP} = -2\sigma(1 - \sigma) \frac{\rho U^2}{2} \text{ and } K_{EXP} = 2\sigma(1 - \sigma) \quad (90)$$

where ( $\Delta P_{EXP}$ ) is the change of pressure through the expansion, and ( $K_{EXP}$ ) is the single-phase pressure loss coefficient through an expansion. In addition, ( $\rho_{out} \neq \rho_{in}$ ), ( $\alpha_{out} \neq \alpha_{in}$ ), and so on for two-phase flow. Two-phase multipliers use these changes, along with basic water properties, to identify how the addition of the vapor phase correlates to the liquid phase. Lottes based his two-phase multiplier for spacers on an expansion; however, since there is both an expansion and contraction, the ( $K_{EXP}$ ) will cancel out. By removing the ( $K_{EXP}$ ), the remaining factor is the pressure change based on the two-phase flow portion of the equation.

The following are very simplified explanations of the multipliers, since this study focuses on the application of existing two-phase multipliers. Lottes, and Lahey and Moody (Lahey and Moody, 1993) have detailed explanations of the derivations of two-phase multipliers. Lahey and Moody also have a detailed explanation of the derivation of the ( $K_{EXP}$ ), and how it is removed from the two-phase multipliers during expansion and contraction for spacer grid pressure loss.

### 6.3.2. Specific Two-Phase Spacer Grid Pressure Loss Models

The Lottes two-phase pressure multiplier was based on all losses taking place in the liquid phase, along with the cross sectional area and velocity of the liquid phase. Its original form was only for the expansion of the channel, and included the ( $K_{EXP}$ ) factor in equation (91): (Lottes, 1961)

$$K_{EXP} \phi_{liq,sp}^{Lottes \text{ exp}} = 2\sigma \left[ \frac{1}{(1-\alpha_{in})(1-\alpha_{out})} - \sigma \left( \frac{1}{(1-\alpha_{out})^2} \right) \right] \quad (91)$$

where, ( $\phi_{liq,sp}^{Lottes \text{ exp}}$ ), is the two-phase spacer pressure loss multiplier, based on the liquid phase, in the fully expanded form. Fully expanded means the equation uses  $\alpha_{in}$  and  $\alpha_{out}$ , which are the void fractions at the inlet and outlet, respectively, which for a spacer grid are

the void fractions at the spacer inlet and spacer outlet. Dividing out ( $K_{EXP}$ ), in its expanded form, the Lottes two-phase spacer pressure multiplier, is calculated by equation (92):

$$\phi_{liq,sp}^{Lottes\ exp} = \left( \frac{1}{1-\sigma} \right) \left[ \frac{1}{(1-\alpha_{sp,in})(1-\alpha_{sp,out})} - \left( \frac{\sigma}{(1-\alpha_{sp,out})^2} \right) \right] \quad (92)$$

By assuming ( $\alpha_{out} \approx \alpha_{in}$ ), across the short distance of the spacer, the simplified and more familiar form of the Lottes two-phase spacer pressure multiplier becomes equation (93): (Lahey and Moody, 1993)

$$\phi_{liq,sp}^{Lottes} = \frac{1}{(1-\alpha_{sp})^2} \quad (93)$$

Another two-phase spacer loss multiplier is commonly known as the ‘‘Romie Multiplier.’’ His multiplier is based on maintaining the mass and momentum balances of the two-phase flow, for both phases, and was published originally as equation (94): (Lottes, 1961)

$$K_{EXP} \phi_{liq,exp}^{Romie\ exp} = 2\sigma \left[ x_{sp}^2 \left( \frac{\rho_{liq,sp}}{\rho_{v,sp}} \right) \left( \frac{1}{\alpha_{in}} - \frac{\sigma}{\alpha_{out}} \right) + (1 - x_{sp})^2 \left( \frac{1}{(1-\alpha_{in})} - \frac{\sigma}{(1-\alpha_{out})} \right) \right] \quad (94)$$

Dividing out ( $K_{EXP}$ ), in its fully expanded form, the Romie two-phase spacer pressure multiplier, ( $\phi_{liq,sp}^{Romie\ exp}$ ), is provided by equation (95): (Lottes, 1961)

$$\phi_{liq,sp}^{Romie\ exp} = \left( \frac{1}{\epsilon} \right) \left[ x_{sp}^2 \left( \frac{\rho_{liq,sp}}{\rho_{v,sp}} \right) \left( \frac{1}{\alpha_{sp,in}} - \frac{(1-\epsilon)}{\alpha_{sp,out}} \right) + (1 - x_{sp})^2 \left( \frac{1}{(1-\alpha_{sp,in})} - \frac{(1-\epsilon)}{(1-\alpha_{sp,out})} \right) \right] \quad (95)$$

As with the Lottes Multiplier, assuming ( $\alpha_{out} \approx \alpha_{in}$ ), across the short distance of the spacer, the simplified and more familiar form of the Romie two-phase spacer pressure multiplier becomes equation (96): (Lahey and Moody, 1993)

$$\phi_{liq,sp}^{Romie} = \left[ \left( \frac{\rho_{liq,sp}}{\rho_{v,sp}} \right) \left( \frac{x_{sp}^2}{\alpha_{sp}} \right) + \frac{(1-x_{sp})^2}{(1-\alpha_{sp})} \right] \quad (96)$$

where ( $\phi_{liq,sp}^{Romie}$ ) is the Romie two-phase spacer pressure loss multiplier that assumes no change in the void coefficient.

An obscure two-phase spacer multiplier by B. L Richardson (Lottes, 1961), in the Lottes compilation, is based on the conservation of energy. He assumed the void fraction did not

change over the spacer, and the energy loss is proportional to the blockage ratio. The original form of the multiplier is equation (97): (Lottes, 1961)

$$K_{EXP} \phi_{liq,sp}^{Richardson} = \frac{(1-x_{sp})^2}{(1-\alpha_{sp})} \sigma(1 - \sigma^2) \quad (97)$$

Removing ( $K_{EXP}$ ), the Richardson two-phase spacer pressure loss multiplier, ( $\phi_{liq,sp}^{Richardson}$ ), becomes equation (98):

$$\phi_{liq,sp}^{Richardson} = \frac{(1-x_{sp})^2}{(1-\alpha_{sp})} \frac{(2-\epsilon)}{2} \quad (98)$$

A familiar two-phase spacer pressure loss multiplier in the compilation was originally published by Mendler (Mendler et al., 1961). He based his model on phase densities at constant void fraction and thermodynamic equilibrium, and assumed there would be no phase increase or decrease across the expansion. The original form of the multiplier is equation (99): (Lottes, 1961)

$$K_{EXP} \phi_{liq,sp}^{Mendler} = \left[ 1 + x \frac{v_v - v_{liq}}{v_{liq}} \right]_{sp} 2\sigma(1 - \sigma) \quad (99)$$

where ( $v_v$ ) is the specific volume of the vapor phase, and ( $v_{liq}$ ) is the specific volume of the liquid phase. Dividing by ( $K_{EXP}$ ), the Mendler two-phase spacer pressure multiplier, ( $\phi_{liq,sp}^{Mendler}$ ), is shown as equation (100): (Todreas and Kazimi, 2012)

$$\phi_{liq,sp}^{Mendler} = \left[ 1 + x \frac{v_v - v_{liq}}{v_{liq}} \right]_{sp} \quad (100)$$

The Mendler Model does not represent many basic water properties. A correctional factor was developed based on the liquid-vapor viscosity ratios using equation (101): (Lahey and Moody, 1993)

$$\text{Viscosity Correctional Factor} = \left[ 1 + x \left( \frac{\mu_{liq}}{\mu_v} - 1 \right) \right]_{sp}^{-n} \quad (101)$$

Based on the literature in Todreas and Kazimi, and Lahey and Moody,  $n \approx 0.25$  for turbulent flow. The Corrected Mandler two-phase spacer pressure multiplier, ( $\phi_{liq,sp}^{Mandler\ corr}$ ) is shown by equation (102):

$$\phi_{liq,sp}^{Mandler\ corr} = \left[ 1 + x \frac{v_g - v_{liq}}{v_{liq}} \right]_{sp} \left[ 1 + x \left( \frac{\mu_{liq}}{\mu_v} - 1 \right) \right]_{sp}^{-0.25} \quad (102)$$

Beattie (Beattie, 1973) later developed a variation of the HEM based on the proportion of the density of the liquid to the density of the mixture. He used empirical observations, based on flow across the spacer, to develop a two-phase spacer pressure multiplier shown in equation (103):

$$\phi_{liq,sp}^{Beattie} = \left[ 1 + x_{sp} \left( \frac{\rho_{liq,sp}}{\rho_{v,sp}} - 1 \right) \right]^{0.8} \left[ 1 + x_{sp} \left( (3.5) \left( \frac{\rho_{liq,sp}}{\rho_{v,sp}} \right) - 1 \right) \right]^{0.2} \quad (103)$$

Chisholm (Rooney et al., 1974) also developed a model based on the HEM and a variation of the Lockhart-Martinelli equation for their two-phase pressure loss multiplier, multiplied by a factor for irreversible loss through a sharp edged orifice, that modified the flow quality. Chisholm's two-phase spacer pressure multiplier is shown in equation (104):

$$\phi_{liq,sp}^{Chisholm} = 1 + \left[ \left( \frac{\rho_{liq,sp}}{\rho_{v,sp}} - 1 \right) [Bx_{sp}(1 - x_{sp}) + x_{sp}^2] \right] \quad (104)$$

where (B) is a coefficient based on density ratios and the Martinelli coefficient. The value of B is given by Fig 24 below (Rooney et al., 1974). Figure 24 is only significant at flow quality below 0.15, and above 0.15 flow quality, the (B) value is a constant value, determined by the pressure. The mass dryness fraction, described in the original table, is a different nomenclature for flow quality.



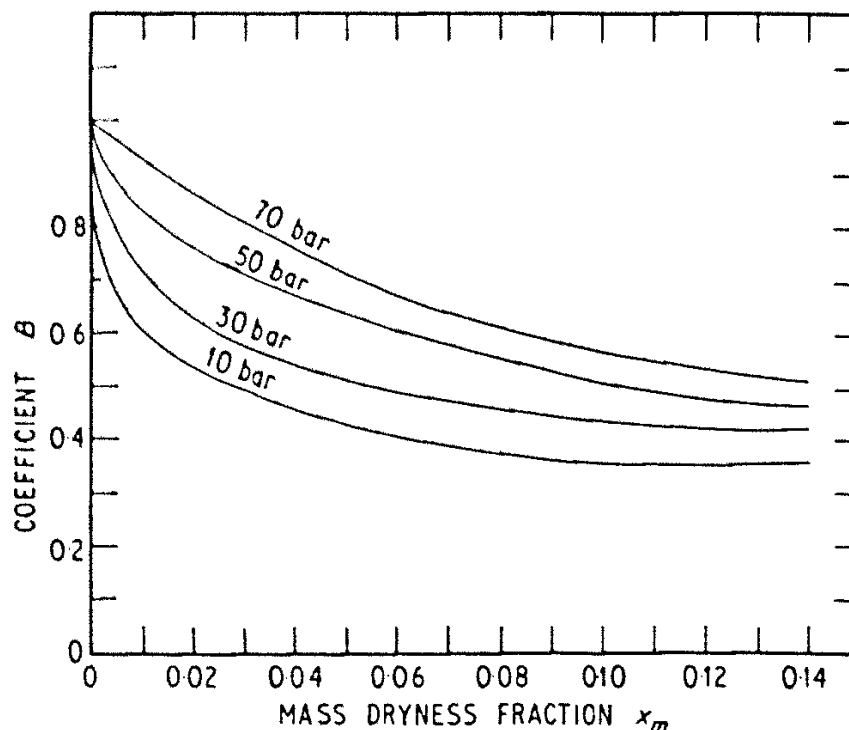


**Figure 24: B factor for the Chisholm Equation (Rooney et al., 1974)**

#### 6.4. References

Beattie, D. R. H., 1973. A Note on the Calculation of Two-Phase Pressure Losses." Nuclear Engineering and Design, Vol. 25, No. 3, pp. 395-402.

Lahey Jr., R. T. Jr. and Moody, F. J., 1993. The Thermal-Hydraulics of a Boiling Water Nuclear Reactor, 2nd Ed. American Nuclear Society Publishing, La Grange Park, Illinois, ISBN: 0-89448-037-5.

Lottes, P., 1961. Expansion Losses in Two-Phase Flow. Nuclear Science and Engineering, Vol. 9, No. 1, pp. 26-31.

Mendler, O.J., Rathbun, A.S.; Van Huff, N.E., and Weiss, A., 1961. Natural Circulation Tests with Water at 800 to 2000 PSIA under Non-Boiling, Local Boiling and Bulk Boiling Conditions. Journal of Heat Transfer, Vol. 83, No. 3, pp. 261-273.

Rooney, D.H., Chisholm, D. and Cornwell, R.S., 1974. Flow of Steam-Water Mixtures through Sharp Edged Orifices. Heat and Fluid Flow in Steam and Gas Turbine Plant Conference, Institute of Mechanical Engineering, London, England, Conference Publication 3-1973, pp. 1-8.

Todreas, N. E., and Kazimi, M. S., 2012. Nuclear Systems, 2nd Ed. CRC Press Publishing, Boca Raton, Florida, ISBN: 978-1-4398-0887-0.

## CHAPTER 7: TWO-PHASE EXPERIMENT AND RESULTS

### 7.1. Experiment Theory and Structure

#### 7.1.1. Experiment Structure

A total of thirty-three two-phase tests in the BFBT were conducted over a variety of characteristic pressures, flow qualities, and flowrates, for the same spacer grid used in the single-phase flow tests. The test used two-pressures, 7.16 MPa and 8.65 MPa, with 4 different flowrates, 5.1, 11.35, 13.85 and 17.65 kg/s for each pressure. At 7.16 MPa, each of the flowrates was measured at a flow quality of 7%, 10%, 14%, 19%, and 24%. At 8.65 MPa, each of the flowrates was measured at a flow quality of 7%, 14%, and 24%. The pressures, temperatures and flowrates of the experimental input conditions were close to the planned values, with minor, insignificant variations as shown in Table 6.

The flow was characterized and the general losses were calculated for each of the thirty-three tests' conditions. The measured properties of the water-vapor mixture were used to calculate the flow characteristics of the Reynolds Number, void fraction and flow regime. The general losses of acceleration, ( $\Delta P_{\text{Accel}}$ ), gravity, ( $\Delta P_{\text{Grav}}$ ), and friction, ( $\Delta P_{\text{Frict}}$ ) were calculated for each experimental test case and subtracted from the measured pressure loss to determine the measured spacer pressure loss. Measured pressure loss values are provided by the BFBT database. Flow characteristics, general and measured losses are shown in Table 6 below:

**Table 6: Two-Phase Flow Characteristics**

Test # <sup>1</sup>	Pressure (Mpa) <sup>1</sup>	Mass Flow (Kg/s) <sup>1</sup>	Flow Quality (Exit) <sup>1</sup>	Void Ratio (spacer)	Re <sub>2P</sub>	$\Delta P_{\text{Accel}}$ (Pa)	$\Delta P_{\text{Grav}}$ (Pa)	$\Delta P_{\text{Frict}}$ (Pa)	Measured Loss (Pa) <sup>1</sup>
P60001	7.16	5.09	0.07	0.49	8.04E+04	9.6	425.1	112.1	1150
P60002	7.16	5.07	0.10	0.58	8.21E+04	13.5	357.8	138.1	1280
P60003	7.16	5.07	0.15	0.67	8.55E+04	20.0	291.1	176.0	1540
P60004	7.16	5.09	0.20	0.73	8.98E+04	27.9	245.2	214.7	1850
P60005	7.16	5.04	0.25	0.77	9.31E+04	35.7	213.1	246.0	2100
P60006	7.16	5.07	0.25	0.77	9.36E+04	36.0	213.0	248.1	2110
P60007	7.17	13.86	0.07	0.52	2.20E+05	79.2	403.7	615.7	5590
P60008	7.17	13.86	0.10	0.60	2.25E+05	111.8	337.9	749.6	7060
P60009	7.17	13.86	0.15	0.69	2.34E+05	165.4	269.9	946.0	9240
P60010	7.17	13.83	0.20	0.76	2.45E+05	223.9	223.3	1137.4	11560
P60011	7.17	13.83	0.25	0.80	2.56E+05	288.0	190.6	1323.7	13560
P60012	7.17	13.86	0.25	0.80	2.56E+05	289.2	190.5	1327.8	13750
P60013	7.16	17.61	0.07	0.53	2.80E+05	135.7	391.5	944.6	8920
P60014	7.16	17.66	0.10	0.61	2.87E+05	183.7	334.1	1122.7	11050
P60015	7.17	17.64	0.15	0.70	2.99E+05	274.3	262.5	1423.2	14930
P60016	7.18	17.66	0.20	0.76	3.12E+05	367.8	217.4	1704.6	18650
P60017	7.16	11.37	0.07	0.51	1.80E+05	51.2	411.9	434.4	3930
P60018	7.17	11.31	0.10	0.60	1.84E+05	72.5	343.5	530.2	4860
P60019	7.17	11.34	0.15	0.69	1.92E+05	109.6	273.3	679.1	6430
P60020	7.16	11.37	0.20	0.75	2.00E+05	146.8	230.2	812.0	7770
P60021	7.16	11.37	0.25	0.79	2.10E+05	192.0	196.0	951.8	9300
P60022	8.64	5.09	0.07	0.45	8.51E+04	8.4	444.0	99.3	1110
P60023	8.63	5.09	0.15	0.63	9.06E+04	17.1	317.9	150.0	1390
P60024	8.63	5.09	0.25	0.74	9.88E+04	30.1	236.2	208.6	1820
P60025	8.64	13.86	0.07	0.46	2.32E+05	65.9	434.7	534.4	4960
P60026	8.64	13.88	0.15	0.65	2.47E+05	136.8	301.8	797.7	7750
P60027	8.64	13.88	0.25	0.77	2.70E+05	241.3	216.0	1109.9	11180
P60028	8.63	13.88	0.25	0.77	2.70E+05	241.6	215.8	1111.1	11200
P60029	8.64	17.66	0.07	0.47	2.95E+05	109.0	431.0	807.5	7600
P60030	8.64	17.69	0.15	0.66	3.15E+05	231.2	293.7	1208.5	12390
P60031	8.64	11.37	0.07	0.46	1.90E+05	43.7	437.4	381.6	3490
P60032	8.63	11.39	0.15	0.65	2.03E+05	92.0	303.5	577.1	5420
P60033	8.63	11.37	0.25	0.76	2.21E+05	158.8	220.7	794.6	7610

<sup>1</sup> Neykov et al., 2006

## 7.1.2. Experiment Purpose and Theory

### 7.1.2.1. Purpose

As with the single-phase models, the purpose of the two-phase flow portion of the study is to compare predicted pressure losses from historical one-dimensional, two-phase spacer pressure loss models to the measured pressure losses, using input conditions from the BFBT bundle experiments and the BFBT test section dimensions. The objectives continue to be to identify if the historical equations are as accurate and precise in different conditions than the equations were developed, using more detailed measurements, and if any of the more precisely measured flow properties demonstrate any trends for further development. A predicted spacer pressure loss was generated for all thirty-three tests, for each of the two-phase spacer grid pressure loss models.

### 7.1.2.2. Two Phase Properties

As stated before in equation (28), to calculate the two-phase pressure change at the spacer, ( $\Delta P_{sp}^{2P}$ ), the two-phase spacer pressure multiplier, ( $\mathcal{O}_{liq,sp}$ ), is multiplied by the single-phase spacer pressure loss coefficient, ( $K_{sp}$ ), and the dynamic pressure factor, ( $G_m^2/2 \rho_{liq,sp}$ ). The previous two-phase general loss factors used specific Reynolds Numbers and dynamic viscosities based on the equations that were used for the general loss factor. The dynamic viscosity and the Reynolds Number used to calculate pressure loss coefficients, and characterize the flow in the results in this study, are based on a two-phase dynamic viscosity, which is calculated by equation (105): (Awad and Muzychka, 2008)

$$\mu_{m,sp} = x_{sp} \mu_{v,sp} + (1 - x_{sp}) \mu_{liq,sp} \quad (105)$$

where ( $\mu_{m,sp}$ ) is the two-phase dynamic viscosity at the spacer. The two-phase Reynolds Number of the fuel bundle at the spacer, ( $Re_{2P\ sp}$ ), using the two-phase viscosity, is calculated by equation (106):

$$Re_{2P\ sp} = \frac{G_m D_H}{\mu_{m,sp}} \quad (106)$$

The pressure, Reynolds Number, flow quality, void fraction and flow regime are the available two-phase flow characteristics. Since more flow characteristics are available than the single-phase portion of the study, analysis can be performed to determine the effects and the feasibility of the different characteristics.

#### 7.1.2.3. Single-Phase Pressure Loss Coefficients

The previously developed one-dimensional single-phase spacer grid pressure loss models, from Chapter 4 of this study, are used for the single-phase spacer pressure loss coefficient, shown in equation (87). The models and their coefficients for the two-phase portion of this study are:

- The Schikorr/Bubelis Single-Phase Pressure Loss Model,  $K_{\text{Schikorr}}$  (Schikorr et al., 2010)
- The In Single-Phase Pressure Loss Model,  $K_{\text{In}}$  (In et al, 2002)
- The Hyun/Oh Single-Phase Pressure Loss Model,  $K_{\text{Hyun/Oh}}$  (Chun and Oh, 1998)
- The Shiralkar Single Phase-Pressure Loss Model,  $K_{\text{Shiralkar}}$  (Glueck, 2008)
- The Rehme Trippe Single-Phase Pressure Loss Model,  $K_{\text{Rehme-Trippe}}$  (Rehme and Trippe, 1980)
- The Rehme Single-Phase Pressure Loss Model,  $K_{\text{Rehme}}$  (Rehme, 1973)
- The DeStourder Single-Phase Pressure Loss Model,  $K_{\text{DeStourder}}$  (DeStourder, 1961)
- The Spengos Single-Phase Pressure Loss Model,  $K_{\text{Spengos}}$  (Spengos, 1959)
- The Idel'chik Single-Phase Pressure Loss Model,  $K_{\text{Idel'chik}}$  (Idel'chik, 1986)
- The Tong/Weisman Single-Phase Pressure Loss Model,  $K_{\text{Tong/Weisman}}$  (Tong and Weisman, 1970)

#### 7.1.2.4. Possible Measurement Errors

The accuracy of the instrumentation measuring the flowrate and pressure continues to be +/- 1.0 %, the same as for single-phase flows. The flowrate continues to affect the flow velocity and mass flux, which is now a combination of vapor and liquid. The pressure continues to

affect the flow properties of density and viscosity, including both the steam and liquid properties. The additional measurement is the quality ratio, which is measured by the equipment in Figure 8, which has an accuracy of +/- 2%. The quality ratio affects the void fraction, which is an input into many of the two-phase pressure loss equations. A change in quality ratio, pressure, and flowrate will not affect all the properties and phases equally. The maximum change was identified with and the maximum increase in pressure and flow quality with a maximum decrease in flowrate.

Based on the factors for spacer grid pressure loss, the maximum variance of the measured loss can be +/- 16%, mainly from the pressure and density changes in the factors to calculate general losses. This variance was input into the models' equations with the other variances to obtain the total possible error in the calculation.

Analysis of a measurement error for two-phase flow is more complex than single-phase because of the added quality ratio factor, the multiple combinations of multipliers and coefficients, and different tables that group the flow characteristics. This study presents almost a thousand results for two-phase flow, each with a possible measurement error, compared to thirty results for single-phase flow. The effect of the error will depend on the specific application and the total errors' prediction is difficult since many equations are involved in a complete calculation. However, this section provides a summary of the effects of the error on the single-phase pressure loss correlations and two-phase multipliers, and a summary of the possible measurement error and the effects on results will be included with the results at the end of Section 7.2.3.

The highest possible measurement errors identified for each single-phase pressure loss correlation are based on the combination of measurement errors that provides the largest variance. The largest contribution to both the single-phase pressure loss correlations and two-phase multipliers is from a pressure variance, while the quality factor variance is less than

0.1%. The variances are shown as a percentage of the calculated value of correlation or multiplier.

- The Schikorr/Bubelis Single-Phase Pressure Loss Model,  $K_{\text{Schikorr}}$ , +/- 1.7%.
- The In Single Phase Pressure Loss Model,  $K_{\text{In}}$ , +/- 1.7%.
- The Hyun/Oh Single-Phase Pressure Loss Model,  $K_{\text{Hyun/Oh}}$ , +/- 1.8%.
- The Shiralkar Single-Phase Pressure Loss Model,  $K_{\text{Shiralkar}}$ , +/- 1.8%.
- The Rehme Trippe Single-Phase Pressure Loss Model,  $K_{\text{Rehme-Trippe}}$ , +/- 1.7%.
- The Rehme Single-Phase Pressure Loss Model,  $K_{\text{Rehme}}$ , +/- 1.8%.
- The DeStourder Single-Phase Pressure Loss Model,  $K_{\text{DeStourder}}$ , +/- 1.8%.
- The Spengos Single-Phase Pressure Loss Model,  $K_{\text{Spengos}}$ , +/- 1.8%.
- The Idel'chik Single-Phase Pressure Loss Model,  $K_{\text{Idel'chik}}$ , +/- 1.8%.
- The Tong/Weisman Single-Phase Pressure Loss Model,  $K_{\text{Tong/Weisman}}$ , +/- 1.8%.

The highest possible measurement errors identified for each two-phase pressure loss multiplier, based on the combination of measurement errors that provides the largest variance:

- The Lottes Two-Phase Pressure Loss Multiplier,  $\emptyset_{\text{liq,sp}}^{\text{Lottes}}$ , +/- 2%.
- The Expanded Lottes Two-Phase Pressure Loss Multiplier,  $\emptyset_{\text{liq,sp}}^{\text{Lottes exp}}$ , +/- 7.5%.
- The Romie Two-Phase Pressure Loss Multiplier,  $\emptyset_{\text{liq,sp}}^{\text{Romie}}$ , +/- 1.1%.
- The Expanded Romie Two-Phase Pressure Loss Multiplier,  $\emptyset_{\text{liq,sp}}^{\text{Romie exp}}$ , +/- 0.5%.
- The Richardson Two-Phase Pressure Loss Multiplier,  $\emptyset_{\text{liq,sp}}^{\text{Richardson}}$ , +/- 1.0%.
- The Mendler Two-Phase Pressure Loss Multiplier,  $\emptyset_{\text{liq,sp}}^{\text{Mendler}}$ , +/- 1.1%.
- The Mendler Corrected Two-Phase Pressure Loss Multiplier,  $\emptyset_{\text{liq,sp}}^{\text{Mendler corr}}$ , +/- 1.0%.
- The Beattie Two-Phase Pressure Loss Multiplier,  $\emptyset_{\text{liq,sp}}^{\text{Beattie}}$ , +/- 1.3%.
- The Chisholm Two-Phase Pressure Loss Multiplier,  $\emptyset_{\text{liq,sp}}^{\text{Chisholm}}$ , +/- 1.0%.

The possible measurement error has no effect on the plotted flow regimes. The maximum variance in the superficial liquid velocity is +/- .2 %, and the maximum variance in the

superficial vapor velocity is +/- 1.1%. This minor amount will not move a flow from one regime to another.

## 7.2. Results

7.2.1. Criteria: The criteria continues to be the accuracy, measured by the bias, or difference, in percentage, from the measured value, and precision, measured by the standard deviation of the biases, in percentage, as previously detailed in paragraph 5.2.1.

### 7.2.2. Flow Characteristics

#### 7.2.2.1. BFBT Flow Regimes

The flow regimes of the thirty-three different BFBT tests are mapped in Figures 25 and 26, to identify which flow regimes are used for the flow pattern across section dPT1 (Figure 7) in the BFBT Fuel Bundle. The flow pattern maps for this study are reprints from Williams and Peterson for 6.9 MPa and 8.3 MPa in Venkateswararao et al, (1982) for the respective 7.16 MPa and 8.65 MPa tests. The 6.9 and 8.3 MPa maps are the closest flow regime maps to the experimental pressure. All but three tests plotted as annular flows on the chart. This flow pattern was expected, since annular flow is the desired flow regime at the top of a BWR fuel bundle. The majority of the liquid phase is around the fuel rod and channel walls while the vapor flows at a faster velocity between the liquid layers (Lahey and Moody, 1993).



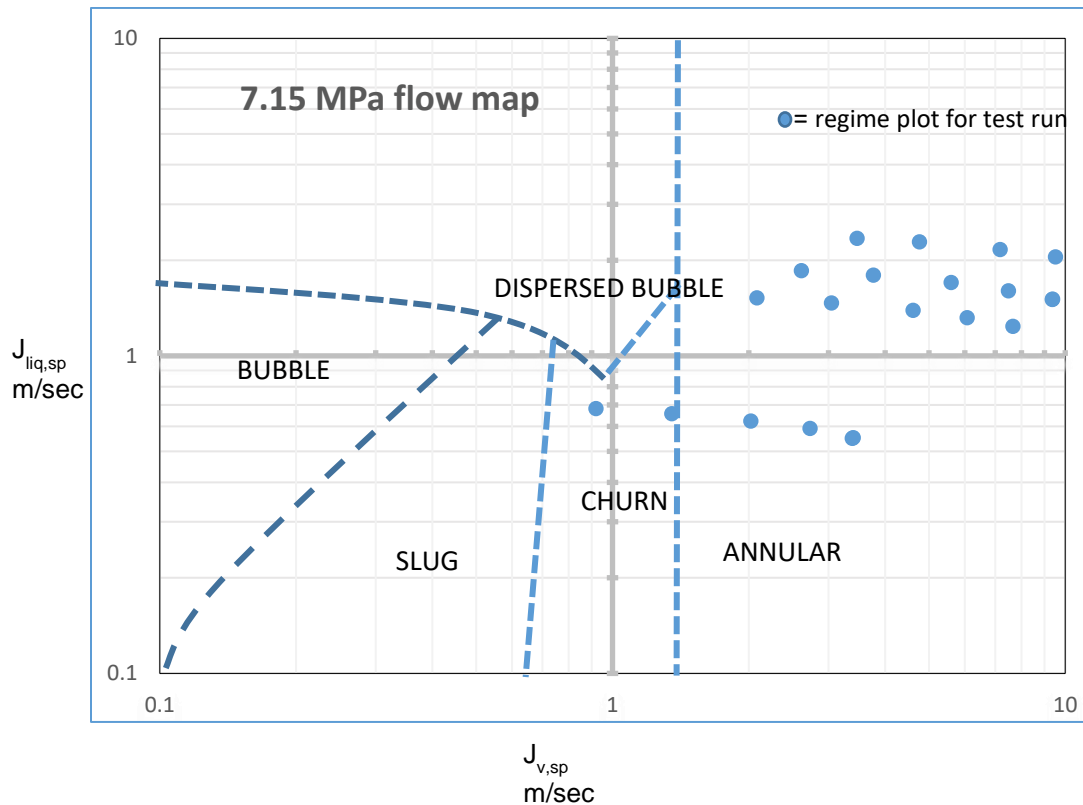


Figure 25: Flow Regimes for 7.16 MPa BFBT Tests

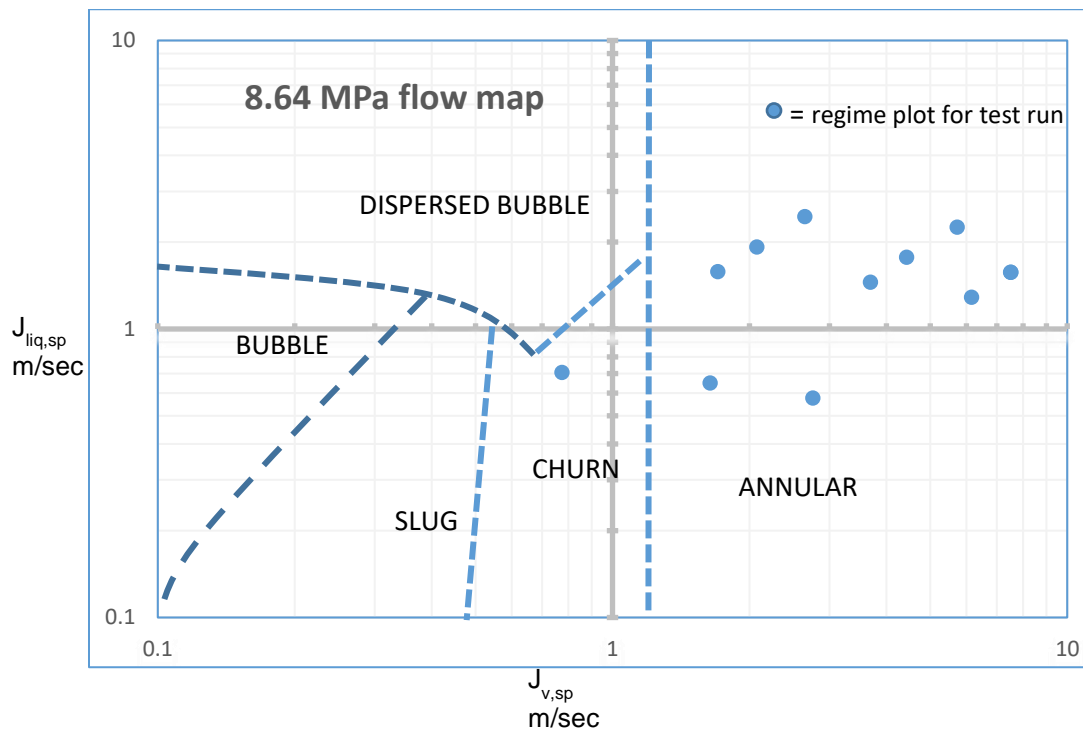


Figure 26: Flow Regimes for 8.65 MPa BFBT Tests

The three plots in the flow regime of churn flow will be treated as annular flow in calculations, for more distinct data groupings. Since the plots were close to the annular boundary, the regimes have imprecise transition areas across the boundaries, and there are not enough churn flow regime plots for a separate analysis, only the annular flow regime will be used, and this study will not analyze the effect of different flow regimes.

#### 7.2.2.2. Two-Phase Reynolds Number and Void Fraction

The Two-Phase Reynolds Numbers of flow, given for the section 301 pressure loss tests of the BFBT, range from  $8 \times 10^4$  to over  $3 \times 10^5$ . These Reynold Numbers place the flow well into the turbulent range where there is a high level of mixing. The void fractions range from 0.49 to over 0.80, reducing the volume of the higher viscosity liquid.

#### 7.2.3. Combined Properties Results

The measured spacer grid pressure losses were compared to the historical models' estimated spacer pressure losses, to determine the accuracy and the precision of the historical models. Since the calculated values consist of both the single-phase spacer pressure loss coefficient ( $K_{sp}$ ) from the liquid phase loss, and the two-phase spacer pressure loss multiplier ( $\phi_{liq,sp}$ ), each test was plotted against a combination of the ten single-phase pressure loss coefficients from Section 4.3, and the nine Two-Phase Multipliers, for a total of ninety results for each average bias and standard deviation. These ninety combinations of multiplier and single-phase pressure loss coefficient were calculated for all thirty-three tests.

The bias and standard deviation, from the measured pressure loss, for each of the two-phase multiplier-pressure loss coefficient combinations are shown respectively in Tables 7 and 8 below. The single-phase pressure loss coefficients are the table columns, the two-phase multiplier-pressure loss coefficient are the table rows, and at their intersection are the thirty-three tests' results combined. To establish a reference, the calculations are for the average bias and the average standard deviation for all thirty-three tests combined. Each result, displayed on the two tables, is the combined result of the thirty-three tests, for each of the ninety combinations of two-phase multiplier and single-phase pressure loss coefficient.

**Table 7: Combined Test Results Bias**

Bias Two-Phase Multiplier	Pressure Loss Coefficients										Average Multiplier Bias
	2P ΔP Schikorr(Pa)	2P ΔP (In) [Pa]	2P ΔP Hyun/Oh (Pa)	2P ΔP Shiralkar (Pa)	2P ΔP Rehme Trippe (Pa)	2P ΔP (Rehme) (Pa)	2P ΔP (DeStour) [Pa]	2P ΔP Spengos (lb-f to Pa)	2P ΔP Idel'chick (Pa)	2P ΔP Tong/Weisman (Pa)	
<b>Lottes</b>	97.01	200.90	348.18	1.95	123.05	91.14	248.92	243.55	272.97	1721.09	180.85
<b>Lottes Expanded</b>	99.16	204.18	353.08	3.07	125.48	97.14	252.74	247.31	277.05	1741.00	184.36
<b>Romie</b>	-43.02	-13.04	29.31	-70.62	-35.64	-44.87	0.60	-0.89	7.49	424.83	-18.96
<b>Romie Expanded</b>	-44.56	-15.40	25.79	-71.42	-37.39	-45.86	-2.14	-3.59	4.56	410.53	-21.11
<b>Richardson</b>	-63.28	-43.96	-16.65	-81.06	-58.53	-64.46	-35.16	-36.14	-30.70	238.35	-47.77
<b>Mendler</b>	-30.97	5.31	56.49	-64.46	-22.06	-33.30	21.74	19.99	30.03	534.90	-1.91
<b>Mendler Corrected</b>	-37.75	-5.04	41.12	-67.95	-29.73	-39.14	9.78	8.19	17.25	472.51	-11.47
<b>Beattie</b>	-34.69	-0.36	48.09	-66.36	-26.22	-36.89	15.22	13.58	23.05	500.83	-7.18
<b>Chisolm</b>	-48.80	-21.89	16.07	-73.64	-42.21	-50.53	-9.72	-11.02	-3.57	370.86	-27.26
<b>Average</b>	-33.67	-10.49	22.25	-55.06	-27.98	-35.01	0.04	-1.10	5.35	328.09	

**Table 8: Combined Test Results Standard Deviation**

Standard Dev	Pressure Loss Coefficients										Average Multiplier Standard Deviation
	Two-Phase Multiplier	2P ΔP Schikorr(Pa)	2P ΔP (In) [Pa]	2P ΔP Hyun/Oh (Pa)	2P ΔP Shiralkar (Pa)	2P ΔP Rehme Trippe (Pa)	2P ΔP (Rehme) (Pa)	2P ΔP (DeStour) [Pa]	2P ΔP Spengos (lb-f to Pa)	2P ΔP Idel'chick (Pa)	
<b>Lottes</b>	55.12	85.05	129.93	30.18	64.06	55.92	102.06	99.17	110.41	539.07	81.32
<b>Lottes Expanded</b>	56.20	86.72	132.46	30.76	65.31	58.95	104.05	101.11	112.54	549.50	83.12
<b>Romie</b>	5.61	8.30	12.35	2.93	5.98	5.40	9.64	9.23	10.73	52.39	7.80
<b>Romie Expanded</b>	5.64	8.34	12.35	2.92	6.01	6.05	9.62	9.25	10.67	52.10	7.87
<b>Richardson</b>	7.85	11.91	17.72	4.07	8.69	7.62	13.76	13.42	14.88	72.67	11.10
<b>Mendler</b>	4.39	5.60	6.29	1.44	3.70	2.64	4.71	5.18	5.26	25.70	4.36
<b>Mendler Corrected</b>	5.75	8.10	10.93	2.48	5.63	6.24	8.35	8.43	9.07	44.31	7.22
<b>Beattie</b>	8.35	12.28	17.60	4.01	9.20	7.44	13.79	13.91	14.68	71.69	11.25
<b>Chisolm</b>	6.69	9.81	13.91	3.15	6.99	5.92	10.70	10.64	11.52	56.24	8.81
<b>Average</b>	4.92	7.15	10.13	2.33	5.13	4.59	7.84	7.78	8.54	41.68	

Each bias and deviation shown in Tables 7 and 8 respectively, combines not only the bias and deviation results for all thirty-three pressure loss estimates for that multiplier-correlation combination, that result also combines all the pressure, void ratio, quality ratio, and Reynolds Number flow characteristics. The Tong/Weisman Single-Phase Coefficient, Lottes Multiplier and Lottes Expanded Multiplier were excluded from the averages, since their large inaccuracies and low precision will preclude their use as feasible models. While some advantage between the combinations of the coefficients and multipliers is displayed, further analyses determine the effects of the flow characteristics.

An additional reference consideration is the possible error from the measuring equipment. The error of measurement's effect on the bias of the two-phase multipliers – single-phase coefficient is given as a range of all the single-phase correlations for each multiplier, based on the largest bias. This is shown as a percentage of the bias's percentage, so a 10% variance in a bias of 11% means the bias can be between 10.9% and 12.1%. The biases do not increase or decrease together. This lack of proportional increase or decrease indicates the measurement error might have minor effects on some results. This would have to be calculated into the specific situation.

- The Lottes Two-Phase Pressure Loss Multiplier,  $\emptyset_{liq,sp}^{Lottes}$ , +/- 25%.
- The Expanded Lottes Two-Phase Pressure Loss Multiplier,  $\emptyset_{liq,sp}^{Lottes\ exp}$ , +/- 30%.
- The Romie Two-Phase Pressure Loss Multiplier,  $\emptyset_{liq,sp}^{Romie}$ , +/- 15%.
- The Expanded Romie Two-Phase Pressure Loss Multiplier,  $\emptyset_{liq,sp}^{Romie\ exp}$ , +/- 20%.
- The Richardson Two-Phase Pressure Loss Multiplier,  $\emptyset_{liq,sp}^{Richardson}$ , +/- 22%.
- The Mendler Two-Phase Pressure Loss Multiplier,  $\emptyset_{liq,sp}^{Mendler}$ , +/- 15%.
- The Mendler Corrected Two-Phase Pressure Loss Multiplier,  $\emptyset_{liq,sp}^{Mendler\ corr}$ , +/- 18%.
- The Beattie Two-Phase Pressure Loss Multiplier,  $\emptyset_{liq,sp}^{Beattie}$ , +/- 17%.
- The Chisholm Two-Phase Pressure Loss Multiplier,  $\emptyset_{liq,sp}^{Chisholm}$ , +/- 15%.

The error of measurement's effect on the standard deviation of the two-phase multipliers-single-phase coefficient is given as a range of all the single-phase coefficients for each multiplier, based on the largest standard deviation. This is shown as a percentage of the standard deviation's percentage, so a 10% variance in a standard deviation of 11% means the bias can be between 10.9% and 12.1%. Any variance will affect all results proportionally. Unlike the biases, the standard deviations increase or decrease together with the variance. This proportional increase or decrease indicates the measurement error will not affect the results.

- The Lottes Two-Phase Pressure Loss Multiplier,  $\emptyset_{liq,sp}^{Lottes}$ , +/- 12%.
- The Expanded Lottes Two-Phase Pressure Loss Multiplier,  $\emptyset_{liq,sp}^{Lottes\ exp}$ , +/- 5%.
- The Romie Two-Phase Pressure Loss Multiplier,  $\emptyset_{liq,sp}^{Romie}$ , +/- 2%.
- The Expanded Romie Two-Phase Pressure Loss Multiplier,  $\emptyset_{liq,sp}^{Romie\ exp}$ , +/- 13%.
- The Richardson Two-Phase Pressure Loss Multiplier,  $\emptyset_{liq,sp}^{Richardson}$ , +/- 14%.
- The Mendler Two-Phase Pressure Loss Multiplier,  $\emptyset_{liq,sp}^{Mendler}$ , +/- 18%.
- The Mendler Corrected Two-Phase Pressure Loss Multiplier,  $\emptyset_{liq,sp}^{Mendler\ corr}$ , +/- 16%.
- The Beattie Two-Phase Pressure Loss Multiplier,  $\emptyset_{liq,sp}^{Beattie}$ , +/- 7%.
- The Chisholm Two-Phase Pressure Loss Multiplier,  $\emptyset_{liq,sp}^{Chisholm}$ , +/- 15%.

#### 7.2.4. Graphical Analysis of the Flow Characteristics

Analysis was accomplished through scatter plots of the thirty-three tests' biases, using a different graph for each calculated pressure loss coefficient-two-phase spacer multiplier combination, and for the flow characteristics in Table 6. Given the large number of combinations to plot, three-hundred-sixty, the plots from the Romie two-phase spacer pressure loss multiplier combined with the Schikorr single-phase pressure loss coefficient were found to summarize the effects of the various characteristics more distinctly than the other models.

The plot of the bias against the two-phase Reynolds Number of the fuel bundle at the spacer grid, shown in Figure 27, resulted in a number of groupings in approximate lines at equal biases from the test result. The lines tend to group by pressure and flow quality, which were measured at the outlet of section 301. All the graphs use the bias in percentage, as the same point of baseline measurement.

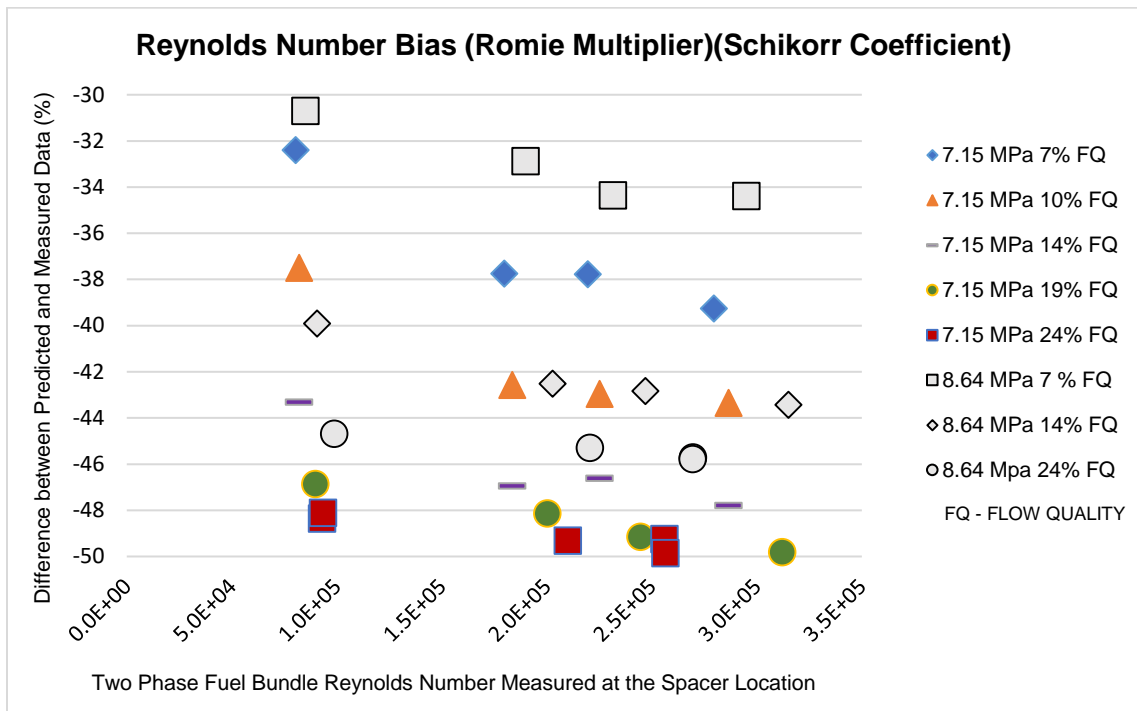


**Figure 27: Effect of the Reynolds Number on the Accuracy of the 2 Phase Multiplier**



Further trending was identified by plotting the bias of the pressure loss against the flow quality in Figure 28 below. Groupings, by each quality and pressure test factor, are identified. Close groups of biases formed at each quality factor of the tests, which further grouped around pressures. By identifying the pressure and Reynolds Number groups, the bias value increases as the pressure decreases and the quality fraction decreases. However, the larger distance between the Reynolds Number plots indicates the Reynolds Number has only a minor effect on the accuracy of the measured values.

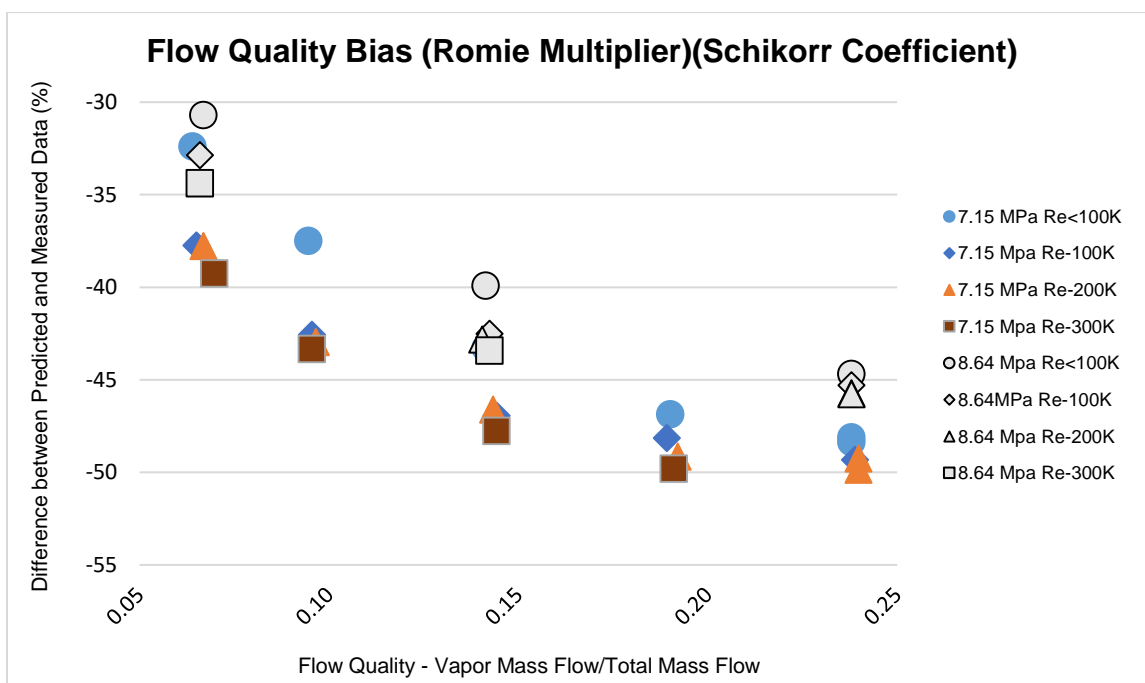


**Figure 28: Effect of the Flow Quality on the Accuracy of the 2 Phase Multiplier**

Plotting the pressure with the flow quality, against the bias, further verifies the indications that pressure and flow quality are significant flow characteristics which affect accuracy. The plots group further from the measured pressure loss as the pressure decreases and the quality factor increases as shown in Figure 29 below:

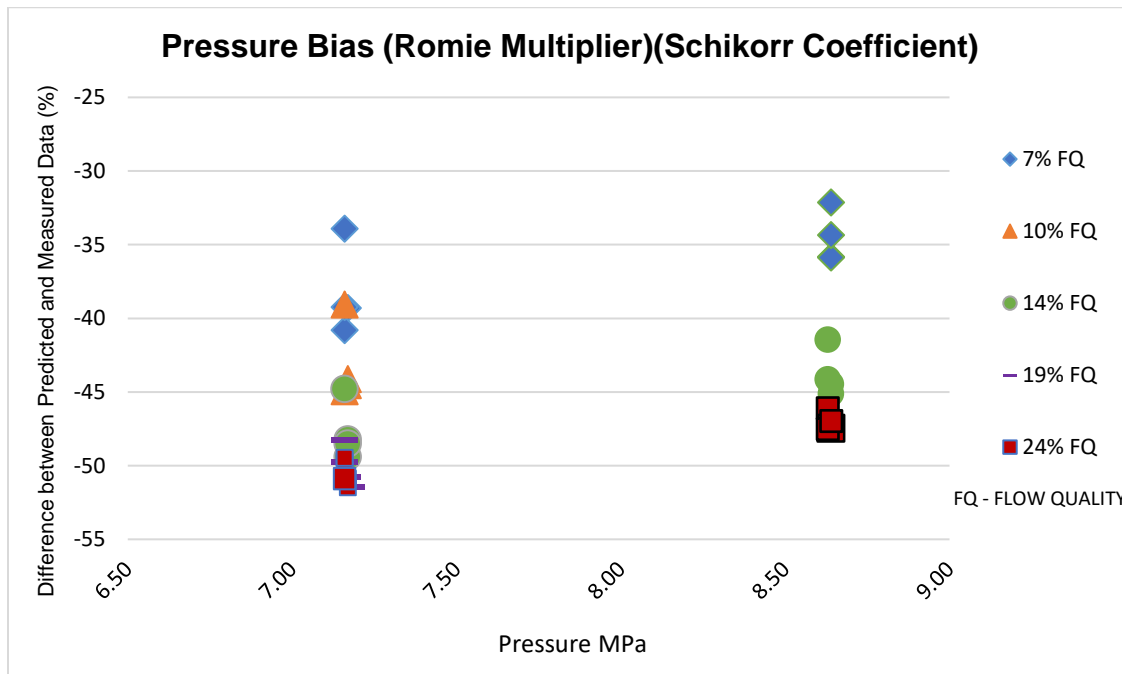


**Figure 29: Effect of the Pressure on the Accuracy of the 2 Phase Multiplier**

The void fraction is directly related to the quality factor and indirectly related to the mass flowrate and pressure. Plotting the calculated void fraction data in Figure 30 against the measured test data, demonstrates an approximate line between the bias and a single flow characteristic, the void fraction. However, establishing a correlation is beyond the scope of this study.

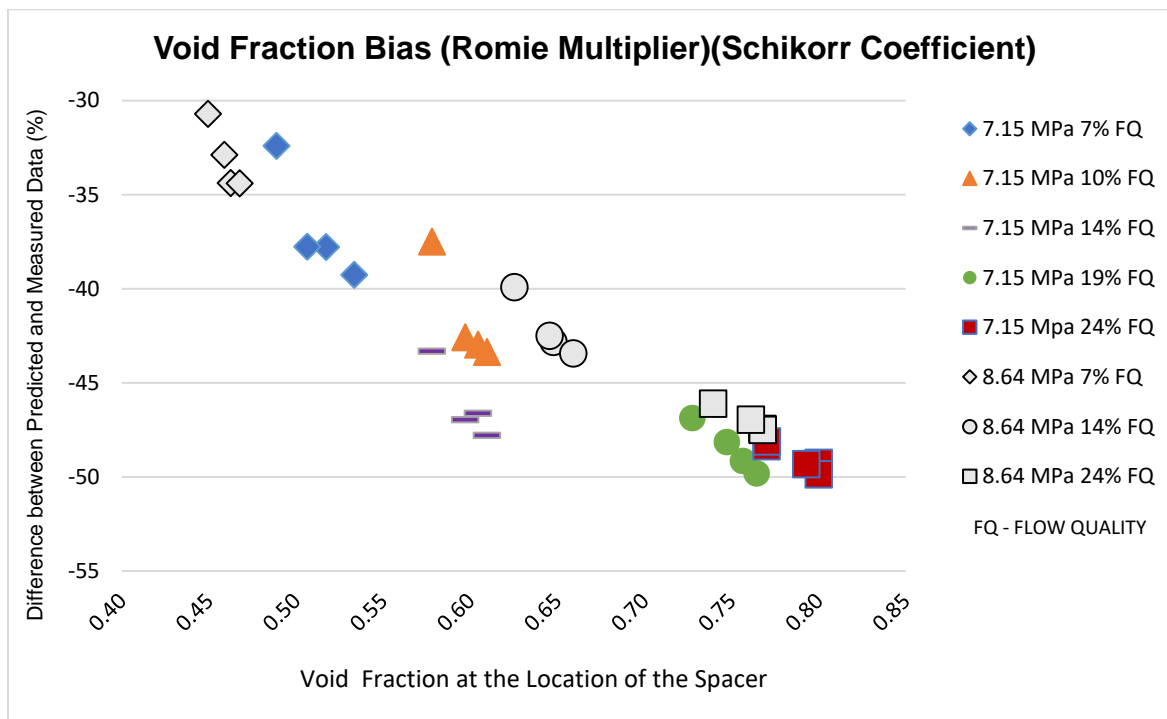


**Figure 30: Effect of the Void Fraction on the Accuracy of the 2 Phase Multiplier**

## 7.2.5. Quality and Pressure Characteristics Effects

### 7.2.5.1. Tabular Summary

Analyses of the results indicate the flow characteristics of quality and pressure significantly affect calculating the accuracy of pressure loss across a spacer. Tables 9 through 18 group the test results into the five different flow quality tests at 7.16 MPa, regardless of mass flowrates and the associated Reynolds Numbers. Tables 19 through 24 group the three flow quality tests at 8.65 MPa. Each bias and deviation shown in Tables 9 through 24, at the intersection of a single-phase pressure loss coefficient table column and the two-phase multiplier-pressure loss table row, combine the biases and deviations for the pressure loss estimates, at the flow quality and pressure shown in the title from that multiplier- coefficient combination

**Table 9: Accuracy of the 2 Phase Multiplier Based on 7% Quality and 7.16 MPa**

Bias 2PØ 7.16 Mpa 7% quality	Pressure Loss Coefficients									
	2P ΔP Schikorr(Pa)	2P ΔP P (In) [Pa]	2P ΔP Hyun/Oh (Pa)	2P ΔP Shiralkar (Pa)	2P ΔP Rehme Trippe (Pa)	2P ΔP (Rehme) (Pa)	2P ΔP (DeStourd) [Pa]	2P ΔP Spengos (Pa)	2P ΔP Idel'chick (Pa)	2P ΔP Tong/Weisman (Pa)
<b>Lottes</b>	35.58	106.65	206.48	-30.48	51.93	30.92	137.84	134.07	154.32	1141.77
<b>Lottes Expanded</b>	36.56	108.14	208.69	-29.98	53.03	31.87	139.56	135.76	156.16	1150.77
<b>Romie</b>	-36.79	-3.70	42.68	-67.66	-29.24	-39.07	10.69	8.99	18.32	477.72
<b>Romie Expanded</b>	-38.30	-6.00	39.26	-68.43	-30.93	-40.53	8.05	6.39	15.49	463.89
<b>Richardson</b>	-53.58	-29.27	4.79	-76.24	-48.03	-55.25	-18.70	-19.95	-13.10	324.32
<b>Mendler</b>	-27.55	10.35	63.45	-62.96	-18.92	-30.21	26.80	24.88	35.51	561.68
<b>Mendler Corrected</b>	-31.48	4.37	54.58	-64.97	-23.31	-34.00	19.92	18.11	28.16	525.78
<b>Beattie</b>	-43.71	-14.25	27.05	-71.20	-36.98	-45.75	-1.43	-2.94	5.36	414.42
<b>Chisolm</b>	-40.45	-9.31	34.32	-69.56	-33.37	-42.65	4.20	2.62	11.35	443.70

**Table 10: Precision of the 2 Phase Multiplier Based on 7% Quality and 7.16 MPa**

Standard Dev 2PØ 7.16 Mpa 7% quality	Pressure Loss Coefficients									
	2P ΔP Schikorr(Pa)	2P ΔP (In) [Pa]	2P ΔP Hyun/Oh (Pa)	2P ΔP Shiralkar (Pa)	2P ΔP Rehme Trippe (Pa)	2P ΔP (Rehme) (Pa)	2P ΔP (DeStourd) [Pa]	2P ΔP Spengos (Pa)	2P ΔP Idel'chick (Pa)	2P ΔP Tong/Weisman (Pa)
<b>Lottes</b>	2.56	4.16	13.87	4.51	5.85	7.31	12.79	9.83	16.50	80.57
<b>Lottes Expanded</b>	2.58	4.27	14.11	4.57	5.95	7.42	12.99	9.99	16.73	81.71
<b>Romie</b>	3.02	2.96	0.95	0.73	1.94	0.87	1.43	2.14	2.67	13.05
<b>Romie Expanded</b>	3.02	3.01	0.92	0.68	1.95	0.79	1.30	2.15	2.47	12.06
<b>Richardson</b>	2.20	2.15	0.62	0.54	1.36	0.63	0.97	1.46	1.96	9.57
<b>Mendler</b>	4.49	4.94	2.46	0.39	3.18	0.60	1.58	3.77	1.43	7.00
<b>Mendler Corrected</b>	4.35	4.83	2.52	0.32	3.08	0.57	1.53	3.67	1.16	5.67
<b>Beattie</b>	2.82	2.86	1.68	0.72	2.13	0.97	1.90	2.60	2.64	12.88
<b>Chisolm</b>	4.00	4.53	2.59	0.15	2.84	0.54	1.44	3.43	0.54	2.65

**Table 11: Accuracy of the 2 Phase Multiplier Based on 10% Quality and 7.16 MPa**

Bias 2PØ 7.16 Mpa 10% quality	Pressure Loss Coefficients									
	2P ΔP Schikorr(Pa)	2P ΔP (In) [Pa]	2P ΔP Hyun/Oh (Pa)	2P ΔP Shiralkar (Pa)	2P ΔP Rehme Trippe (Pa)	2P ΔP (Rehme) (Pa)	2P ΔP (DeStourd) [Pa]	2P ΔP Spengos (Pa)	2P ΔP Idel'chick (Pa)	2P ΔP Tong/Weisman (Pa)
<b>Lottes</b>	54.45	135.55	249.81	-20.58	73.56	49.56	171.71	167.39	190.54	1318.64
<b>Lottes Expanded</b>	55.78	137.58	252.83	-19.89	75.05	50.85	174.05	169.69	193.05	1330.88
<b>Romie</b>	-41.59	-10.96	32.10	-70.03	-34.42	-43.54	2.58	1.01	9.65	435.38
<b>Romie Expanded</b>	-43.16	-13.35	28.56	-70.83	-36.18	-45.05	-0.17	-1.70	6.71	421.01
<b>Richardson</b>	-59.09	-37.63	-7.45	-79.00	-54.06	-60.44	-28.13	-29.24	-23.17	275.11
<b>Mendler</b>	-30.27	6.26	57.57	-64.26	-21.75	-32.67	22.35	20.51	30.74	538.38
<b>Mendler Corrected</b>	-35.42	-1.59	45.93	-66.90	-27.53	-37.64	13.30	11.60	21.08	491.20
<b>Beattie</b>	-37.96	-5.45	40.21	-68.20	-30.38	-40.08	8.87	7.22	16.34	468.06
<b>Chisolm</b>	-47.13	-19.43	19.46	-72.91	-40.67	-48.95	-7.25	-8.64	-0.89	383.94

**Table 12: Precision of the 2 Phase Multiplier Based on 10% Quality and 7.16 MPa**

Standard Dev 2PØ 7.16 Mpa 10% quality	Pressure Loss Coefficients									
	2P ΔP Schikorr(Pa)	2P ΔP (In) [Pa]	2P ΔP Hyun/Oh (Pa)	2P ΔP Shiralkar (Pa)	2P ΔP Rehme Trippe (Pa)	2P ΔP (Rehme) (Pa)	2P ΔP (DeStourd) [Pa]	2P ΔP Spengos (Pa)	2P ΔP Idel'chick (Pa)	2P ΔP Tong/Weisman (Pa)
<b>Lottes</b>	1.97	3.73	15.29	5.07	5.93	8.17	14.13	10.32	18.56	90.65
<b>Lottes Expanded</b>	1.97	3.86	15.59	5.16	6.05	8.31	14.38	10.52	18.86	92.10
<b>Romie</b>	2.75	2.70	1.18	0.74	1.94	0.89	1.68	2.25	2.69	13.15
<b>Romie Expanded</b>	2.76	2.75	1.13	0.68	1.94	0.81	1.56	2.26	2.48	12.11
<b>Richardson</b>	1.70	1.56	1.12	0.63	1.24	0.83	1.48	1.51	2.31	11.30
<b>Mendler</b>	4.91	5.65	3.54	0.23	3.68	0.81	2.23	4.55	0.85	4.15
<b>Mendler Corrected</b>	4.57	5.27	3.34	0.22	3.44	0.77	2.11	4.27	0.80	3.92
<b>Beattie</b>	4.23	4.82	2.86	0.21	3.13	0.63	1.79	3.83	0.78	3.80
<b>Chisolm</b>	3.96	4.64	3.21	0.24	3.06	0.82	2.08	3.86	0.88	4.27



**Table 13: Accuracy of the 2 Phase Multiplier Based on 14% Quality and 7.16 MPa**

Bias 2PØ 7.16 Mpa 14% quality	Pressure Loss Coefficients									
	2P ΔP Schikorr(Pa)	2P ΔP (In) [Pa]	2P ΔP Hyun/Oh (Pa)	2P ΔP Shiralkar (Pa)	2P ΔP Rehme Trippe (Pa)	2P ΔP (Rehme) (Pa)	2P ΔP (DeStourd) [Pa]	2P ΔP Spengos (Pa)	2P ΔP Idel'chick (Pa)	2P ΔP Tong/Weisman (Pa)
<b>Lottes</b>	89.25	189.05	330.62	-2.02	113.88	83.75	235.07	229.59	258.42	1650.07
<b>Lottes Expanded</b>	91.22	192.06	335.12	-1.00	116.12	85.67	238.58	233.04	262.18	1668.39
<b>Romie</b>	-46.15	-17.82	22.25	-72.21	-39.22	-47.86	-4.91	-6.38	1.66	396.36
<b>Romie Expanded</b>	-47.72	-20.21	18.68	-73.02	-41.00	-49.39	-7.68	-9.11	-1.32	381.84
<b>Richardson</b>	-65.31	-47.06	-21.22	-82.09	-60.84	-66.40	-38.72	-39.68	-34.48	219.90
<b>Mendler</b>	-32.85	2.44	52.28	-65.40	-24.26	-35.08	18.43	16.64	26.56	517.96
<b>Mendler Corrected</b>	-39.71	-8.03	36.72	-68.94	-32.00	-41.71	6.33	4.72	13.63	454.80
<b>Beattie</b>	-32.75	2.61	52.53	-65.35	-24.14	-34.97	18.63	16.83	26.78	519.00
<b>Chisolm</b>	-52.95	-28.22	6.71	-75.76	-46.93	-54.51	-17.01	-18.27	-11.32	333.02

**Table 14: Precision of the 2 Phase Multiplier Based on 14% Quality and 7.16 MPa**

Standard Dev 2PØ 7.16 Mpa 14% quality	Pressure Loss Coefficients									
	2P ΔP Schikorr(Pa)	2P ΔP (In) [Pa]	2P ΔP Hyun/Oh (Pa)	2P ΔP Shiralkar (Pa)	2P ΔP Rehme Trippe (Pa)	2P ΔP (Rehme) (Pa)	2P ΔP (DeStourd) [Pa]	2P ΔP Spengos (Pa)	2P ΔP Idel'chick (Pa)	2P ΔP Tong/Weisman (Pa)
<b>Lottes</b>	5.87	13.19	32.31	9.31	12.93	15.91	27.72	22.14	34.04	166.22
<b>Lottes Expanded</b>	6.07	13.53	32.95	9.47	13.21	16.21	28.24	22.61	34.65	169.17
<b>Romie</b>	1.97	1.71	1.66	0.92	1.27	1.35	2.03	1.53	3.36	16.43
<b>Romie Expanded</b>	2.02	1.82	1.41	0.84	1.29	1.21	1.81	1.50	3.07	14.98
<b>Richardson</b>	0.91	0.64	1.89	0.79	0.82	1.22	1.96	1.29	2.88	14.08
<b>Mendler</b>	4.57	5.30	3.22	0.24	3.31	0.85	1.82	4.02	0.89	4.34
<b>Mendler Corrected</b>	4.15	4.83	3.00	0.22	3.02	0.80	1.72	3.70	0.82	3.99
<b>Beattie</b>	4.43	5.08	2.88	0.24	3.14	0.76	1.55	3.76	0.89	4.33
<b>Chisolm</b>	3.22	3.74	2.29	0.17	2.34	0.61	1.31	2.85	0.63	3.08

**Table 15: Accuracy of the 2 Phase Multiplier Based on 19% Quality and 7.16 MPa**

Bias 2PØ 7.16 Mpa 19% quality	Pressure Loss Coefficients									
	2P ΔP Schikorr(Pa)	2P ΔP (In) [Pa]	2P ΔP Hyun/Oh (Pa)	2P ΔP Shiralkar (Pa)	2P ΔP Rehme Trippe (Pa)	2P ΔP (Rehme) (Pa)	2P ΔP (DeStourd) [Pa]	2P ΔP Spengos (Pa)	2P ΔP Idel'chick (Pa)	2P ΔP Tong/Weisman (Pa)
<b>Lottes</b>	130.07	251.90	425.97	19.93	161.58	125.43	310.03	303.16	338.73	2042.19
<b>Lottes Expanded</b>	132.85	256.15	432.33	21.38	164.74	128.16	314.99	308.03	344.04	2068.12
<b>Romie</b>	-48.49	-21.29	17.42	-73.26	-41.54	-49.73	-8.51	-9.94	-2.18	377.62
<b>Romie Expanded</b>	-50.04	-23.66	13.88	-74.07	-43.30	-51.25	-11.27	-12.66	-5.13	363.20
<b>Richardson</b>	-69.67	-53.64	-30.80	-84.24	-65.56	-70.37	-46.08	-46.94	-42.34	181.55
<b>Mendler</b>	-34.17	0.55	49.88	-65.89	-25.34	-35.87	16.76	14.98	24.78	509.28
<b>Mendler Corrected</b>	-42.49	-12.16	30.93	-70.20	-34.78	-43.98	1.99	0.44	9.01	432.24
<b>Beattie</b>	-29.61	7.51	60.25	-63.53	-20.17	-31.42	24.84	22.94	33.43	551.48
<b>Chisolm</b>	-54.97	-31.21	2.53	-76.66	-48.93	-56.13	-20.13	-21.34	-14.63	316.81

**Table 16: Precision of the 2 Phase Multiplier Based on 19% Quality and 7.16 MPa**

Standard Dev 2PØ 7.16 Mpa 19% quality	Pressure Loss Coefficients									
	2P ΔP Schikorr(Pa)	2P ΔP (In) [Pa]	2P ΔP Hyun/Oh (Pa)	2P ΔP Shiralkar (Pa)	2P ΔP Rehme Trippe (Pa)	2P ΔP (Rehme) (Pa)	2P ΔP (DeStourd) [Pa]	2P ΔP Spengos (Pa)	2P ΔP Idel'chick (Pa)	2P ΔP Tong/Weisman (Pa)
<b>Lottes</b>	13.68	25.90	53.91	14.62	22.70	26.84	45.00	37.87	53.49	261.17
<b>Lottes Expanded</b>	14.05	26.54	55.04	14.90	23.22	27.36	45.92	38.70	54.52	266.22
<b>Romie</b>	1.28	0.94	2.65	1.14	0.47	1.92	2.61	1.03	4.16	20.30
<b>Romie Expanded</b>	1.38	1.08	2.28	1.04	0.45	1.74	2.29	0.79	3.79	18.50
<b>Richardson</b>	0.22	0.67	2.94	0.98	0.85	1.73	2.64	1.68	3.60	17.58
<b>Mendler</b>	4.20	4.92	2.99	0.42	2.77	0.43	1.34	3.25	1.53	7.49
<b>Mendler Corrected</b>	3.69	4.32	2.66	0.37	2.44	0.39	1.21	2.86	1.36	6.66
<b>Beattie</b>	4.45	5.20	3.08	0.44	2.93	0.45	1.34	3.41	1.60	7.81
<b>Chisolm</b>	2.87	3.35	2.03	0.29	1.89	0.29	0.90	2.21	1.04	5.09

**Table 17: Accuracy of the 2 Phase Multiplier Based on 24% Quality and 7.16 MPa**

Bias 2PØ 7.16 Mpa 24% quality	Pressure Loss Coefficients									
	2P ΔP Schikorr(Pa)	2P ΔP (In) [Pa]	2P ΔP Hyun/Oh (Pa)	2P ΔP Shiralkar (Pa)	2P ΔP Rehme Trippe (Pa)	2P ΔP (Rehme) (Pa)	2P ΔP (DeStourd) [Pa]	2P ΔP Spengos (Pa)	2P ΔP Idel'chick (Pa)	2P ΔP Tong/Weisman (Pa)
<b>Lottes</b>	172.32	315.01	515.11	39.47	207.66	160.86	378.66	373.06	410.21	2391.18
<b>Lottes Expanded</b>	175.92	320.51	523.27	41.32	211.74	164.32	385.02	379.33	416.99	2424.29
<b>Romie</b>	-48.98	-22.35	14.82	-74.01	-42.45	-51.37	-10.68	-11.58	-4.91	364.28
<b>Romie Expanded</b>	-50.47	-24.62	11.46	-74.77	-44.13	-52.79	-13.30	-14.16	-7.70	350.66
<b>Richardson</b>	-73.09	-59.03	-39.37	-86.27	-69.63	-74.31	-52.83	-53.33	-49.77	145.25
<b>Mendler</b>	-32.86	2.15	50.91	-65.86	-24.30	-36.11	17.38	16.27	24.90	509.83
<b>Mendler Corrected</b>	-42.80	-12.98	28.56	-70.92	-35.51	-45.58	-0.01	-0.95	6.39	419.49
<b>Beattie</b>	-25.09	13.96	68.37	-61.91	-15.55	-28.72	30.95	29.72	39.34	580.37
<b>Chisolm</b>	-53.73	-29.61	4.00	-76.47	-47.83	-55.97	-19.11	-19.87	-13.93	320.26

**Table 18: Precision of the 2 Phase Multiplier Based on 24% Quality and 7.16 MPa**

Standard Dev 2PØ 7.16 Mpa 24% quality	Pressure Loss Coefficients									
	2P ΔP Schikorr(Pa)	2P ΔP (In) [Pa]	2P ΔP Hyun/Oh (Pa)	2P ΔP Shiralkar (Pa)	2P ΔP Rehme Trippe (Pa)	2P ΔP (Rehme) (Pa)	2P ΔP (DeStourd) [Pa]	2P ΔP Spengos (Pa)	2P ΔP Idel'chick (Pa)	2P ΔP Tong/Weisman (Pa)
<b>Lottes</b>	23.83	42.41	80.19	20.89	32.60	38.02	64.51	54.43	76.40	373.05
<b>Lottes Expanded</b>	24.43	43.41	81.89	21.31	33.36	38.80	65.86	55.64	77.94	380.56
<b>Romie</b>	0.72	0.39	3.62	1.34	0.56	2.31	3.21	1.44	4.91	23.99
<b>Romie Expanded</b>	0.86	0.36	3.16	1.22	0.47	2.09	2.84	1.15	4.47	21.83
<b>Richardson</b>	0.41	1.24	3.58	1.08	1.03	1.92	2.99	2.01	3.97	19.38
<b>Mendler</b>	3.48	3.73	1.25	0.51	2.57	0.69	0.60	2.80	1.86	9.09
<b>Mendler Corrected</b>	2.99	3.22	1.12	0.42	2.22	0.57	0.53	2.43	1.54	7.54
<b>Beattie</b>	3.84	4.09	1.31	0.59	2.82	0.81	0.64	3.05	2.16	10.53
<b>Chisolm</b>	2.39	2.55	0.84	0.36	1.76	0.49	0.40	1.91	1.30	6.36

**Table 19: Accuracy of the 2 Phase Multiplier Based on 7% Quality and 8.65MPa**

Bias 2PØ 8.65 Mpa 7% quality	Pressure Loss Coefficients									
	2P ΔP Schikorr(Pa)	2P ΔP (In) [Pa]	2P ΔP Hyun/Oh (Pa)	2P ΔP Shiralkar (Pa)	2P ΔP Rehme Trippe (Pa)	2P ΔP (Rehme) (Pa)	2P ΔP (DeStourd) [Pa]	2P ΔP Spengos (Pa)	2P ΔP Idel'chick (Pa)	2P ΔP Tong/Weisman (Pa)
<b>Lottes</b>	30.23	98.78	195.71	-32.78	46.89	25.81	129.96	126.31	145.90	1100.63
<b>Lottes Expanded</b>	31.09	100.10	197.67	-32.34	47.86	26.65	131.48	127.80	147.52	1108.59
<b>Romie</b>	-33.08	2.12	51.86	-65.49	-24.55	-35.40	18.08	16.23	26.24	516.41
<b>Romie Expanded</b>	-34.53	-0.10	48.56	-66.24	-26.19	-36.80	15.51	13.71	23.50	503.01
<b>Richardson</b>	-50.65	-24.68	12.01	-74.54	-44.35	-52.35	-12.90	-14.27	-6.88	354.69
<b>Mendler</b>	-25.97	12.96	67.92	-61.85	-16.55	-28.57	30.56	28.54	39.56	581.44
<b>Mendler Corrected</b>	-29.59	7.43	59.70	-63.72	-20.64	-32.07	24.17	22.25	32.73	548.10
<b>Beattie</b>	-48.15	-20.89	17.59	-73.28	-41.56	-49.98	-8.57	-9.98	-2.27	377.19
<b>Chisolm</b>	-37.40	-4.48	42.00	-67.74	-29.44	-39.60	10.40	8.69	18.02	476.25

**Table 20: Precision of the 2 Phase Multiplier Based on 7% Quality and 8.65MPa**

Standard Dev 2PØ 8.65 Mpa 7% quality	Pressure Loss Coefficients									
	2P ΔP Schikorr(Pa)	2P ΔP (In) [Pa]	2P ΔP Hyun/Oh (Pa)	2P ΔP Shiralkar (Pa)	2P ΔP Rehme Trippe (Pa)	2P ΔP (Rehme) (Pa)	2P ΔP (DeStourd) [Pa]	2P ΔP Spengos (Pa)	2P ΔP Idel'chick (Pa)	2P ΔP Tong/Weisman (Pa)
<b>Lottes</b>	1.37	1.86	11.19	3.90	3.57	5.78	10.38	6.73	14.28	69.74
<b>Lottes Expanded</b>	1.35	1.92	11.34	3.95	3.63	5.86	10.51	6.83	14.44	70.50
<b>Romie</b>	1.74	1.14	3.29	1.44	1.03	1.90	3.37	1.70	5.28	25.80
<b>Romie Expanded</b>	1.76	1.19	3.10	1.39	1.01	1.80	3.21	1.60	5.07	24.76
<b>Richardson</b>	1.1	0.63	1.57	4.24	1.16	20.68	1.49	0.81	1.10	2.83
<b>Mendler</b>	2.99	2.79	1.50	1.07	1.55	1.09	1.93	1.44	3.92	19.12
<b>Mendler Corrected</b>	2.83	2.63	1.47	1.03	1.45	1.05	1.87	1.34	3.76	18.38
<b>Beattie</b>	2.26	2.19	0.78	0.67	1.26	0.62	1.12	1.23	2.45	11.94
<b>Chisolm</b>	2.50	2.32	1.33	0.92	1.27	0.95	1.68	1.18	3.37	16.47



**Table 21: Accuracy of the 2 Phase Multiplier Based on 14% Quality and 8.65MPa**

Bias 2PØ 8.65 Mpa 14% quality	Pressure Loss Coefficients									
	2P ΔP Schikorr(Pa)	2P ΔP (In) [Pa]	2P ΔP Hyun/Oh (Pa)	2P ΔP Shiralkar (Pa)	2P ΔP Rehme Trippe (Pa)	2P ΔP (Rehme) (Pa)	2P ΔP (DeStourd) [Pa]	2P ΔP Spengos (Pa)	2P ΔP Idel'chick (Pa)	2P ΔP Tong/Weisman (Pa)
<b>Lottes</b>	79.67	174.75	310.57	-6.40	104.37	75.15	220.12	214.92	242.41	1571.90
<b>Lottes Expanded</b>	81.45	177.49	314.66	-5.47	106.40	109.15	223.31	218.05	245.83	1588.57
<b>Romie</b>	-42.17	-11.61	31.93	-69.95	-34.29	-43.73	2.84	1.23	9.94	436.83
<b>Romie Expanded</b>	-43.79	-14.09	28.23	-70.79	-36.13	-41.12	-0.05	-1.61	6.86	421.75
<b>Richardson</b>	-62.20	-42.22	-13.73	-80.34	-57.03	-63.20	-32.75	-33.81	-28.09	251.10
<b>Mendler</b>	-31.32	4.93	56.53	-64.36	-22.00	-33.26	21.99	20.13	30.39	536.64
<b>Mendler Corrected</b>	-37.69	-4.80	42.01	-67.66	-29.24	-33.58	10.68	8.99	18.30	477.61
<b>Beattie</b>	-35.41	-1.32	47.21	-66.48	-26.65	-37.23	14.73	12.98	22.62	498.74
<b>Chisolm</b>	-50.27	-24.02	13.33	-74.19	-43.53	-51.67	-11.67	-13.02	-5.59	360.97

**Table 22: Precision of the 2 Phase Multiplier Based on 14% Quality and 8.65MPa**

Standard Dev 2PØ 8.65 Mpa 14% quality	Pressure Loss Coefficients									
	2P ΔP Schikorr(Pa)	2P ΔP (In) [Pa]	2P ΔP Hyun/Oh (Pa)	2P ΔP Shiralkar (Pa)	2P ΔP Rehme Trippe (Pa)	2P ΔP (Rehme) (Pa)	2P ΔP (DeStourd) [Pa]	2P ΔP Spengos (Pa)	2P ΔP Idel'chick (Pa)	2P ΔP Tong/Weisman (Pa)
<b>Lottes</b>	4.55	10.74	28.20	8.29	11.02	13.51	24.40	19.09	30.34	148.14
<b>Lottes Expanded</b>	4.70	11.02	28.73	8.43	11.25	52.74	24.84	19.47	30.85	150.62
<b>Romie</b>	1.55	1.02	2.53	1.20	1.01	1.65	2.76	1.48	4.38	21.40
<b>Romie Expanded</b>	1.62	1.17	2.21	1.11	0.99	7.21	2.49	1.34	4.05	19.78
<b>Richardson</b>	0.61	0.16	2.60	1.00	0.83	1.48	2.54	1.54	3.64	17.78
<b>Mendler Mendler Corrected</b>	3.72	4.07	1.24	0.49	2.38	0.58	0.36	2.57	1.78	8.69
<b>Beattie</b>	3.38	3.70	1.14	0.44	2.17	11.72	0.35	2.34	1.61	7.87
<b>Chisolm</b>	3.48	3.81	1.13	0.47	2.22	0.42	0.34	2.39	1.71	8.34
	2.70	2.95	0.90	0.35	1.73	0.44	0.28	1.87	1.29	6.30

**Table 23: Accuracy of the 2 Phase Multiplier Based on 24% Quality and 8.65MPa**

Bias 2PØ 8.65 Mpa 24% quality	Pressure Loss Coefficient									
	2P ΔP Schikorr(Pa)	2P ΔP (In) [Pa]	2P ΔP Hyun/Oh (Pa)	2P ΔP Shiralkar (Pa)	2P ΔP Rehme Trippe (Pa)	2P ΔP (Rehme) (Pa)	2P ΔP (DeStourd) [Pa]	2P ΔP Spengos (Pa)	2P ΔP Idel'chick (Pa)	2P ΔP Tong/Weisman (Pa)
<b>Lottes</b>	165.72	306.98	509.44	39.11	203.35	160.24	375.57	367.57	408.90	2384.79
<b>Lottes Expanded</b>	169.22	312.35	517.49	40.95	207.35	163.68	381.85	373.74	415.62	2417.63
<b>Romie</b>	-45.37	-16.39	25.01	-71.49	-37.69	-46.64	-2.47	-4.01	4.28	409.17
<b>Romie Expanded</b>	-47.01	-18.90	21.26	-72.35	-39.56	-48.24	-5.40	-6.89	1.15	393.86
<b>Richardson</b>	-70.19	-54.37	-31.74	-84.43	-65.99	-70.86	-46.74	-47.60	-43.04	178.11
<b>Mendler</b>	-32.29	3.60	54.80	-64.72	-22.81	-33.93	20.76	18.90	29.08	530.23
<b>Mendler Corrected</b>	-41.54	-10.56	33.65	-69.54	-33.35	-42.96	4.26	2.66	11.44	444.15
<b>Beattie</b>	-27.21	11.37	66.41	-62.07	-17.02	-28.98	29.81	27.82	38.76	577.51
<b>Chisolm</b>	-52.24	-26.92	9.19	-75.11	-45.55	-53.40	-14.82	-16.13	-8.95	344.56

**Table 24: Precision of the 2 Phase Multiplier Based on 24% Quality and 8.65MPa**

Standard Dev 2PØ 8.65 Mpa 24% quality	Pressure Loss Coefficients									
	2P ΔP Schikorr(Pa)	2P ΔP (In) [Pa]	2P ΔP Hyun/Oh (Pa)	2P ΔP Shiralkar (Pa)	2P ΔP Rehme Trippe (Pa)	2P ΔP (Rehme) (Pa)	2P ΔP (DeStourd) [Pa]	2P ΔP Spengos (Pa)	2P ΔP Idel'chick (Pa)	2P ΔP Tong/Weisman (Pa)
<b>Lottes</b>	17.88	32.41	63.64	16.84	25.34	28.86	51.51	42.72	61.62	300.88
<b>Lottes Expanded</b>	18.34	33.17	64.98	17.18	25.93	29.45	52.57	43.67	62.84	306.84
<b>Romie</b>	0.50	0.45	3.90	1.40	0.59	2.01	3.41	1.61	5.12	24.98
<b>Romie Expanded</b>	0.65	0.29	3.43	1.28	0.44	1.79	3.03	1.29	4.67	22.81
<b>Richardson</b>	0.44	1.27	3.68	1.11	1.08	1.76	3.08	2.09	4.07	19.87
<b>Mendler</b>	2.75	2.81	0.80	0.70	1.84	0.48	0.62	1.74	2.55	12.47
<b>Mendler Corrected</b>	2.37	2.43	0.69	0.60	1.59	0.42	0.53	1.51	2.21	10.77
<b>Beattie</b>	2.95	3.03	0.87	0.75	1.98	0.52	0.67	1.87	2.75	13.41
<b>Chisolm</b>	1.94	1.98	0.56	0.49	1.30	0.34	0.44	1.23	1.80	8.80

Tables 9 through 24 result in 720 biases and 720 standard deviations for comparison. To further organize these results for clarification of the pressure-flow quality groupings, the models which have the lowest bias and the lowest standard deviation are listed for each quality ratio and pressure in Table 25. The models which have the lowest bias are compiled from the bias pressure-quality characteristics in Tables 9, 11, 13, 15, 17, 19, 21 and 23. The models, which have the lowest standard deviation from the standard deviation are compiled from the standard deviation pressure-quality characteristics Tables 10, 12, 14, 16, 18, 20, 22 and 24. The accompanying standard deviation and bias for each model are also listed in Table 25.

**Table 25: Highest Accuracy and Highest Precision Two-Phase Models at each Quality Ratio and Pressure**

Quality/ Pressure	Multiplier	Loss Coefficient	Lowest Bias	Standard Deviation	Multiplier	Loss Coefficient	Bias	Lowest Standard Deviation
<b>7.16 Mpa 7% quality</b>	Beattie	DeStourder	-1.43	1.90	Mendler Corr	Shiralkar	-64.97	0.15
<b>7.16 Mpa 10% quality</b>	Romie Exp	DeStourder	-0.17	1.56	Beattie	Shiralkar	-68.20	0.21
<b>7.16 Mpa 14% quality</b>	Lottes Exp	Shiralkar	-1.00	9.47	Chisholm	Shiralkar	-75.76	0.17
<b>7.16 Mpa 19% quality</b>	Mendler Corr	Spengos	0.44	2.86	Chisholm	* Shiralkar/ Rehme	-76.66/ -56.13	0.29/0.29
<b>7.16 Mpa 24% quality</b>	Mendler Corr	DeStourder	-0.01	0.53	* Chisholm/ Romie Exp	* Shiralkar/ In	-76.47/ -24.62	0.36/0.36
<b>8.65 Mpa 7% quality</b>	Romie Exp	In	-0.10	1.19	* Beattie/ Richardson	* Rehme/ In	-49.98/ -24.68	0.62/0.63
<b>8.65 Mpa 14% quality</b>	Romie Exp	DeStourder	-0.05	-2.49	Richardson	In	-42.22	0.16
<b>8.65 Mpa 24% quality</b>	Romie Exp	Idel'chik	1.15	4.67	Romie Exp	In	-18.90	0.29

\* Less than .01% separated the lowest deviation. Loss Coefficient, Bias and Standard Deviation are shown in order for the Listed Multiplier.

#### 7.2.5.2 Graphical Analysis of Two-Phase Spacer Grid Pressure Loss Models

Further analysis is performed through graphical comparisons of the two-phase multiplier-single-phase coefficient combinations over the change in flow quality for each pressure, to provide better visual comparison. Some of the models are eliminated; the Lottes Multipliers and the Tong/Weisman pressure loss factors have a comparatively high deviation and bias, and will not be shown. Only one version of the Romie and Mandler multipliers are shown, the version with the lowest deviation. The five chosen multipliers were then applied to each of the single-phase spacer pressure loss coefficients, in Figures 31 through 39, to compare the effect of the different two-phase spacer pressure multipliers on each of the single-phase spacer pressure loss coefficients.

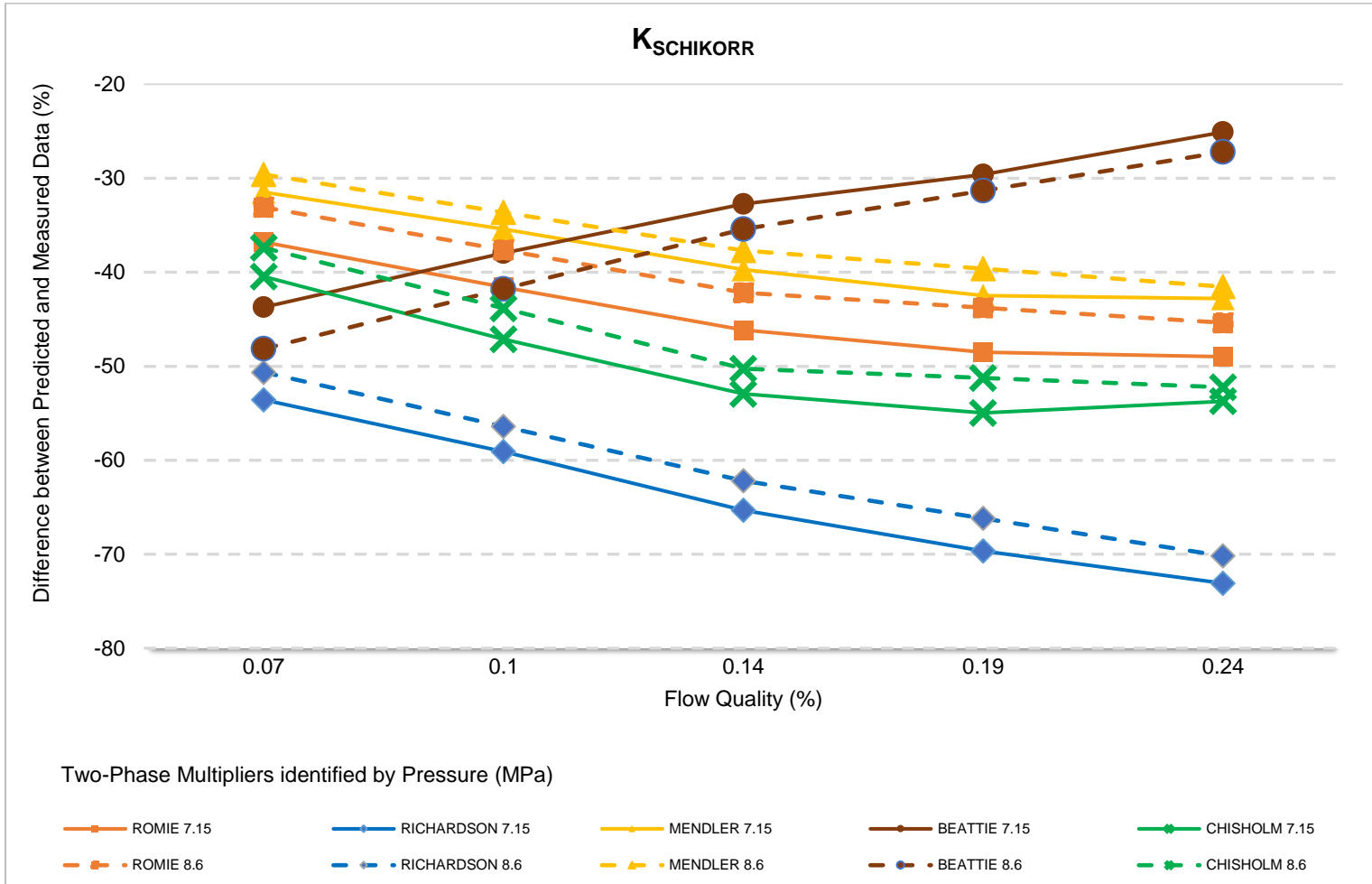


**Figure 31: Effect of Quality and Pressure on Accuracy – K<sub>Schikorr</sub>**



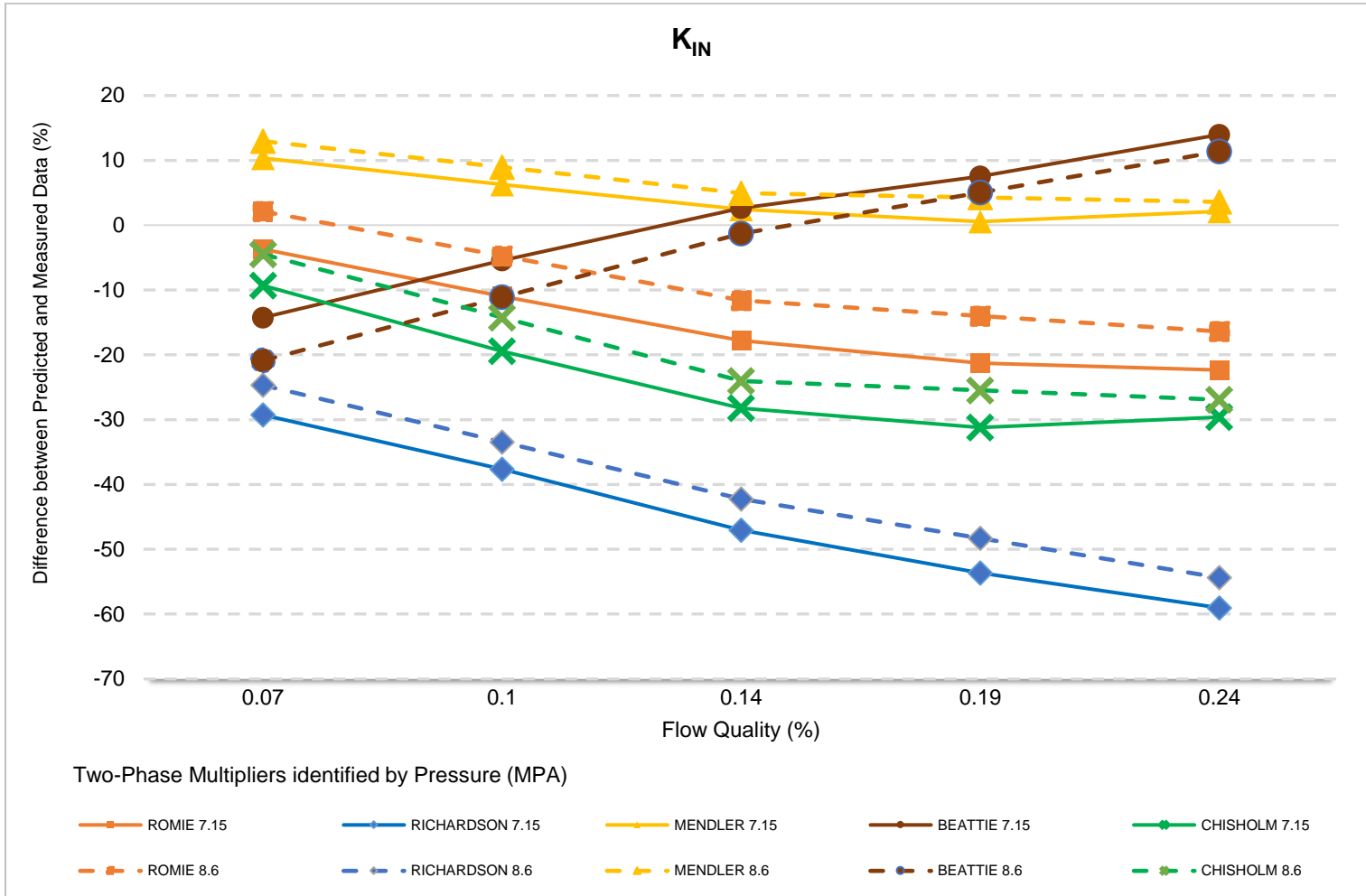


**Figure 32: Effect of Quality and Pressure on Accuracy -  $K_{IN}$**

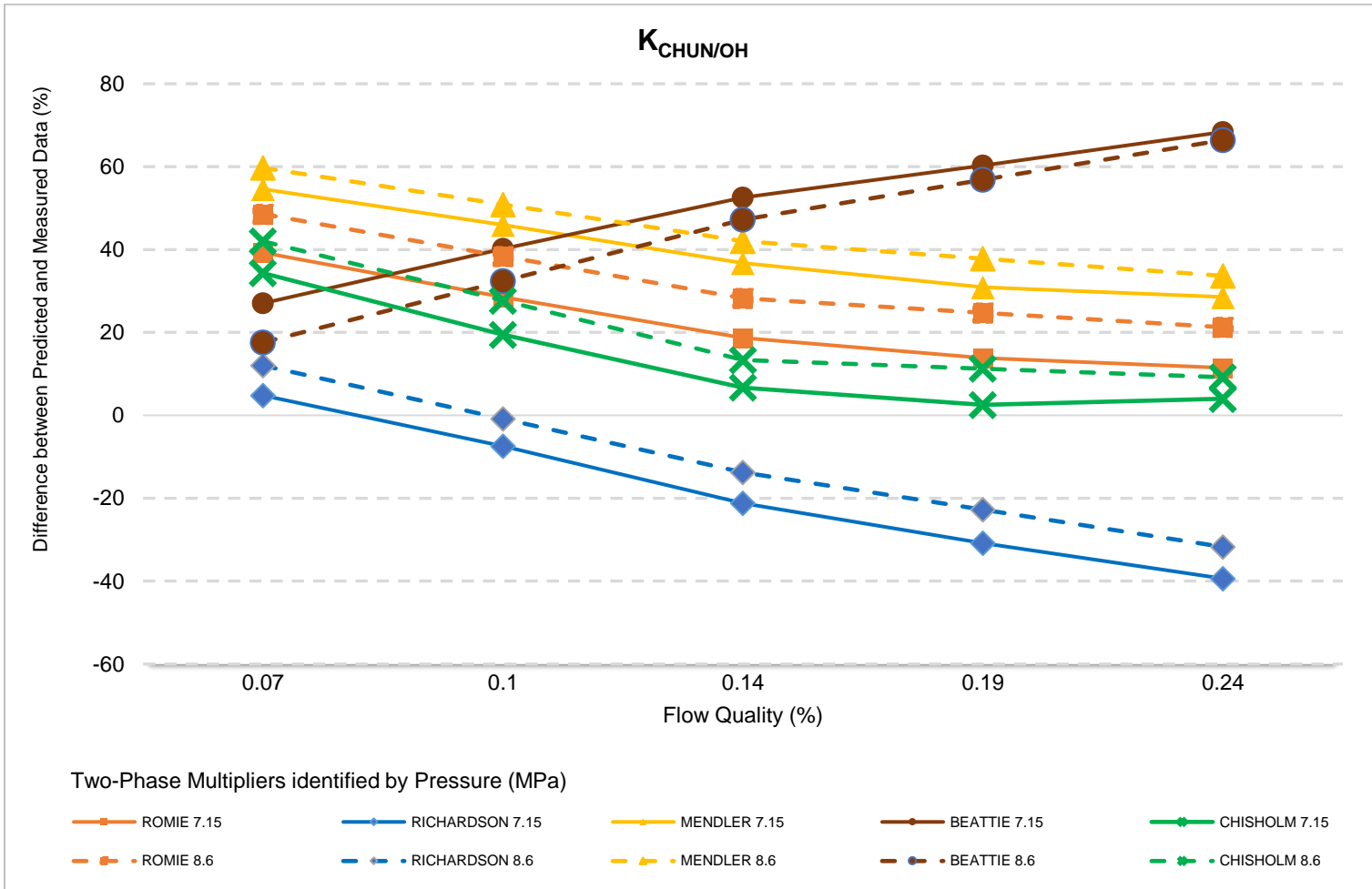
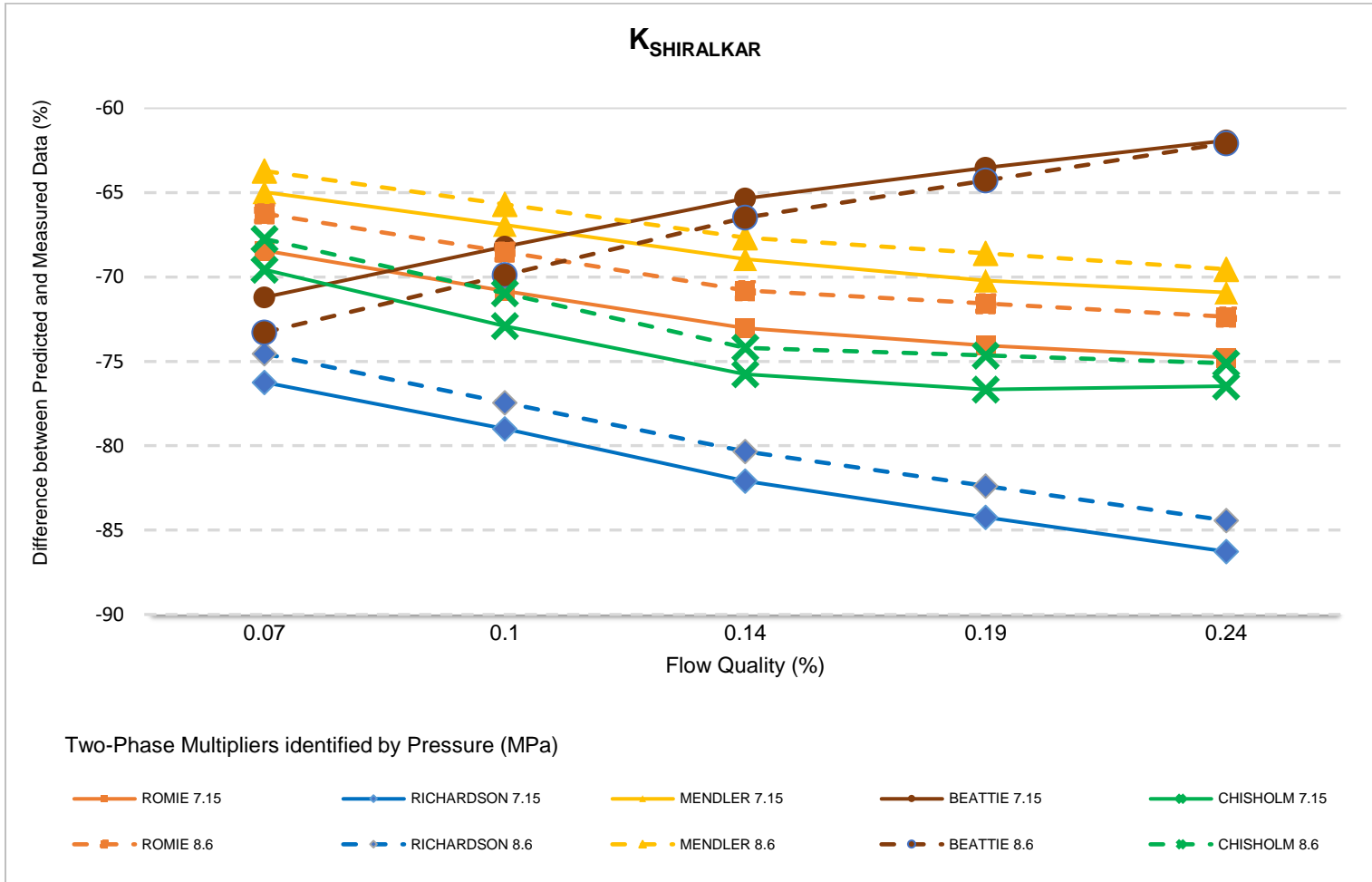


Figure 33: Effect of Quality and Pressure on Accuracy –  $K_{Co}$



**Figure 34: Effect of Quality and Pressure on Accuracy – K<sub>Shiralkar</sub>**

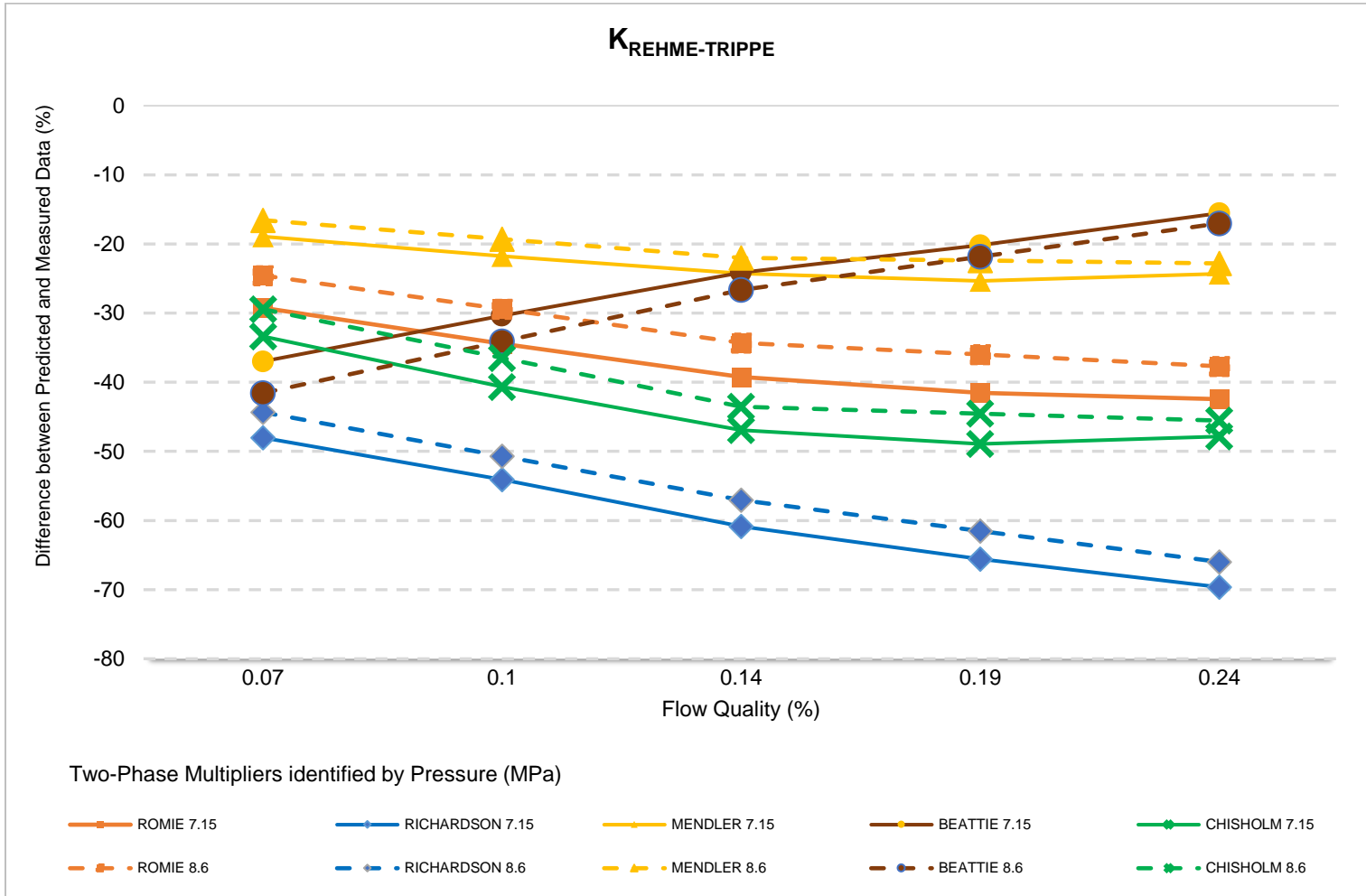


Figure 35: Effect of Quality and Pressure on Accuracy –  $K_{Rehme-Tripp}$

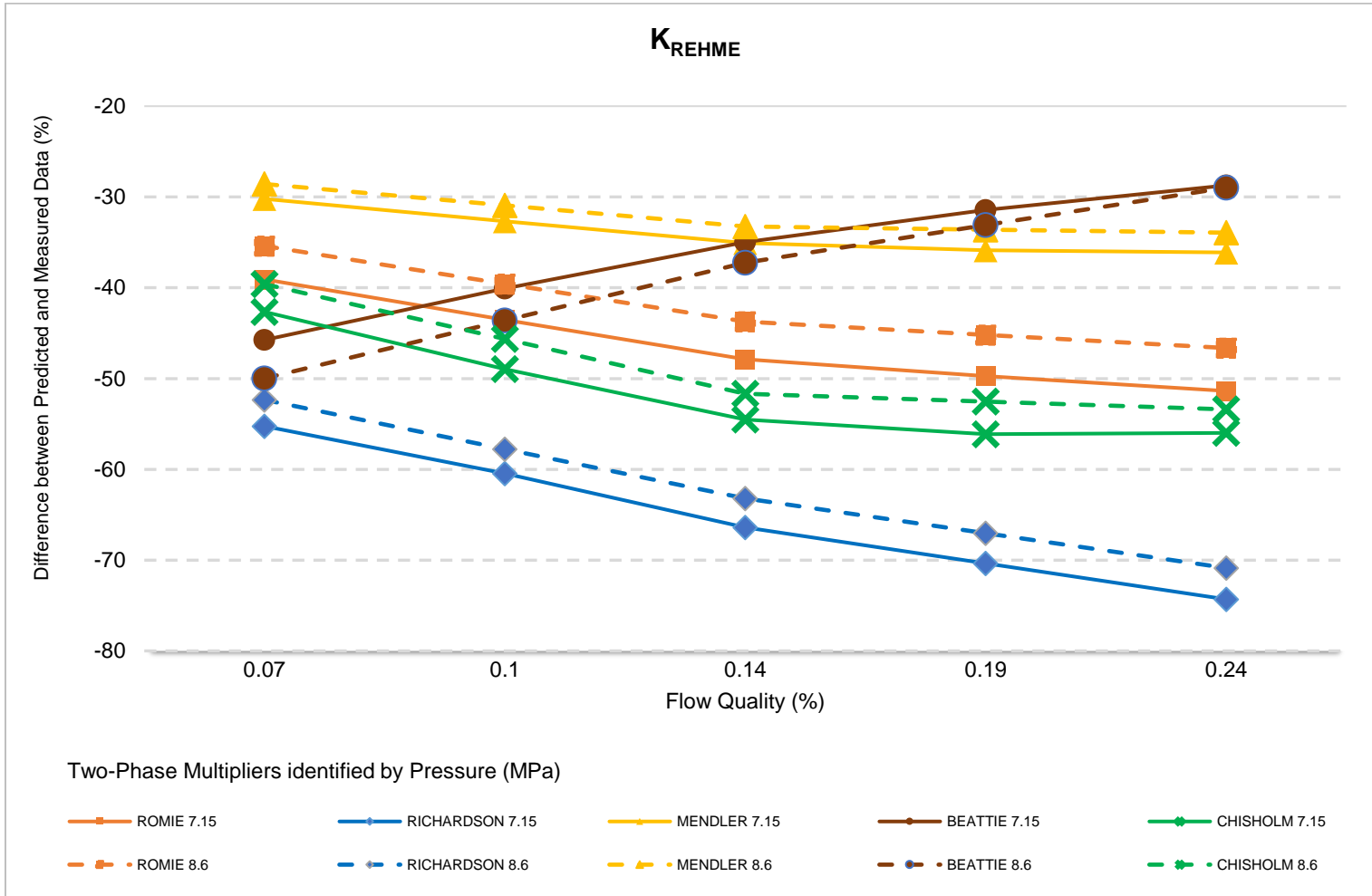
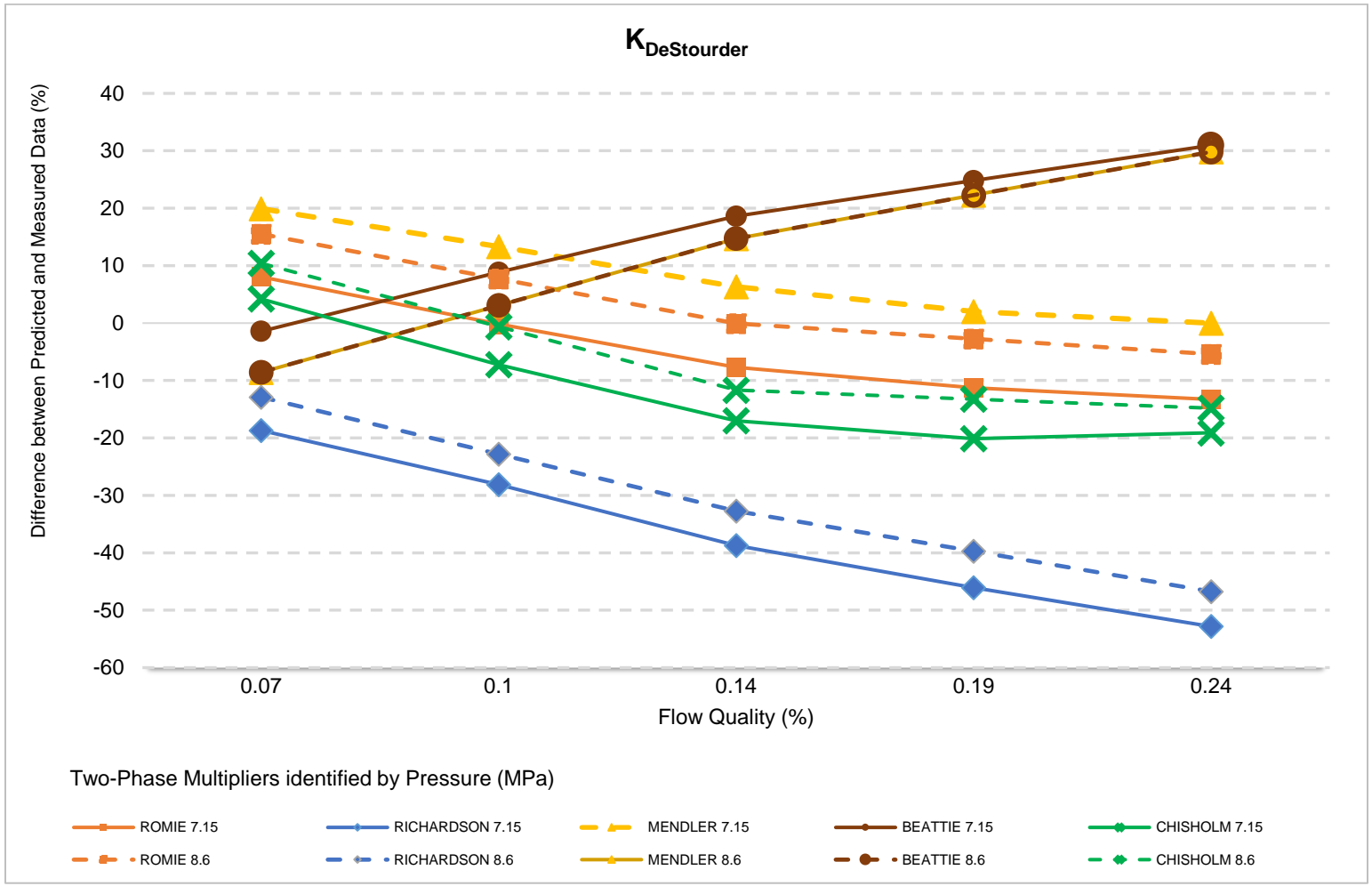
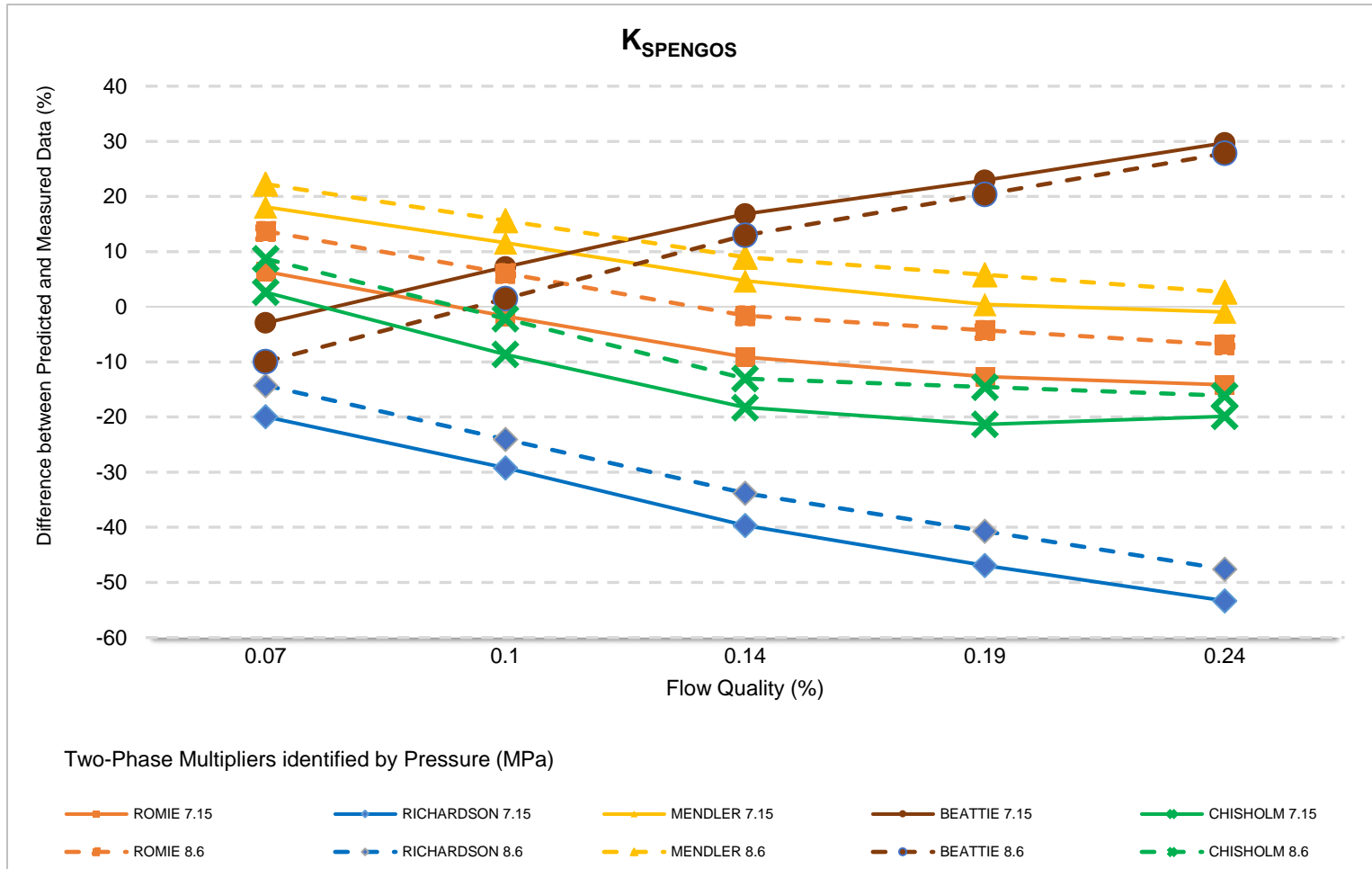


Figure 36: Effect of Quality and Pressure on Accuracy –  $K_{Rehme}$



**Figure 37: Effect of Quality and Pressure on Accuracy –  $K_{DeStourder}$**



**Figure 38: Effect of Quality and Pressure on Accuracy – K<sub>Spengos</sub>**

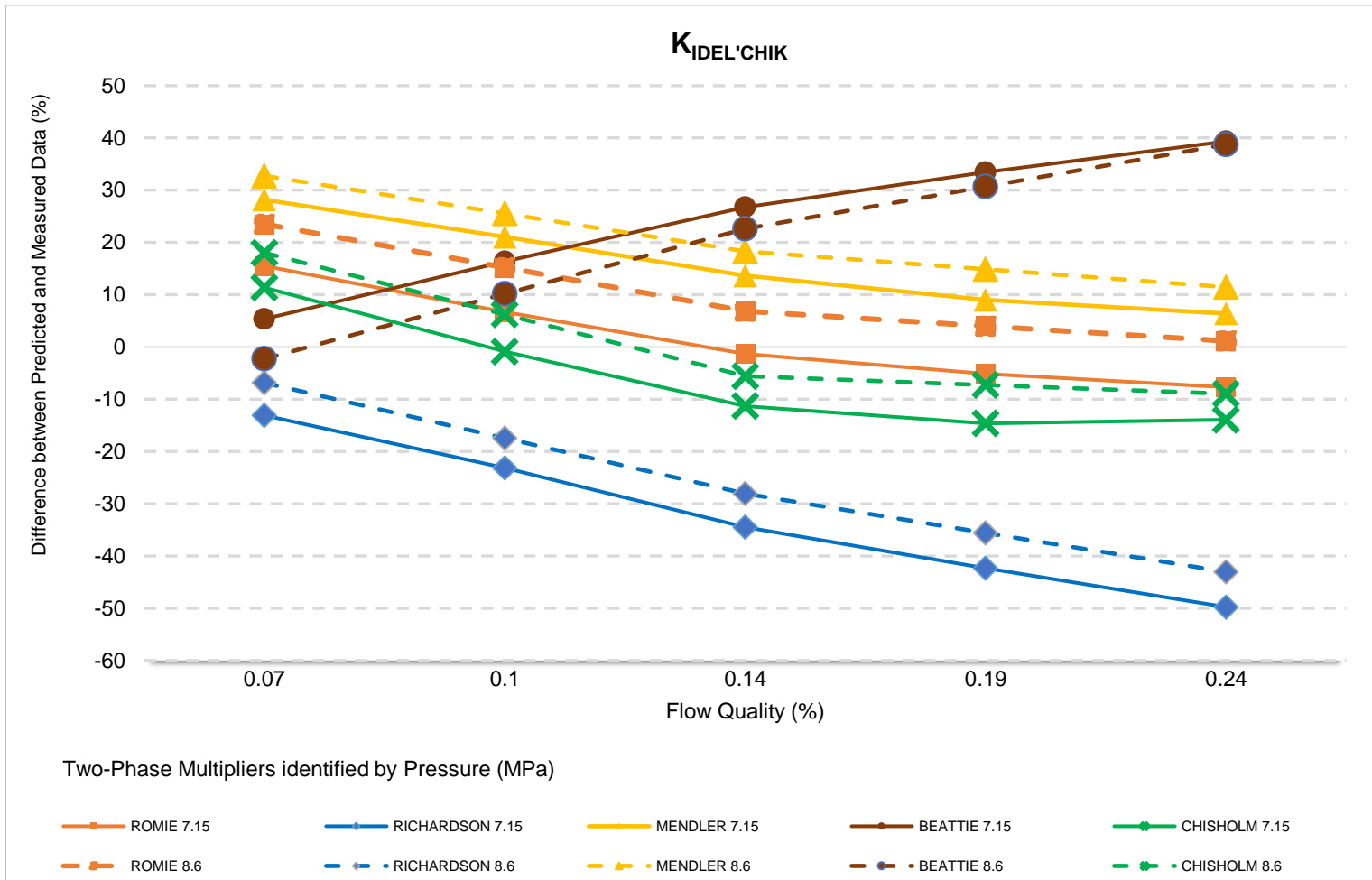


**Figure 39: Effect of Quality and Pressure on Accuracy -  $K_{IDEL'chik}$**



### 7.3. Observations

#### 7.3.1. Two-Phase Spacer Multipliers and Single-Phase Coefficients Observations

Descriptions of the models for two-phase spacer grid pressure loss, and the two-phase models' analyses of the results are more complex than the single-phase spacer grid pressure loss results. The first reason two-phase models are more complex is there is not a distinct model, the two-phase model consists of a correlation factor, which is the two-phase spacer grid pressure loss multiplier ( $\emptyset$ ), which can be multiplied by any one of ten single-phase spacer grid pressure loss coefficients (K). The second reason is the number of results, nine two-phase multipliers multiplied by ten single-phase coefficients provide results for ninety models, compared to ten results for single-phase models. The third reason is the necessity to organize the effect of multiple flow characteristics on the bias and standard deviation, compared to only Reynolds Number and pressure for the single-phase results.

For brevity, the two-phase models will be described using the term "multiplier-coefficient combination" instead of "two-phase multiplier single-phase coefficient spacer grid pressure loss model." Tables 7 and 8, which combine the bias and deviation results for all thirty-three pressure loss estimates, for each multiplier-coefficient combination, will be described by the term "combined characteristics tables." Tables 9 through 24, which combine the bias and deviation for the pressure loss estimates from the flow quality and pressure shown in the title of the table, will be described by the term "pressure-quality characteristics tables." Table 25 identifies the multiplier-coefficient combination, which has the lowest bias and standard deviation from each bias and standard deviation pressure-quality characteristic table, will be described by the term "lowest bias-deviation table."

To assist in comparisons, models with large variances in comparison to other models are eliminated. The Tong/Weisman Pressure Loss Factor has a significantly higher bias and deviation. This is likely because it was developed for expansions and contractions in a PWR,

so its function and factors from its drag coefficients chart were based on single-phase flows and a different fuel channel. The Lottes and Lottes Expanded Multipliers also demonstrated a significantly higher bias and deviation using the BFBT flow characteristics. Therefore, these models will not be analyzed further, because these models' results do not produce useable data.

For the same reasons as the results for single-phase pressure loss tests, the measures of performance are only by comparison. Comparison of Table 7, the bias combined characteristics table, to Table 25, the lowest bias-deviation table, identifies that the lowest bias in each grouping of flow quality and pressure, was lower than all the two-phase multiplier averages. The lowest bias from Table 25 was also lower than all the single-phase spacer grid pressure loss coefficients averages except for the DeStourder single-phase loss coefficient.

Comparison of Table 8, standard deviation combined characteristics tables, to Table 25, lowest bias-deviation table, identifies that the lowest standard deviation in each grouping of flow quality and pressure, was lower than all the two-phase multiplier averages, and also lower than all the single-phase coefficients' averages. In addition, the lowest standard deviation, from Table 25, was less than 20% of any of the single-phase pressure loss coefficients averages and two-phase multiplier averages. This low deviation was expected from the closeness of the bias grouping in Figures 28 and 29 at specific flow qualities and pressures.

From the combined results shown in Table 7, the most precise and accurate two-phase multiplier, using the BFBT test data, was the Mandler Two-Phase Multiplier, with the lowest average bias of -1.91 % and the lowest average standard deviation of 4.36%. The single-phase coefficient with lowest average bias was the DeStourder Single-Phase Loss Coefficient, with an average bias of 0.04% and an average standard deviation of 7.78%. From the combined results shown in Table 8, the single-phase coefficient with lowest average

standard deviation was the Shiralkar Coefficient, with an average standard deviation of 2.33% and an average bias of -55.06%.

From the combined results shown in Table 7, the most accurate multiplier–coefficient combination using the BFBT test data was the Beattie-In Two-Phase Model, with the lowest average bias of -0.36% and a standard deviation of 12.28%. From the combined results shown in Table 8, the most precise multiplier–coefficient combination was the Mandler-Shiralkar Two-Phase Model, with the lowest average standard deviation of 1.44% and an average bias of -64.46%.

From Table 25, the lowest bias-deviation table, in the 7.16 MPa pressure range, no multiplier indicates any advantage for the accuracy of calculated estimates. Four different two-phase multipliers providing the lowest bias in the five possible quality-pressure groupings provides this indication. The DeStourder Single-Phase Coefficient indicates an advantage for the bias of calculated estimates, by providing the lowest bias for three of the five possible flow quality groupings. However, this single-phase coefficient combined with different two-phase multipliers for every occurrence and the three values were not consecutive.

From Table 25, at the 7.16 MPa pressure range, the Chisolm Multiplier and Shiralkar multiplier-coefficient combination indicates a comparative advantage for precision, by providing 60% of the lowest standard deviations in the five possible pressure-quality groupings, all grouped in the higher flow quality sub-groups. Also, the Shiralkar Single-Phase Coefficient indicates a comparative advantage for precision by providing the lowest standard deviation for all five quality-pressure groupings, however it combined with different two-phase multipliers for the lowest two-flow qualities.

From Table 25, the lowest bias-deviation table, at the 8.65 MPa pressure range, the Romie Expanded Multiplier indicates a comparative advantage for accuracy by providing the lowest bias for all three quality-pressure groupings. However, the Romie Expanded Multiplier

combined with a different single-phase coefficient for each occurrence. The Richardson Two-Phase Multiplier indicates a comparative advantage for precision by providing the lowest standard deviation for the first two of the three quality-pressure groupings. The In Pressure Loss Coefficient indicates a comparative advantage for precision, by providing the lowest standard deviation for all three quality-pressure groupings. By providing the lowest standard deviation, it means other multiplier-coefficient combinations may have provided an equal value, as annotated in Table 25.

Other significant observations from Tables 7, 8, and 25, and a broad observation of tables 9 through 24, are the majority of the multiplier – coefficient combinations with the lowest bias or standard deviation do not have a comparatively low bias or standard deviation. Also, the In-Expanded Romie Multiplier- Coefficient Combination was the model providing the lowest bias for the highest flow quality in both pressure groups.

#### 7.3.2. General Observations and Trends

Comparing Tables 9, 11, 13, 15, 17, 19, 21 and 23, the bias pressure-quality characteristics tables, to Table 7, the bias combined characteristics table, the biases of all the multiplier-coefficient combinations, from the bias pressure-quality characteristics tables, are both above and below the average bias in Table 7. Comparing Tables 10, 12, 14, 16, 18, 20, 22 and 24, the standard deviation pressure-quality characteristics tables, to Table 8, the standard deviation combined characteristics table, the standard deviations of all the multiplier-coefficient combinations from the pressure-quality characteristics table are below the average standard deviation in Table 8 by at least 50%.

The lower deviation was expected from the closeness of the bias grouping in Figures 28 and 29 at specific flow qualities and pressures. This verifies the biases group according to pressure and quality ratio. The variance in the biases was also expected from the range of

the bias groups' values in Figures 28 and 29, which was better explained by graphical analysis.

Graphical analysis of the multipliers in Figures 31 through 39, across the flow qualities and by pressure, provided clarification of the results and variances in the tabular results. For all the two-phase spacer grid pressure loss multipliers, except the Beattie and Lottes multipliers, the bias calculated at a quality ratio is a lower value than the bias calculated at the lower quality ratio. The value declines whether it overestimates the bias, a positive value, or underestimates the bias, a negative value. An example is: The bias ranges from +5% at 10% quality, to -5% at 14% quality, to -15% at 19% quality. The Beattie and the Lottes multipliers move in the opposite direction from the other multipliers, and the calculated bias at a quality ratio, is a higher value than the bias calculated for the previous quality ratio.

The general plots, for the 7.16 MPa and 8.65 MPa pressures follow the same general trend as each other, for each model, as shown in the graphs in Figures 31 through 39. For all the multipliers except the Beattie multiplier, the calculated bias at 8.65 MPa has a higher value than the 7.16 MPa pressure bias. For the Beattie multiplier, the calculated bias at 8.65 MPa, is a lower value than the 7.16 MPa pressure bias.

These graphs indicate the effects of flow quality and pressure in Figures 31 through 39 confirm the initial trends identified in Figures 28, 29 and 30. For the BFBT test set, the quality ratio increase, at a specific pressure, affects each group of biases with a consistent increase or decrease, causing the groups of biases to occupy a range of values. The effect is the highest accuracy multiplier-coefficient combination is random for a given flow quality. However, the average bias for a specific pressure and flow quality grouping has a low deviation, enabling an estimated bias with a high degree of certainty.

#### 7.4. References

Awad, M.M. and Muzychka, Y.S., 2008. Effective Property Models for Homogenous Two-Phase Flows. *Experimental Thermal and Fluid Science*, Vol. 33, No. 1, pp. 106-113.

Chun, T.H. and Oh D.S., 1998. A Pressure Drop Model for Spacer Grids with and without Flow Mixing Vanes. *Journal of Nuclear Science and Technology*, Vol.35, No. 7, pp. 508-510.

DeStourder, A. N., 1961. Drag Coefficients for Fuel Element Spacers. *Nucleonics*, Vol. 19, No. 6, pp. 74-79.

Glueck, M., 2008. Validation of the Sub-Channel Code F-COBRA-TF, Part I. Recalculation of Single-Phase and Two-Phase Pressure Loss Measurements. *Nuclear Engineering and Design*, Vol. 238, No. 9, pp. 2308-2316.

Idel'chik, I. E., 1986. *Handbook of Hydraulic Resistance*, 2<sup>nd</sup> ed. Hemisphere Publishing Corporation, New York, ISBN: 978-0-8911-6284-1.

In, W.K., Oh, D.S. and Chun, T.H., 2002. Empirical and Computational Pressure Drop Correlations for PWR Spacer Grids. *Nuclear Technology*, Vol. 139, No. 1, pp. 72-79.

Lahey Jr., R. T. Jr. and Moody, F. J., 1993. *The Thermal-Hydraulics of a Boiling Water Nuclear Reactor*, 2nd Ed. American Nuclear Society Publishing, La Grange Park, Illinois, ISBN: 0-89448-037-5.

Neykov, B., Aydogan, F., Hochreiter, L., Ivanov, K., Utsuno, H., Kasahara, F., Sartori, E., and Martin, M., 2006. NUPEC BWR Full-size Fine-mesh Bundle Test (BFBT) Benchmark, Vol. I: Specifications. OECD, Nuclear Energy Agency, NEA No. 6212, ISBN: 92-64-01088-2.

Rehme, K., 1973. Pressure Drop Correlations for Fuel Element Spacers. *Nuclear Technology*, Vol. 17, No. 1, pp. 15-23.

Rehme, K. and Trippe, G., 1980. Pressure Drop and Velocity Distribution in Rod Bundles with Spacer Grids. *Nuclear Engineering Design*, Vol. 62, No. 1, pp. 349-359.

Schikorr, M., Bubelis, E., Mansani, E. L., and Litfin, K., 2010. Proposal for Pressure Drop Prediction for a Fuel Bundle with Grid Spacers using Rehme Pressure Drop Correlations. *Nuclear Engineering and Design*, Vol. 240, No. 7, pp. 1830-1842.

Spengos, A. C., 1959. Tests on Models of Nuclear Reactor Elements, IV. Model Study of Fuel Element Supports. UMRI-2431-4-P, University of Michigan Research Institute, Ann Arbor.

Tong, L.S., and Weisman, J., 1970. *Thermal Analysis of Pressurized Water Reactors*, 1st Ed. American Nuclear Society Publishing, La Grange Park, Illinois, ISBN: 978-0-8944-8038-6.

Venkateswararao, P., Semiat, R. and Dukler, A.E., 1982. Flow Pattern Transition for Gas-Liquid Flow in a Vertical Rod Bundle. *International Journal of Multiphase Flow*, Vol. 8, No. 5, pp. 509-524.

## CHAPTER 8: CONCLUSIONS

The BWR Full-Size Fine Mesh Bundle Test (BFBT) results were selected to analyze flow characteristics and pressure loss, through nuclear fuel bundle spacer grids, because of the detailed flow data available. The BFBT benchmark study provides the most extensive data available on a full-size fuel rod bundle spacer grid in a variety of operational conditions with detailed measurements of the flow properties. The BFBT test results are used to calculate accurate friction, gravity, and acceleration loss factors using accurate BFBT pressure drop measurements across the spacer grid.

These measurements enable application of precise data to individual historical models, so the models' predictive capabilities could be defined and evaluated. The detailed measurements from BFBT also enable accurate calculation of flow characteristics, such as Reynolds Number and flow quality. This resolution enables observation of these characteristics' effects on the accuracy and the deviation of available spacer grid pressure loss models.

In the scope of this thesis, ten single-phase spacer grid models and nine two-phase multipliers were chosen because the available literature provides enough supporting data to separate them from other models. These mathematical models predict pressure losses, which are evaluated against the BFBT measured losses and detailed flow characteristics. Single-phase flow characteristics consist of Reynolds Number and pressure, while two-phase flow characteristics include Reynolds Number, pressure, quality ratio and void coefficient. The flow regime was also evaluated. However, because the selected spacer grid locations are near the end of the BFBT experimental simulator flow, the flow regime map verified that all the test flows can be considered annular. Since different flow regimes are not available, different results cannot be compared to each other.

The single-phase models' comparisons to the experimental data demonstrate that the historical models' predictions have a bias from almost every measured value. The range of each model's bias value is larger at a lower pressure and Reynolds Numbers. The comparison of the models' accuracy identifies trends which could lead to further study. However, the results indicate no clear trends in the models' bias across the Reynolds Numbers. Comparison of the models' precision identifies a trend in the precision of the models at lower Reynolds Numbers. As the Reynolds Number decreases, the single-phase spacer grid pressure loss models' standard deviations tend to increase. In the lower pressure range, the plot, or the calculated value, of the models' drag coefficient has a wider variation. Identifying an exact drag coefficient makes the models more difficult to mathematically model at the lower tested pressures and flowrates in the BFBT. This deviation is important particularly in startup, shut down and low power conditions.

The first model, that demonstrates a comparative averaged advantage using the BFBT flow characteristics, is the Trippe/Rehme Model in the criterion of accuracy, with a below the median variance. The Shiralkar Model demonstrates an overall averaged advantage in the criterion of precision, however the bias is above the median. Further analysis of individual spacer grid models identifies advantages and disadvantages based on accuracy and precision, within specific groupings of flow characteristics. The Rehme-Trippe Model and the Shiralkar Model have the lowest bias and precision, respectively, in the higher-pressure conditions. However, in the 200 KPa flow pressure, other models demonstrate a lower bias and lower standard deviation.

The results of the graphical analyses and summarized calculations demonstrate the conditions at which specific single-phase models perform better than others. Almost every model that demonstrates a low bias or low standard deviation cannot consistently demonstrate an accompanying low standard deviation or bias, or any distinct trends in the



flow characteristics that could affect the accuracy. The existing models were developed under various conditions, using equipment designed for specific operations. No single historical one-dimensional single-phase spacer grid pressure loss model has demonstrated it can provide the comparatively best accuracy and precision under all the tested conditions.

The two-phase models' comparison of the flow characteristics of Reynolds Number, pressure, void fraction, and flow quality, demonstrates a correlation between the bias, and flow quality and pressure. A correlation between the bias and the flow characteristic of void fraction is indicated. However, flow quality and pressure provide a more distinct relation.

Based on the results of the flow characteristics' analyses, the ninety two-phase multiplier-coefficient combinations' biases and variances were grouped by the eight pressure-flow quality groupings in separate tables. Graphically, nine single-phase coefficients were combined with five different two-phase multipliers, enabling improved comparison of the effects of flow quality and pressure on multiplier-coefficient combinations' biases. The bias to the measured pressure loss was then plotted across the range of flow qualities. Grouping by pressure and flow quality verified that those flow characteristics caused those biases to group together with a below average deviation, while the groups of biases are both above and below the initial reference table's average. The explanation from the analyses is the bias proportionately increases or decreases across the range of flow qualities for every two-phase multiplier, placing the models' biases both above and below the measured bias as a function of the specific flow quality and pressure.

Comparison of the models with the lowest biases and deviations demonstrated only the Romie Expanded Two-Phase Multiplier demonstrates a consistent advantage in the criterion of bias at higher pressures. More consistent advantages were demonstrated in the criterion of deviation with the Chisholm-Shiralkar and Richardson-In Multiplier-Coefficient Combinations, and the Shiralkar and In Single-Phase Coefficients. However, the

accompanying biases are all above the average. No single multiplier-coefficient combination demonstrated the lowest bias or deviation consistently and no multiplier-coefficient combination can provide both a low bias and low deviation consistently in every pressure-quality group.

The conclusions from the application of the BFBT to historical two-phase spacer grid pressure loss models are given below:

- Multiplier-coefficient combinations exist that can provide accuracy and precision within specific conditions of the BFBT. However, no single two-phase spacer grid pressure loss models can be applied to all flow conditions.
- The accuracy of the two-phase multiplier-coefficient combination is a function of the flow quality and pressure variables, so improvements to the two-phase spacer grid pressure loss models need to include these flow characteristics.
- This study indicates the accuracy of the two-phase multiplier-coefficient combination is possibly a function of a single flow characteristic, the void coefficient.

The results of this thesis can lead to further study in refinement of mathematical models and then applying those models to different spacer grid configurations. The scope of this study was to apply one-dimensional mathematical models from available literature to a spacer grid, that had detailed flow characteristic measurements from the BFBT. The objective of this study was to identify a one-dimensional mathematical model, that incorporates the factors causing pressure loss across spacer grids accurately and precisely, in all conditions. This scope and objective focused the study on one specific grid location and fuel bundle, and the development of a framework to analyze and compare numerous possible models.

The results identified that the single-phase mathematical models require further development of the flow characteristics in the lower Reynolds Numbers, where friction and drag have a greater effect. The two-phase mathematical models identified that grouping the models' biases by flow quality and pressure forms a precise line, with a distinctive slope, compared to the measured pressure loss. Further study would develop factors for the equations, which would align the bias with the measured pressure loss. The models in both phases, demonstrating the best accuracy and precision, require further refinement to develop factors to increase their accuracy and precision, over the entire range of conditions. Based on the results from this study, further research would begin with the Shiralkar Model, the Rehme-Trippe Model, The Chisolm-Shiralkar Two Phase Combination and the Romie Expanded-In Two Phase Combination.

Further study to refine the equations would consist of applying the framework developed in this study, to the remainder of the spacers in the fuel bundle. These spacer grids are all in the flow prior to this study's spacer, so the flow would be less turbulent, have different Reynolds Numbers, and provide more flow regimes. This would provide a wider range of flow characteristic measurements, in order to refine the models.

Detailed flow measurements from other spacer grids and configurations are necessary to achieve the BFBT goal of identifying critical flow properties, which enable application over a wide range of conditions. The framework developed for this study would be applied to compare the results from different configurations, and further refine the model's predictions, from the effect of critical properties on the different configuration. The different configurations would consist of different geometries, and different materials, coatings and surfaces. Based on the factors in the better performing models, a coating or a configuration that reduces either the length of contact through the spacer grid, blockage ratio, or reduces the drag through the spacer grid, is likely to reduce the pressure losses and provide a more accurate and precise model.